Development of bispecific antibodies with optimized T cell costimulatory activity

Dissertation

der Mathematisch-Naturwissenschaftlichen Fakultät

der Eberhard Karls Universität Tübingen

zur Erlangung des Grades eines

Doktors der Naturwissenschaften

(Dr. rer. nat.)

vorgelegt von

Dipl. Biologe (t.o.) Timo Manz

aus Reutlingen

Tübingen

2020

Gedruckt mit Genehmigung der Mathematisch-Naturwissenschaftlichen Fakultät der Eberhard Karls Universität Tübingen.

Tag der mündlichen Qualifikation:	19.10.2020
Stellvertretender Dekan:	Prof. Dr. József Fortágh
1. Berichterstatter:	Prof. Dr. Gundram Jung
2. Berichterstatter:	Prof. Dr. Hans-Georg Rammensee

Meiner Familie und Freunden

Abstract

In recent years, the clinical application of therapeutic antibodies has already significantly improved the therapy and prognosis of various malignant diseases. Notably, immunomodulating antibodies demonstrated the possibility to selectively modify the T cell-response and thus represent an attractive therapeutic strategy. However, in many cases, the therapeutic success of monospecific antibodies is limited or comes with severe systematic side-effects in patients. In comparison, the use of bispecific antibodies demonstrated several advantages by enabling the recruitment and activation of effector cells such as T cells, specifically at the tumor side.

This thesis presents the *in vitro* generation, characterization and optimization of novel immunomodulating bispecific antibodies for target cell-restricted modulation of T cell activation. The bispecific endoglinxCD28 antibodies were subjected to an extensive characterization process aiming at the identification of the optimal antibody format and clone. Finally, secondary work focused on a successful humanization by CDR grafting to decrease the risk of immunogenicity.

In further work, proof of concept studies were performed to evaluate the suitability of 4-1BB or PD-1 targeting bispecific antibodies. Novel antibodies were generated using hybridoma generation and phage display technology and underwent an extensive characterization to identify agonistic and antagonistic antibodies. The bispecific antibodies directed against 4-1BB revealed a target cell-restricted activation of T cells with a correlation between affinity and the induced activation. In further studies, target-cell restricted blockade using the bispecific PD-1 antagonist TIM4-E6 could not be archived.

Taken together, certain immunomodulating antibodies described in this work demonstrated a beneficial effect on activated T cells only in a target cell-restricted manner and demonstrate the potential of a novel promising therapeutic candidate for selective cancer treatment.

Zusammenfassung

In den letzten Jahren hat die klinische Anwendung therpaheutischer Antiköper die Therapie und Prognose verschiedener maligner Erkrankungen deutlich verbessert. Insbesondere Antikörper mit immunmodulierender Wirkung zeigten die Möglichkeit einer selektiven Beeinflussung der T-Zell-Antwort und stellen somit eine vielversprechende therapeutische Strategie dar.

In vielen Fällen ist jedoch der therapheutische Erfolg monospezifischer Antikörper begrenzt und oft zu schwerwiegenden Nebenwirkungen bei den Patienten. Im Vergleich dazu zeigen der Einsatz bispezifischer Antikörper Vorteile in der selektiven Rekrutierung und Aktivierung von Effektorzellen wie beispielsweise T-Zellen im Tumor.

Die vorliegende Arbeit präsentiert die *in vitro* Generierung, Charakterisierund und Otimierung neuer immunmodulierender bispezifischer Antikörper für eine Ziellzell-restringierte Modulierung der T-Zell-Aktivierung. Die bispezifische EndoglinxCD28 Antikörper wurden einer intensiven Charakterisierung unterzogen, um die Verwendung eines optimalen Antikörperformats und Antikörperklones zu ermöglichen. Darüber hinaus erfolgte zur Minimierung des Risikos der Immunogenität eine Hummanisierung über die Transplantation der Komplementaritäts-bestimmenden Regionen.

Des Weiteren erfolgte ein konzeptioneller Beweis für die Verwendung von 4-1BB und PD-1 gerichteten bispezifischen Antikörpern. Hierfür wurden neue Antikörper über die Hybridomgenerierung sowie das Phagendisplay generiert und wurden einer intensiven Charakterisierung unterzogen um etwaige agonistische oder antagonistische Antikörper zu identifizieren. Die gegen 4-1BB gerichteten bispezifischen Antikörper zeigten eine Zielzell-gerichtete Aktivierung von T-Zellen mit einer Korrelation zwischen ihrer Affinität und der induzierten Aktivierung. Mit der Verwendungen des PD-1 gerichteten Klones TIM4-E6 konnte in weiteren Experimenten keine zielzellgerichtete Blockade von PD-1 erreicht werden.

Die hier beschriebenen immunmoduliernden Antikörper zeigen in Teilen eine deutliche Zielzell-gerichtet Wirkung auf aktivierte T-Zellen und zeigen so das Potential einer neuartigen selektiven Tumortherapie.

Table of Contents

1. Introduction

1.1 The immune system

Every living organism needs do defend itself from harmful invaders such as viruses, bacteria, and parasitic worms, collectively called pathogens. For this purpose, vertebrates have developed the immune system, a complex of interactions involving protective barriers, toxic molecules, restriction factors, and phagocytic cells to prevent entry and survival of such pathogens. Two distinctive types of immune responses can be distinguished to protect the host from infections, the innate, and the adaptive immune response (Figure 1). The innate immune system is broadly considered to be the first line of host defense in vertebrates. In contrast, adaptive immunity is establishing overtime upon the contact of hosts with pathogens. It has evolved to provide a broader and fine-tuned repertoire of recognition for both self- and nonself-antigens. Nonetheless, both types of responses are closely connected and work together to eliminate pathogens.

1.1.1 Innate immune system

The innate immune system refers to the concept of first-line host defense in vertebrates to recognize microorganisms and other pathogens. Basic molecular modules serving this purpose are found in plants and animals, proving it to be an evolutionarily ancient host defense mechanism [7]. The first layer of defense is a physical and chemical barrier. Antimicrobial chemicals associated with epithelial layers can block the entrance of pathogens into the host. Blood proteins, including members of the complement system and other mediators of inflammation such as cytokines, form the second component of the innate immune system. A series of sequentially activated proteins in a complex enzymatic cascade constitute the complement system. Effector functions of the complement system include the opsonization of antigen followed by phagocytosis via effector cells such as macrophages. Promotion of the inflammatory response and the formation of membrane attack complexes to induce lysis are the effector functions of the innate immune system.

Finally, the innate immune system is programmed to detect invariant features of invading pathogens and compromises different immune cells (Figure 1) such as NK cells, macrophages, monocytes, dendritic cells, neutrophils, eosinophils, basophils and mast cells [8]. Pattern recognition receptors (PRRs) specifically recognize proteins, carbohydrates, lipids and nucleic acids. PRRs are germline-encoded, limiting their overall number. Prominent members of the PRRs are Toll-like receptors, scavenger receptors, C-type lectin receptors, nucleotide-binding oligomerization domain-like receptors, and beta 2-integrins, which are expressed by antigen-presenting cells (APCs) such as macrophages and dendritic cells. APCs, play an essential role in the activation of the adaptive immune system. Thus, these cells are linking the innate and adaptive parts of the immune system.

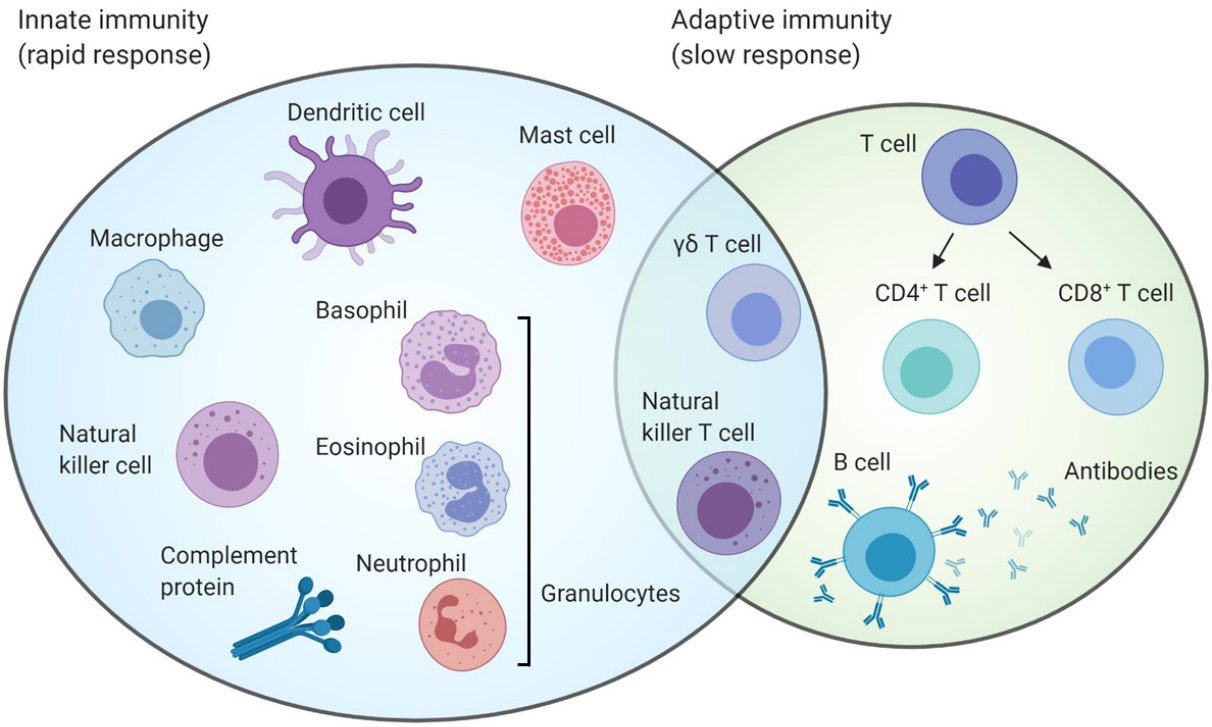

Figure 1: The innate and adaptive immune response. The innate immune response functions as an initial line of defense against pathogens. Its fast response consists of soluble factors such as complement proteins and cellular components including mast cells, dendritic cells, macrophages, natural killer cells, and granulocytes (basophils, eosinophils, and neutrophils). The development of the adaptive immune response is slower but results in a more defined specificity. It consist of antibody secreting B cells and CD4/CD8 T cells. In between, natural killer T cells and γδT cells straddle the interface of both immune responses. Adapted from Dranoff [3].

1.1.2 Adaptive immune system

Limited PRR diversity enables pathogens with a high mutation rate, such as viruses, to escape recognition by the innate immune system [9]. The adaptive immune system uses a mechanism of generating significant receptor variability by gene rearrangement and, thus, avoids genetic limitation. This leads to the conclusion of the adaptive immune system being an evolutionary newcomer [10]. Gene rearrangement provides specific recognition of foreign antigens, immunological memory of infection, and pathogen-specific adaptor proteins. The primary effector cells involved in an adaptive immune response are lymphocytes, the B cells and T cells in particular (Figure 1). Expression of the highly divergent B cell receptors (BCR) and T cell receptors (TCR), respectively, ensure high antigen specificity. Antibody-secreting B cells drive the humoral immune response, while the cellular immune response is dependent on T cells. Together, both cells comprise different methods of recognition of foreign antigen and effector mechanisms.

1.1.2.1 B-cell response

B cells are best known for being central components of the adaptive immune response because of their ability to secrete antibodies, also called immunoglobulins (Ig). Antibodies are glycoproteins with highly specific binding to their antigen. The BCRs consist of membrane-bound antibodies with each B cell clone expressing a specific antibody. Thus, a nearly infinite number of clones, each equipped with a specific receptor, are available to detect and eliminate a large number of pathogens by secreting antibodies. This enormous diversity reaches a magnitude of up to 10^{12} different clones, ensuring a broad immunity against a variety of different antigens. This number is by far exceeding the complete number of human genes. Through a complex sequence of somatic recombination and mutation, a limited number of genes can generate variety and a vast number of immunoglobulins [11]. The exons encoding the variable regions of the antibody are assembled from V (variable), D (diversity), and J (joining) gene segments. The rearrangement is occurring in an ordered fashion with an initial joining of D to J segments before the V segments are joining the DJ segments. The diversity significantly amplified by the variability at the junctions. A loss or gain of a small number of amino acids between the various gene segments dramatically increases the number of potential antigen binding proteins to a sheer limitless number. This process is termed V(D)J recombination and is involved not only in the BCR but also in the TCR generation.

Upon binding of the BCR with its specific antigen, the B cell differentiates into an antibody-secreting plasma cell or a memory B cell. Large numbers of specific antibodies are secreted into the blood and other bodily fluids and are referred to as the humoral immune response. Long-lived plasma cells are responsible for the long-lasting antibody production and protection against pathogens of the adaptive immune response.

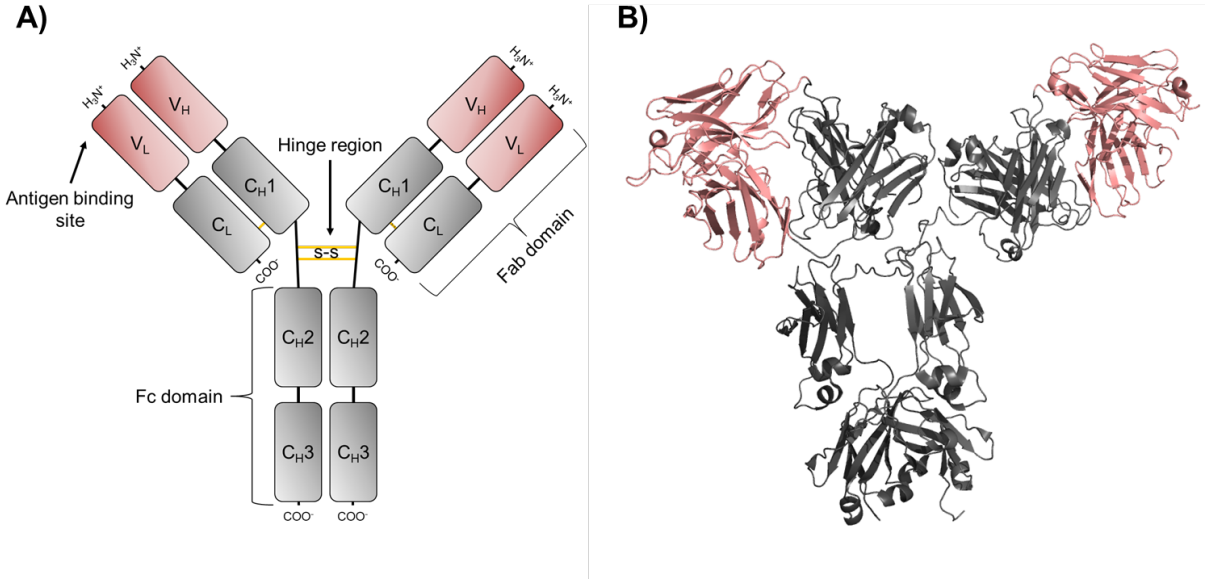

Figure 2: The antibody structure. Variable and constant regions are indicated in red and grey respectively. Disulfid bonds are shown in orange. **A)** Representative visualization of the antibody structure adapted from Moser and Leo [1] and **B)** the representative crystal structure [2]. The figure was generated using PyMol software with the PDB ID: 1HZH.

A representative visualization of the antibody structure is shown in Figure 2. Antibodies are Y-shaped consisting of two heavy chains (Hc) and two light chains (Lc) (Figure 2 A). The first crystal structure was published by Harris et al. [12], and a representative structure is shown in Figure 2 B [2]. The antibody chains fold into repeated immunoglobulin domains, with each consisting of anti-parallel β-sheets. Each chain comprises a variable region and a constant region which is acting as a structural framework region. The variable regions are part of the Fab domain, which consists of a total of two variable and two constant domains. Each variable domain contains three hypervariable loops within four less variable framework sequences. These hypervariable loops are known as complementary determining regions (CDRs) and provide the antigen-specific recognition of antibodies. Structural and functional analysis of antibodies in complex with their respective antigen revealed the critical role of CDRs in the specificity and affinity of antibodies [13-15].

The constant region of the heavy chain is defining the antibody's isotype and is responsible for its effector mechanism. The effector mechanisms of antibodies are mediated either by direct binding of the antibody to its antigen or via interaction of its fragment crystallizable (Fc) region with Fc-receptors expressed by effector cells. The main effector mechanisms are neutralization of target cells via binding, complement-dependent cytotoxicity (CDC), antibody-dependent cellular cytotoxicity (ADCC), and cross-presentation of antigens. Antibodies also participate in the innate immune system by activating its complement system.

1.1.2.2 T cell-based immune response

Several pathogens such as viruses render their detection by the innate immune response and the antibody-mediated immune response ineffective by their ability to replicate intracellularly. Due to their size, antibodies are not capable of crossing the plasma membrane and are therefore unable to detect intracellular pathogens. T cells play a central role in the adaptive immune system by overcoming the limitations of the humoral immune response. Whereas B cells recognize intact antigen on the surface, T cells recognize pathogens inside infected cells. T cell-mediated immunity works *via* direct interaction of the TCR with the MHC complex on the surface of the presenting cell. MHC complexes present protein antigens, which have been partly degraded inside the anigen presenting cell and which are then carried to the cell surface. The T cells release cytotoxic factors to kill infected cells and other pathogens to prevent their survival.

Lymphoid progenitor cells, derived from hematopoietic stem cells, migrate from the bone marrow to the thymus in order to complete their maturation into functional effector cells expressing CD4+ or CD8+, natural killer and memory T cells, the four major types of T cells. Being long-lived, memory T cells provide the immune system with a long-lasting memory in which they can quickly expand into large numbers of effector T cells upon re-exposure of their antigen. Effector CD8 expressing cytotoxic cells cause lysis of virus-infected or tumor cells. CD4 expressing T helper cells support the maturation of B cells into plasma cells and memory B cells. Besides, they help activate cytotoxic T cells and macrophages. Natural Killer cells play a role as a bridge between the adaptive and the innate immune system. Antigen recognition of natural killers cells can be independent of the major histocompatibility complex (MHC) and upon activation, can perform the same functions as CD4+ and CD8+ T cells. The four major tasks combine but are not limited to the promotion of inflammation by cytokine production (by Th1 and Th7 cells), supporting B cells (by Th2 cells), the regulation of immunosuppressive responses (by T regulatory cells) and the killing of unwanted target cells (by CTL).

1.1.2.3 T cell activation

Similar to the B cells, T cells are specific to one particular antigen and this specificity is mediated by the TCR. A total of three major signals are needed for a complete T cell activation (Figure 3) and are described in the following with TCR binding to the peptide-bound MHC is the primary signal. Specific binding of the TCR to an MHC on the surface of APCs [16, 17] triggers a complex intracellular signaling pathway, which leads to the induction of cell proliferation, cytokine production, and T cell differentiation [18, 19].

Upon recognition of the peptide/MHC complex on a presenting cell, TCR associated molecules cluster in the contact area between T cell and APC, leading to the formation of the immunologic synapse upon activation. The TCR complex consists of the TCR α, β chains, and CD3 chains (γ, δ, ε , and ζ). Additional bnding to non-polymorphic regions of the MHC via CD4 or CD8 molecules further stabilizes the interaction of T cells and antigen APCs.

Sole activation via the TCR might be ineffective and lead to an unresponsive state of anergy or cell death [20-22]. Besides the primary signal, further signals are essential for a complete T cell response. Constitutively expressed molecules like the member of the Ig superfamily CD28 induce secondary signaling.

Costimulatory receptors can provide further stimulation upon engagement with their ligands. Several members of the tumor necrosis family receptors (TNFR) such as Ox40 (or CD134) and 4-1BB (or CD137) exhibit stimulatory effects on T cell activation upon engagement with their ligands [26-29]. In contrast to the constitutively expressed CD28, however, the expression of these molecules is upregulated hours to days after activation on the T cell surface [30]. In addition to CD28, TNFRs appear to provide further proliferation-inducing signals [28] and thus, providing a long-term stimulatory effect on the T cells. After activation by its antigen, T cells mature into various effector cells and collectively play a central role in the orchestration of diverse functions of the adaptive immune system.

Additional signals from the environment can further influence the activation of T cells. Cytokines are often referred to as the third signal needed for a complete T cell activation. Inflammatory cytokines enhance both CD4 and CD8 T cell responses *in vitro.* In presence of the inflammatory cytokine IL-2 and antibody-based stimulation, CD4 T cells require IL-1 for effective stimulation, whereas CD8 T cells require IL-12 to augment the response [19]. The cytokine milieu experienced by antibody activated cells can further enhance the level of signal 2 availability by enhancing the expression of costimulatory molecules [23-25]

Advances discovery of new classes of immunomodulating receptors led to the further understanding of T cell response of the human immune system. One of such receptors is the inhibitory programmed cell death protein 1 (PD-1, or CD279) together with its ligands PD-L1 and PD-L2, which have been identified to play a critical role in co-inhibitory pathways of T cell response. Their interaction is often described as “breaks” keeping the immune response in check and are generally named checkpoint inhibitors. PD-1 is a cell surface-expressed receptor molecule [31]. It is expressed on a variety of lymphocytes such as activated T cells and B cells [32] and was also reported to be expressed by natural killer T cells (NKT), NK cells, activated monocytes and DC subsets [33, 34]. Various studies have shown a strong expression on tumor-infiltrating CD4+ and CD8+ T cells [35]. Upon activation of the TCR or BCR, a persistent stimulation maintains a durable and long-lasting PD-1 expression level [36] with a peak at 48 hours after initiation of stimulation [37]. PD-1 signaling regulates T cell response to maintain peripheral tolerance by inhibiting alloreactive T cells responses. The T cells lacking PD-1 expression are shown to be hyperactive in comparison with wildtype (wt) cells [38-41]. The interaction of PD-1 and its ligands provides an inhibitory signal in the presence of TCR or BCR activation [41-43] and is reported to target the CD28 signaling pathway directly [44] and thus, having a direct inhibitory effect on T cell proliferation [41, 45, 46]. However, PD-1 blockage can be prevented by a strong activation via CD28 or IL-2, PD-1 and T cell proliferation and survival can be maintained [47].

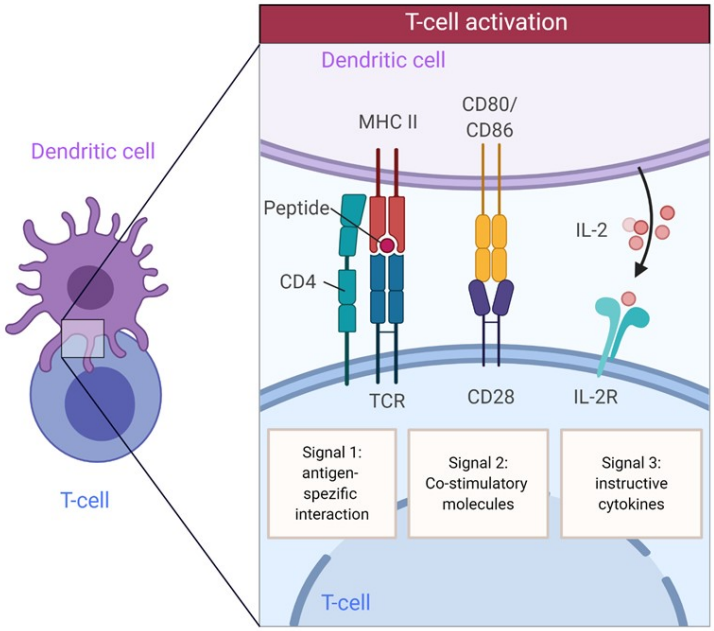

Figure 3: The three signals of T cell activation by antigen presenting cells. T cells require three stimulatory signals for a sustaining and prolonged activation. Representative activation shown for the CD4 T cells via the T cell receptor (TCR). Adapted from Kambayashi et al. [5].

For their essential role in potentiating the T cell response while also showing potential to fine-tune the immune response, the stimulatory and inhibitory receptors have emerged as potential therapeutical targets for either enhancing or dampening the immune response in various diseases.

1.2 Stimulation of the adaptive immune system for cancer immunotherapy

In general, antibodies protect the host from invading pathogens. Due to their high level of diversity, antibodies can recognize virtually all known molecular structures whether or not these are biological structures such as proteins [48-50], lipids [51-53], nucleic acids [54, 55] or synthetic organic compounds [56, 57]. Upon binding, antibodies can mediate various effector mechanisms. It is for these effector mechanisms that antibodies emerged as the only established immunotherapy up to now in the treatment of cancer and autoimmune diseases.

1.2.1 Effector mechanisms of antibodies

Antibodies act by a number of mechanisms, most of which can be separated into two distinct modes of action. The first one is mediated by directly binding the antigen by which antibodies can mediate a steric blockage of a receptor-ligand interaction. The second mode of action for mAbs is the harnessing of Fc-part mediated effector mechanisms and recruiting effector cells to induce cell lysis.

1.2.1.1 Exclusively antibody binding-dependent effector mechanisms

Neutralizing pathogens is one of the central tasks of the immune system. Antibodies directly attach selectively to the surface of a virus or bacterium, rendering the invading microbes immobile or preventing the pathogen from attaching itself to healthy cells and avoid the infection of such [58, 59]. Besides pathogens, antibodies are capable of binding bacterial produced toxins. The biological effect of a toxin depends on the binding to specific receptors. Therefore, antibodies can function as antitoxins neutralize the toxin upon binding [60-62]. With Bezlotoxumab, targeting the toxin B of *Clostridium difficile*, the first antitoxin antibody got approved in 2016.

The class of agonistic and antagonistic antibodies can modulate the response upon binding of a receptor. The agonistic activity of an antibody can occur when it binds a receptor in a manner that mimics the binding to the ligand. In general, immunomodulating receptors such as CD3, CD28, and members of the TNFR superfamily such as 4-1BB, OX40, TNFR, and CD40 are interesting targets in the clinical use of agonistic antibodies.

Antagonistic antibodies can inhibit a receptor by binding to it and block rather than activating it. One of such antibodies is Infliximab, which neutralizes the ligand TNFα. TNFα is inducing inflammatory responses upon binding with its receptor. Infliximab is used in the treatment of inflammatory and autoimmune diseases such as rheumatoid arthritis, Crohn's disease, and ulcerative colitis.

1.2.1.2 Fc-mediated effector mechanisms

In addition to the directly mediated effector mechanism, the Fc-part of the antibody can interact with complement proteins and specialized Fc-receptors. Such mediated-effector mechanisms include antibody-dependent cell-mediated cytotoxicity (ADCC), induction of phagocytosis, and complement-dependent cytotoxicity (CDC).

A larger number of plasma proteins participate in the CDC. One of such, C1q binds the Fc-part of IgG or IgM. The binding of at least two of these tulip-like structures leads to the activation of two additional C1 subunits, C1r and C1s. Several plasma proteins participating in the CDC are enzymes. Upon activation of such, an enzymatic cascade is triggered, which further increases the CDC-mediated immune response. In this way, a small number of activated complement proteins results in the amplification and, thus, a rapid generation of a strong complement response. Triggering of the complement cascade leads to the formation of the membrane attack complex, which forms transmembrane channels. These channels disrupt the cell membrane, resulting in cell lysis and death of the target cells [63]. In addition, the CDC mediates a series of inflammatory responses that further boost the response against the infection.

Fc gamma receptors (FcγR) trigger cell-mediated cytotoxic effector functions such as ADCC. FcγRs are expressed on the surface of immune effector cells and bind the Fc-part of antibodies. Effector cells of the ADCC include nonspecific cytotoxic cells such as natural killer cells, macrophages, monocytes, and eosinophils. The expression of Fc receptors is reported for all hematopoietic cells, excluding αβT cells [64]. All receptors of the Fcγ receptor family are members of the immunoglobulin superfamily and consist of inhibitory (FcγRIIB) and stimulatory (FcγRI, FcγRIIA, and FcγRIII) Fcγ receptors.

The level of antibody-induced ADCC is highly dependent on its isotype due to varying binding to the various Fcγ receptors. For the IgG1 and IgG3 isotype, the ADCC effector function is high and low if compared to IgG2 and IgG4.

Thus, the latter isotypes are most suitable for the use of therapeutic antibodies. IgG1 is the most frequently used antibody isotype in antibody engineering for it is less polymorphic and has a shorter hinge than IgG3 and can engage in both humoral and cellular immune responses. Advantages in the understanding of the impact of single amino acids and glycosylation in the backbone resulted in advanced technologies altering the ADCC and CDC activity of antibodies [65].

1.2.2 Therapeutic antibodies

In 1975 when Köhler and Milstein developed a method for the generation of antibody-secreting hybridoma cells [66], the opportunity was offered to produce monoclonal antibodies (mAbs) in large quantities and with defined specificity, which enabled their use as therapeutic drugs.

1.2.2.1 Antibody technology

A majority of therapeutic antibodies in the clinic are approved for oncology indications. In combination with cytotoxics or radiation therapy, these mAbs have delivered significant improvements in the treatment of patients.

However, the first mAbs were mouse molecules that may elicit immune responses when administered to patients [67-69]. The mouse protein sequences in the first therapeutically used antibodies are recognized as foreign, eliciting an immune response that leads to the formation of human anti-mouse antibodies (HAMAs). HAMAs may result in the clearance of antibodies, thus, limiting their therapeutic efficacy [70, 71]. Also, the low affinity to the human Fc receptor [72] can render mouse mAbs inefficient in recruiting human effector cells such as macrophages or T cells when being compared to human IgGs. Human hybridomas were produced, following the methods established by Köhler and Milstein [73], to avoid the limitations of mouse antibodies. However, these human IgG secreting cell lines proved to be genetically unstable, yielding only a small amount of antibodies. Subsequent efforts were put into genetic engineering of antibodies, by joining the variable region of a mouse antibody with the human constant region, the first chimeric antibodies were described by Morrison in 1984 [74]. The use of a human constant region in chimeric antibodies led to the hope of a higher effector function in combination with a lowered risk of immunogenicity resulting in various engineered antibodies [75-77].

However, the mouse variable regions were still prone to generate anti-idiotypic responses *in vivo* [78, 79], indicating the need to substitute the mouse framework regions in the variable antibody sequences with the closest human framework sequences. With the development of more refined genetic engineering techniques, a further decreasing percentage of mouse-derived sequences became possible. Exchanging the hypervariable loops of a mouse antibody of interest with loops of a human acceptor sequence was first described by Jones in 1986 [80] and called CDR crafting. The first commercially sponsored chimeric humanized mAb, Abciximab, entered the clinic in 1994 to an ever-increasing number of mouse mAbs entering the clinical trials [81].

The main limitation of CDR grafting is a grade of unpredictability. CDRs of a human framework sequence, with the highest sequence similarity possible, are substituted with mouse CDRs. The straightforward exchange of CDRs does not affect the affinity of an antibody in some cases, while in others, it drastically lowers the affinity [80, 82, 83] or overall stability of the antibody [84]. Residues in the mouse framework sequence of antibodies have been demonstrated to have an impact on the conformation of the hypervariable CDR loops and the affinity of an antibody as such [85, 86]. These amino acids are referred to as vernier zone residues, which are located in close proximity to the CDR loops and are orientated towards them. Mutations of vernier zone residues can impact the thermodynamics of the interaction of an antibody with its antigen [87]. These findings resulted in the development of novel methods, including the vernier zone residues in the humanization of antibodies [88]. Even with further improvements [89], CDR Crafting remains to be challenging and time consuming up to today. A second challenge to tackle is the persistent immunogenicity of humanized antibodies. The mouse CDRs in humanized antibodies were sufficient to elicit an immune response leading to the generation of HAMAs [90]. Therefore, fully human antibodies were considered to be the optimal solution for therapy, for they have the lowest risk of inducing an immune response *in vivo*.

Based on the work of Smith et al. [91], phage display technology emerged as one possibility of generating fully human antibodies. Antibodies are genetically linked to a surface protein and thus expressed on the surface of the phage. Vast repertoires of either Fab (fragment antigen binding) [92, 93] or scFv (single chain fragment variable) [94-96] genes were cloned into engineered phages in a way that these antibody fragments are displayed on the phage surface. With the construction of large and highly diverse phage display libraries consisting of human antibody genes, the generation of complete human antibodies *in vitro* became a reality. Without the need for a prior immunization, the process of generating human antibodies against almost any target became possible in weeks rather than months. Antibody phage display technology was developed in parallel in Cambridge by McCafferty et al. [97], in Heidelberg by Breitling et al. [98] and in California by Barbas et al. [99]. Following initial improvements [100, 101], several phage display-derived antibodies went into clinical development [102], with Adalimumab being the first antibody accepted in the clinic in 2002.

1.2.2.2 T cell modulating antibodies

The immune system has evolved a variety of methods to challenge infection and disease while maintaining tolerance both centrally and in the periphery. This regulation is a highly complex balance between inhibitory and stimulatory receptors and molecules. The discovery of the hybridoma technology and the generation of monoclonal antibodies enabled not only the identification of these receptors but also their manipulation via the use of immunomodulating antibodies. In general, Immunomodulating antibodies can be separated into agonistic or antagonistic agents that affect an ongoing immune response via binding to either cellular or soluble targets. The use of immunomodulating antibodies has emerged as one of the most effective ways to modulate the immune responses against inflammatory diseases, infectious agents, or in the fight against malignant tumors.

Muromonab was the first immunomodulating antibody described, and it binds to the CD3 domain of the TCR complex [103]. As previously described, the first signal of T cell activation is mediated by the TCR complex. Muromonabwas clinically approved by the US Food and Drug Administration in 1986 for the treatment of transplant rejection [104]. However, Muromonab was first described to have potent mitogenic properties on T cells [105]. In addition, the antibody demonstrated was highly immunogenic in humans. Moreover, the potent mitogenic effect of Muromonab resulted in a wide spectrum of side effects that include fever, chills, nausea, vomiting, and headache with a small number of patients suffering from even more severe side-effects such as cardiopulmonary distress, seizures, encephalopathy, meningitis, renal insufficiency, and graft thrombosis [106]. Later research demonstrated the unspecific T cell activation was mediated by cross-linking on the Fcγ receptor.

The primary activating by the TCR complex is reported to be insufficient for a complete and long-lasting T cell response. Lacking secondary signaling is resulting in an ineffective and unresponsive state of anergy or cell death of the T cells [20-22]. Additional stimulatory receptors came into focus in the development of immunomodulating antibodies targeting for instance CD28 [107-112] or 4-1BB [113-116].

As one of the first of such antibodies, the CD28 binding clone 9.3 was first described in 1982 by Lum and his colleagues [117]. In the presence of immobilized CD3 antibody, 9.3 demonstrated the capability of inducing proliferation and cytokine secretion on T cells. The identification of a CD28 stimulatory antibody enabled further research into CD28 and its role in T cell activation [118-121]. CD28 expression is found on CD4+ T cells and CD8+ T cells. It costimulates T cell responses upon interaction with its ligands CD80 and CD86 and provides an essential regulatory step in the triggering of a specific immune response. Upon the binding of MHC to the TCR, the CD28 expression of the T cell is sharply upregulated, which is further increasing its interaction with its ligands.

CD28 binding superagonists (SA) proved to show particularly strong signaling capacity without the need for immobilization [122]. Epitope characterization and the crystal structure indicated the reasons to be distinctive epitopes that enable the activating properties of SAs [123, 124]. Lateral binding of the SA to the CD28 homodimer enables the clustering of the receptor resulting in T cell activation without the need for a TCR mediated signal by antigen recognition [125]. However, T cells lacking TCR signaling [126, 127] were resistant to CD28 super agonists. Thus, the loss of the ability for CD28 activation in the absence of a primary signal was later linked to the need for a tonic TCR signaling induced by cellular interaction in the tissue or high-density cell cultures *in vitro* [128].

The ability of SA to induce potent T cell activation without TCR stimulus indicated the possibility of an administration for CD28 SAs in patients for the treatment of immunodeficiency illnesses [129] or autoimmune diseases [108]. Following a successful pre-clinical safety test, the mAb TGN1412 was the first CD28 targeting antibody being approved for a first-in-man Phase I clinical trial. When TGN1412 was applied to healthy volunteers, however, it resulted in the induction of a severe cytokine storm and multi-organ failure [107]. Such severe side effects were not being anticipated due to the lack of toxicity in preclinical animal studies. The following research showed strong activation of tissue-resident CD4 effect memory cells [128, 130]. In primates, the CD28 expression is downregulated on this specific T cell subset, which is resulting in a better tolerance compared to the application in man [130]. The failure of the phase I clinical trial of TGN1412 illustrated the need for a defined and well-controlled use of CD28 SA in the clinic. Two major strategies resulted from this trial. Low doses of TGN1412 (renamed TAB08 or Theralixumab) induced expansion of Treg cells from healthy donors while obtaining a dose range for a safe administration where pro-inflammatory cytokine secretion from convention T cells is absent [131].

Activation of T cells via the TNFR 4-1BB has emerged as an additional and promising strategy for immunotherapy [132] besides targeting CD28 or CD3. The stimulation of this receptor enhances the activation, proliferation, and amplification of a cytotoxic CD8+ T cell response [133]. Besides its effect on proliferation and cytotoxicity, 4-1BB stimulation also enhances cytokine secretion and T helper cell polarization [134-136] but also metabolic fitness [137], modification of DNA methylation [138], the formation of T cell memory [137], and showed a counteracting function in T cell exhaustion [136] and activation-induced cell death [134]. Today, two major approaches have entered clinical trials, which are relying on 4-1BB agonism, the use of 4-1BB targeting agonistic antibodies [132, 139], and chimeric antigen receptor (CAR) T cells carrying intracellular 4-1BB signaling domains [137].

The IgG4 antibody Urelumab (or BMS-663513) was the first agonistic antibody that entered clinical trials. Patients treated with Urelumab experienced dose-dependent hepatitis [116, 139, 140] most likely caused by its immobilization on FcγRIIB expressing cells. The activation of TNFRs is reported to be cross-linking dependent [141-143]. Limiting toxicity by lowering its dose led to a safe administration with only limited efficacy [116]. A second agonistic antibody targeting 4-1BB was the IgG2 Utomilumab (PF-05082566) showed a better safety profile with lower agonistic potency [132]. Both trials were hampered by their dependency on Fcγ receptor-mediated clustering and hepatoxicity. Thus, despite the fact that a considerable effort was put into their clinical development, 4-1BB agonistic antibodies have not progressed beyond early stages in clinical trials.

Another class of immunomodulatory antibodies targets the inhibiting safeguard systems that are frequently harnessed by cancer cells to establish immunological tolerance, the so-called immune checkpoints. In recent years a considerable number of inhibitory receptors have been discovered and since then been well described. Several findings include the identification and first characterization of the inhibitory cytotoxic T lymphocyte-associated antigen 4 (CTLA-4) and PD-1.

Early preclinical research showed the importance of the PD-1/PD-L1 signaling in the evasion of antigen-specific T cell response by tumor cells [144, 145]. Indicating its primary responsibility in the regulation of T cell activation in peripheral tissues and, therefore, its importance in the context of solid tumors as an immune escape mechanism [145]. Thus, it resulted in the clinical development of PD-1/PD-L1 targeting therapy as cancer immunotherapy. In mouse models with various tumor types expressing PD-L1, anti-PD-1 and anti-PD-L1 antibodies demonstrated an enhanced T cell function, resulting in an increased antitumor response [47, 144, 146]. Antibody-based inhibition showed acceptable safety and tolerability and promising antitumor activity in patients with advanced solid tumors targeting PD-1 [147, 148] or its ligand [149].

In September 2014, the PD-1 inhibitor Pembrolizumab was approved for the treatment of metastatic melanoma by the FDA, followed by Nivolumab. Both antibodies are targeting the PD-1 pathway by binding PD-1, blocking its interaction with its ligands and thus, resulting in response rates of 40-45% in melanoma and non-small lung cancer [150, 151]. Regulating inhibitory immune checkpoint signals *via* the use of antibodies opens a wide window of possible further treatment in a combination of adoptively transferred T cells [152]. The use of immune checkpoint modulating mAbs is associated with immune-related adverse events. These side-effects are affecting the dermatologic [148, 153], gastrointestinal [148, 154], hepatic [147, 148, 155], endocrine [156] and other organs [147, 157-159]. It is highlighting the critical problem of a systemic therapy that might be overcome by a more targeted approach.

1.2.3 T cell modulating bispecific antibodies

Immunomodulating antibodies proved to have a T cell-stimulating effect and produced potent anti-tumor responses. These responses came with a downside in the form of strong side effects, a systemic cytokine release syndrome and the organ-specific autoimmunity. This raises the question of whether a more localized and focused therapy can harness the positive T cell response while avoiding severe side effects or not. To further improve the efficacy of immunomodulating antibodies, new approaches included the molecular engineering of new antibody formats such as bispecific antibodies.

1.2.3.1 Bispecific antibody technology

Bispecific antibodies can harness a variety of strategies for therapeutic effect. The first major strategy when using bispecific antibodies is the direct binding to the target structure such as cell surface receptor or soluble factors such as cytokines to either block the ligand-receptor interaction or to achieve neutralization of the soluble ligand (Figure 4 A). Bispecific molecules can simultaneously block two different antigens or pathways and bispecific binding can lead to a potentially increased affinity on overlapping antigens or different epitopes [160-162].

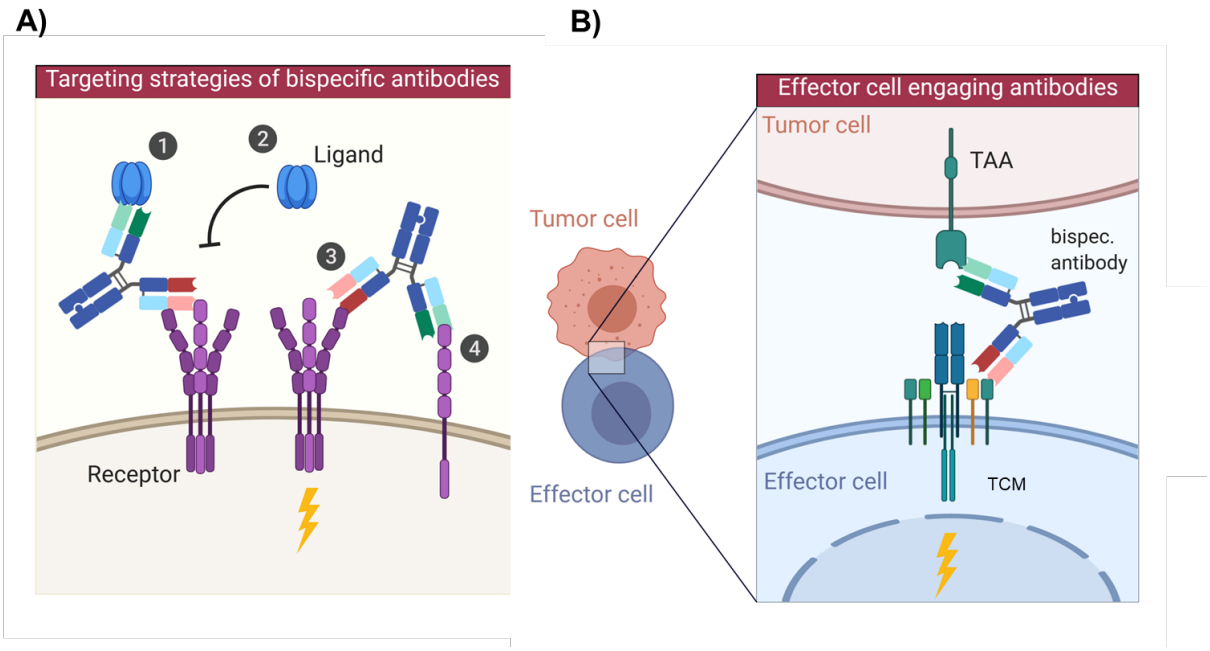

Figure 4: Examples of targeting strategies utilizing bispecific antibodies. A) Dual-targeting strategies. (1) Neutralization of receptor-activating ligands, (2) neutralizing of a receptor, (3) activating of a receptor. and (4) deactivation of a receptor. Strategies are exemplified with various combinations of (1-4) being possible. **B)** Dual-retargeting strategy with retargeting of effector cells via the binding to a tumor-associated antigen (TAA) and a T cell modulating receptor (TMR)**.** Strategies are exemplified with bispecific IgG molecules. Addapted from Kontermann [4].

In the past, the first bispecific antibodies were generated by fusing two different hybridoma cell lines resulting in quadroma cell lines producing bispecific molecules [163, 164]. A disadvantage of this approach was the promiscuous rearrangement of heavy and light chains leading to the secretion of a heterogeneous antibody population with the same molecular mass, including bispecific molecules but also monospecific mAbs. An alternative approach was the chemical conjugation of different antibodies to generate bispecific antibodies [165-167]. Already in 1961, Nisonoff and his colleagues demonstrated the possibility of conjugating two different monoclonal antibodies via oxidative recombination [168].

However, separating the bispecific heterodimers and homodimers proved to be challenging in the purification due to the heterogeneity of the end product. Another drawback of chemical cross-linking is the possibility of poor stability a decreased activity of antibodies. The breakthrough in their availability came with the development of novel genetic engineering methods. Recombinant DNA technology in the development of bispecific antibodies led to an increased understanding, and the ability to modulate valency [169-171], flexibility [172], half-life [173-175], biodistribution [173, 176] and Fc based effector mechanism [177, 178], resulting in an ever-increasing variety of novel bispecific formats [4, 6], as seen in Figure 5. The structure and size of these different formats are various, and advantages or disadvantages can determine the therapeutic efficacy [6].

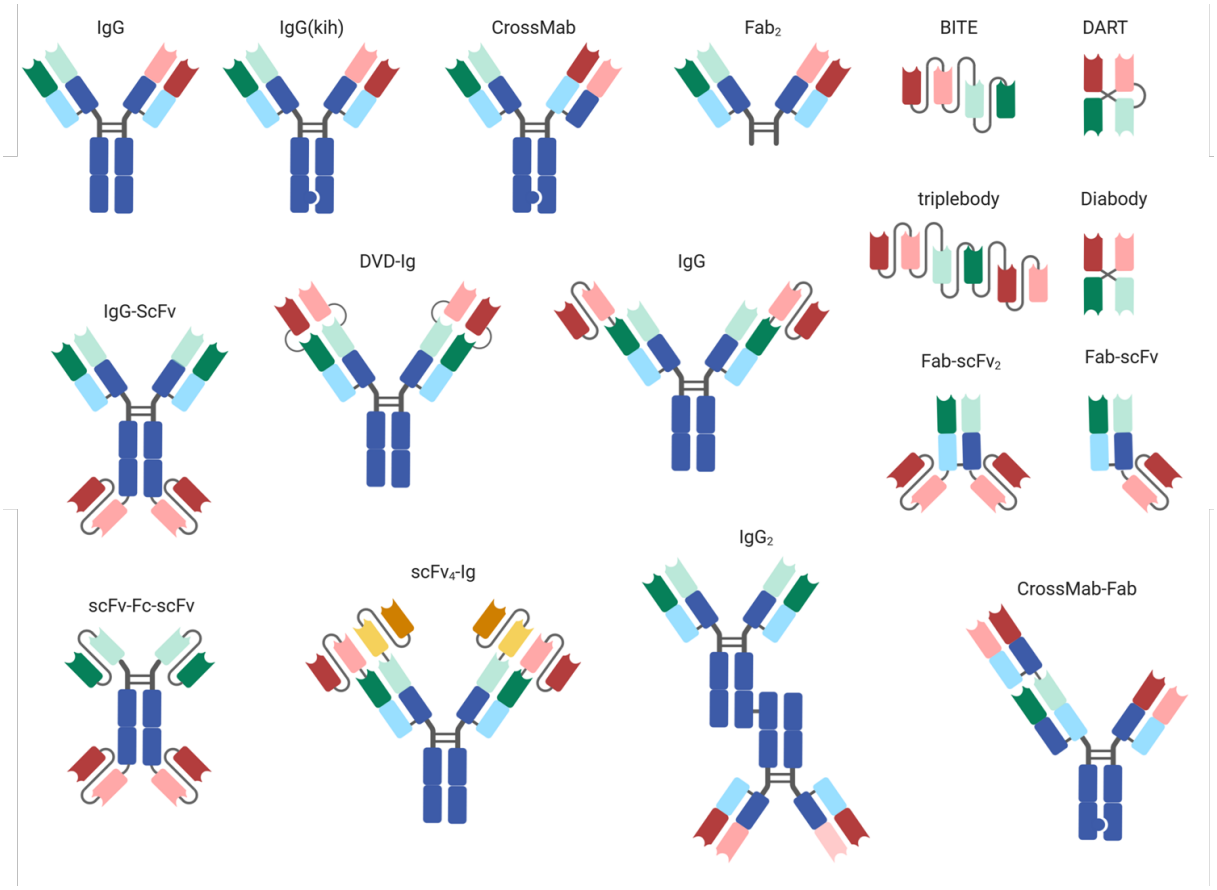

Figure 5: Various of bi- and trispecific antibody formats. Constant regions are shown in dark blue for the heavy chain domains and light blue for light chain domains. Variable heavy chain domains are shown in dark red, green, and yellow. Variable light chain domains are shown in light red, green, and yellow with each colour indicating different specificities. Adapted from Kontermann [4] and Brinkmann [6].

Approved in the year 2009, the trifunctional antibody Catumaxomab [182] was the first bispecific antibody entering the clinic. Catumaxomab is produced via quadroma technology [163, 164] and consists of mouse IgG2a and rat IgG2b. Catumaxomab is a trifunctional antibody targeting epithelial cell adhesion molecule, CD3, and is recruiting effector cells via its binding to the Fc-receptor. In 2013, Catumaxomab was voluntarily withdrawn from the market for commercial reasons. The CD19 and CD3 binding antibody Blinatumomab was the first bispecific antibody approved for the clinic in 2015 for the treatment of Philadelphia chromosome-negative relapsed or refractory B-cell precursor acute lymphoblastic leukemia. The basis of the BiTe format used in the development of Blinatumomab is a bispecific scFv that comprises two different scFv moieties connected by a linker [183]. A second IgG-like bispecific format is the CrossMAB format [179] developed by Roche. By exchanging C_H and C_L domains within the antigen-binding fragment (Fab) of one half of the IgG arm, bispecificity could be archived while retaining the affinity and avoiding light-chain missparing. The first clinically developed antibody using CrossMAB technology is Faricimab [180]. Simultaneous binding and inhibiting the vascular endothelial growth factor A and Angiopoietin 2, it finished Phase 2 [181] and is currently undergoing Phase 3 trials.

Up to date, the majority of bispecific antibodies focus on the recruitment of T cells as effector cells. These T cells engaging antibodies are designed to bind T cells simultaneously to tumor cell antigens, leading to a localized and focused T cell activation, proliferation, and tumor cell death.

By binding their antigen on the tumor cell with one binding site and binding a T cell modulating receptor, T cells are temporarily forced to interact with the cancer cell (Figure 4 B). Any cytotoxic T cell will become activated and can induce a directed lyses of the tumor cells [183-185], which is otherwise performed by antigen-specific cytotoxic T cell clones.

1.2.4 Immunostimulatory bispecific antibodies

The Idea of harnessing bispecific antibodies to kill tumor cells dates back to the work of Staerz et al. in 1985 [186] and the first bispecific antibodies. CD3 specific bispecific antibodies trigger CD3 on the surface of the T cells by binding to their target protein on the surface of the target cells. Briding the T cells and tumor cells can result in tumor regression and even complete remission [187, 188].

Up to date, most of the T cell activating bispecific antibodies target the CD3 domain of the T cell receptor complex. Currently, there are multiple CD3 bispecific antibodies in the clinical development for the treatment of hematological malignancies and solid tumors. In general, these CD3 targeting bispecific antibodies are relatively well tolerated. However, the primary signals induced by activation via the TCR is often not sufficient for a complete T cell response. Lacking the secondary signaling is resulting in an ineffective and unresponsive state of anergy or cell death of the T cells [20-22].

CD28 targeting bispecific antibodies with a TAA specificity offered the possibility of promoting targe-cell restricted CD28 stimulation without the systemic toxicity demonstrated by the superagonist TGN1412. Initial versions of CD28 bispecific antibodies were already proposed in 1987 by Jung et al. [165] and resulted in an extensive evaluation in the early 1990s [109-111, 189]. Recently, Skokos et al. described the generation of two bispecific antibodies targeting CD28 and the tumor antigens MUC16 and PSMA [190]. Paired with a respective TTAxCD3 bispecific, these CD28 bispecific could efficiently promote T cell activation and tumor cell killing in an antigen-dependent manner. However, these bispecific antibodies demonstrated limited activity in the absence of signal 1.

Several clinical and preclinical studies have demonstrated the importance of 4-1BB stimulation on the maintenance of long-lasting T cell functionality. However, agonistic 4-1BB targeting antibodies have not moved beyond early clinical trials. Recent publications focused on the selective activation of 4-1BB by the use of antibody 4-1BBL fusion proteins [115] or bispecific antibodies [113]. Hinner et al. focused on the development of a bispecific Antibody-Anticalin fusion protein targeting HER2 and 4-1BB [113]. This bispecific molecule facilitated tumor-localized T cell activation and did not show significant toxicity in a 4-week GLP compliant toxicity study in cynomolgus monkeys.

Using the physiological ligand 4-1BBL in a fusion protein with antibodies targeting either FAP or CD19, Claus and her colleagues demonstrated tumor remission in mouse models in combination with TAAxCD3. Tumor remission got accompanied by an increased intratumoral accumulation of activated effector CD8+ T cells. However, the 4-1BBL fusion protein demonstrated 4-1BB activation in the presence of cells lacking the TAA expression.

As previously discussed, the use of monoclonal antibodies blocking PD-1 shows remarkable efficacy against various cancers. However, the systemic administration of antagonistic PD-1 antibodies exhibits strong side effects in patients.

The only PD-1 blocking bispecific known to date is described in the work of Sun et al. [191]. Sun and his colleagues combined a PD-1 specific antibody with an antibody specific to c-MET. This bispecific antibody rescued T cell activation and, furthermore, markedly inhibited the growth of subcutaneously implanted tumors and chronic inflammation in xenograft mouse models. Several other approaches focused on a bispecific blockade of PD-L1 in combination with another growth factor receptors [192-194], which resulted in a dual-blocking strategy.

1.2.4.1 Targets for bispecific antibodies

Treating lymphoma and leukemia patients *via* antibody-mediated therapy demonstrated impressive responses as seen for Rituximab [195, 196] and Blinatumomab [187, 188]. The critical difference between soluble and solid tumors is the relative inaccessibility of solid tumors for immunological effector cells. The microenvironment of tumors exhibits barriers which hinder the penetration of antibodies into the tumor following their systemic administration [197]. A limiting penetration reduces the overall amount of antibodies that reach the tumor tissue, leading to sub-therapeutic concentrations, which resulted in therapy resistance and treatment failure [197, 198]. As a result, therapeutic antibodies are often administered in combination with chemotherapeutics to increase their efficacy and overcome limitations [199]. Extensive research has highlighted the significance of tissue penetration to the outcome of therapeutic efficacy [200, 201]. An approach to increase the efficacy of tumor-targeting antibodies consists of employing smaller antibody formats such as single-chain variable fragments or Fab fragments [202]. While the smaller antibody size increases the diffusion rate, the rapid clearance of these molecules led to a reduced therapeutic efficacy in physiological settings [200, 203]. Up to date, increasing tumor tissue penetration poses a significant challenge in the use of therapeutic antibodies.

The tumor microenvironment is characterized by factors such as hypoxia and a chronic growth factor stimulation, which is resulting in endothelial dysfunction. The growth of tumors with a tumor-size of more than 1-2 mm is restricted by the generation of novel blood vessels. This process of angiogenesis is highly dependent on the temporal coordination of factors that regulate the establishment of novel blood vessels. Endothelial cells in the tumor have irregular sizes and forms. The blood flow is abnormal and leaky because of a defective endothelial monolayer. These abnormalities might contribute to tumor growth, metastasis, and maybe a prominent target of antibody-mediated therapy.

Studies on the gene expression patterns of endothelial cells derived from blood vessels of malignant and healthy colorectal tissue led to the identification of tumor-specific up-regulation of several genes [207]. These findings demonstrate the molecular differences between healthy and malignant endothelium, which may have significant implications in further antibody-based therapies. A possible target for anti-tumor vascular mediated immunotherapy is the glycoprotein endoglin.

Endoglin (or Eng, CD105) is a transmembrane glycoprotein with a size of approximately 180 kDa [208, 209]. It is composed of two disulfide-linked subunits, and its expression is upregulated in tumor cells while resting endothelial cells only exhibit a mild expression [210-212]. High endoglin expression is a prognostic factor for patients with different solid tumors [213-218]. A promising expression pattern of endoglin led to the development of Carotuximab, which finished phase II trial in 2017 and was well-tolerated in patients [219]. However, the single-agent activity of Carotuximab was not significant. Currently, Carotixumab is in phase II clinical trial, suggesting endoglin to be a promising target for further antibody-mediated therapy.

1.3 Preliminary Work and Study Content

In this work, the main goal was to generate optimal costimulatory bispecific antibodies that are capable of inducing a target-cell restricted modulation of T cell activation together with CD3 targeting bispecific antibodies.

High endoglin expression is a prognostic factor for patients with different solid tumors [213-218] and was selected as the tumor-associated antigen of choice in the use of a bispecific antibody format. Based on the work of Coloma and Morrison [239], varying tetravalent antibodies, comprising a T cell modulating moiety and endoglin binding antibody, should be designed in the IgG(scFv)$_2$ format. The focus in their analysis should be set on the effect of format, affinity, epitope, and binding kinetic in the target cell-mediated activation of T cells.

Initial work focused on clones that were already described in the literature. Endoglin binding clones Kro-10, Kro-22, and Kro-23 were generated and described in great detail in the work of Karolin Schwartz [237] and were selected for initial comparison in this thesis. These clones were selected because of their differences in biochemical characterization, such as affinity, ADCC induction, and immunohistochemistry, while not sharing the same epitope.

The T cell receptors CD28, 4-1BB, and PD-1 were selected for target cell-specific T cell modulation. For T cell stimulation, the anti-CD28 clone 9.3 was selected. Hansen and his colleagues first described the clone 9.3 in 1980 [243], and subsequently, it was reported to induce proliferation on T cells [64, 65, 126].

Additional focus was set on the generation of additional immunomodulating antibodies targeting either the stimulatory 4-1BB or the inhibitory PD-1 T cell receptor. For the generation of novel antibodies, hybridoma technology and phage display technology were used. Both approaches have theoretical and practical limitations and advantages. In general, hybridoma technology allows the generation of highly specific monoclonal antibodies due to the natural affinity maturation, which is occurring *in vivo*. The obtained antibodies are ensured to bind the cellular-expressed antigen when using cells for the immunization. However, the hybridoma generation is generally time-consuming. Counting from the initial immunization, it takes at least 3 to 4 months to obtain a monoclonal hybridoma clone. In addition, the animal origin of the obtained antibodies requires further humanization for therapeutic use, adding to the time of development.

Unlike the hybridoma techniques, the naïve library used in phage display technologies can result in fully-human antibodies in less than two weeks. The sheer size of phage display libraries ensures the screening of billions of different clones. Nonetheless, missing the affinity maturation, the chance of obtaining clones with moderate affinity is higher using phage display technology. In general, the clones are screened *in vitro* using recombinant protein, which may result in diminished affinity to cellular expressed protein.

In this work, novel 4-1BB or PD-1 targeting antibodies were generated via hybridoma generation and phage display technology, harnessing the advantages of both these approaches. These novel generated clones should be compared to antibodies in the literature to identify possible agonistic and antagonistic antibody clones. With a successful identification of such, their potential as bispecific T cell engaging antibodies should be assessed, following the criteria described above.

2. Results

2.1 Development of a bispecific antibody comprising endoglin and CD28 binders

As outlined before, following a primary signal of the TCR, T cells need additional signaling in order to achieve a sustaining activation leading to long-lasting proliferation, differentiation, and cytokine release. Hence, next to an anti-CD3 stimulus, the costimulatory CD28 molecule is a promising candidate for antibody therapy, as its activation leads to a sustained T cell response inducing cytokine release [240] and proliferation [121, 223, 224]. However, previous studies have shown the problems associated with the systematic application of monospecific superagonistic antibodies targeting CD28 causing systemic inflammatory response [107] and have pointed to the necessity to restrict costimulatory activity to the tumor site.

Thus, the first part of this study was subjected to the generation of a bispecific antibody format combining anti-CD28 and anti-endoglin binding.

2.1.1 Validation of different antibody formats using muKro-23xmu9.3 in IgG(scFv)$_2$ format.

For the generation of a bispecific antibody, including endoglin and CD28 binding, the IgG(scFv)$_2$ format was selected based on the work of Coloma and Morrison [239] with modifications in the C_{H2} domain consisting of the amino acid substitutions and deletions E233P, L234V, L235A, ΔG236, D265G, A327Q, and A330S (EU-index) which abrogate FcR binding and complement activation.

On the one hand, the generated bispecific formats comprise endoglin binding to the IgG backbone together with a covalently linked CD28 binding scFv on the C-terminus of the heavy chain (Hc) or the light chain (Lc). The scFv was attached using either a 15 amino acid residue glycin-serin linker (+L) to increase its flexibility or without any linker (-L), as shown in Figure 6 A, while Figure 6 B illustrates the varying formats. Thus, a total of four different bispecific antibody formats were designed, comprising the clones Kro-23 and 9.3, binding to endoglin and CD28, respectively. The productions for each variant were accomplished in CHO cells via transient transfection. The supernatant was purified via protein A-based affinity purification. Purity and integrity of each variant were confirmed via SDS-Page analysis and size exclusion chromatography, respectively. (Figure 6)

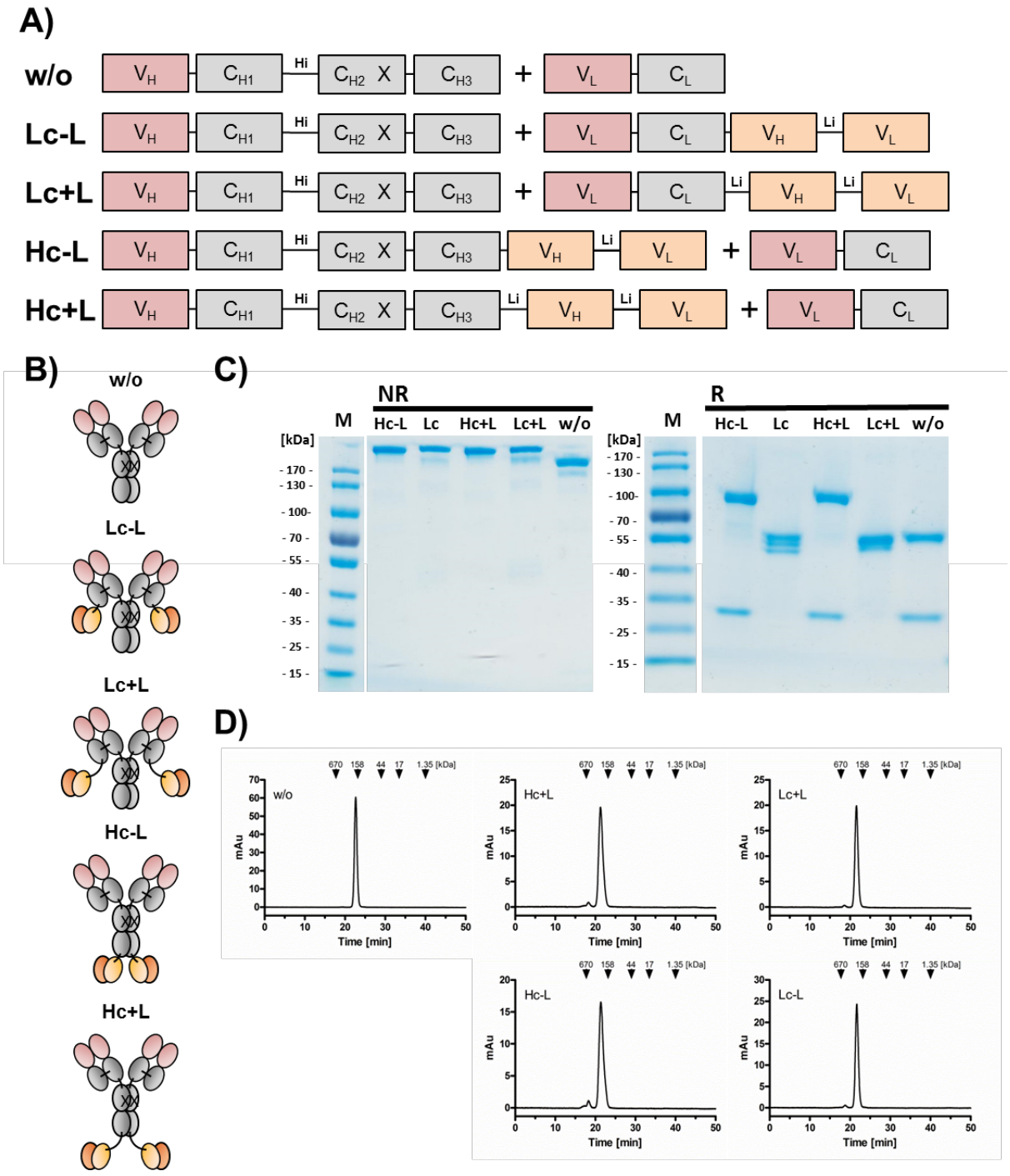

Figure 6: Design and biochemical characterization of different muKro-23xmu9.3 variants. A) Illustration of the genotype of the different muKro-23xmu9.3 IgG(scFv)$_2$ variants with the hinge region (Hi) and glycine-serin linker (Li) consisting of (Gly-Gly-Gly-Ser)$_3$. ScFv of the CD28 antibody 9.3 was either attached to the light chain (LC) or the heavy chain (HC) with (+L) or without (-L) linker. **B)** Graphical illustration of the constructs. **C)** SDS-Page analysis (10 % PAA, 2 µg/lane) of purified antibodies under non-reducing (NR) and reducing (R) conditions. **D)** Analytical size exclusion chromatography with standard proteins and their corresponding molecular masses indicated by arrows.

All IgG(scFv)2 migrated as double bands corresponding to their expected size of approximately 55 kDa for the heavy chain and 27 kDa for the lights chain under reducing conditions in SDS-Page analysis (Figure 6 C). The C-terminal addition of the scFv increased the corresponding molecular weight by approximately 27 kDa.

Furthermore, biochemical characterization was performed by size exclusion chromatography to elaborate protein integrity under native conditions. The elution profiles showed a major peak at the retention time corresponding to the expected molecular sizes at 150 kDa for the w/o format or 200 kDa with c-terminally linked scFv (Figure 6 D). A small amount of aggregates with ≥ 600 kDa was detectable in all antibody formats containing the CD28-specific scFv but was generally below 1%.

The binding of the antibodies to endoglin and CD28 was analyzed by flow cytometry-based methods. The half-maximum binding values (EC_{50}) of all variants were assessed using Jurkat (CD28+) and Nalm16 (Eng+), and the results are shown in Figure 7.

All bispecific molecules revealed a concentration-dependent binding for CD28 and endoglin. Binding of the HC proteins to CD28 resulted in EC_{50} values ranging from 0.48 to 0.84 nM, which was lower in comparison to the Lc-linked scFv (EC_{50} of 1.83 to 5.56 nM) and revealed a difference of up to 11.5-fold in the EC_{50} values between the Hc and Lc format. Adding a linker to the CD28 binding scFv, led to increased half-maximum binding of approximately 2.5 – fold in Hc and Lc format. Binding of bispecific antibodies to endoglin was comparable to that of the parental χIgG Kro-23 with EC_{50} values in a sub-nanomolar range of 0.11 to 0.25 nM (Figure 7 B).

To summarize these results, CD28-binding showed format-specific differences, with Hc+L providing the highest affinity in comparison to other generated formats. The endoglin binding maintained a constant affinity for all formats.

In addition to assessing the affinity of all antibody variants, further parameters are essential for clinical development. Target-cell restricted activation of T cells was assessed via [methyl-3H] thymidine incorporation by co-incubation of bispecific antibodies in the presence of resting PBMCs and Nalm16 cells that that express endoglin and, in addition, a tumor-associated antigen (TAA). A TAA-specific antibody was used as a subunit in a bispecific antibodiy with TAA^{+}xCD3 specificity in the HC-L format. An analog bispecific antibody directed to a non-expressed target antigen (TAA^{-}xCD3) was used as a control (Figure 8). The level of incorporated [methyl-3H] thymidine indicates the induced proliferation of T cells and thus, correlates with T cell activation.

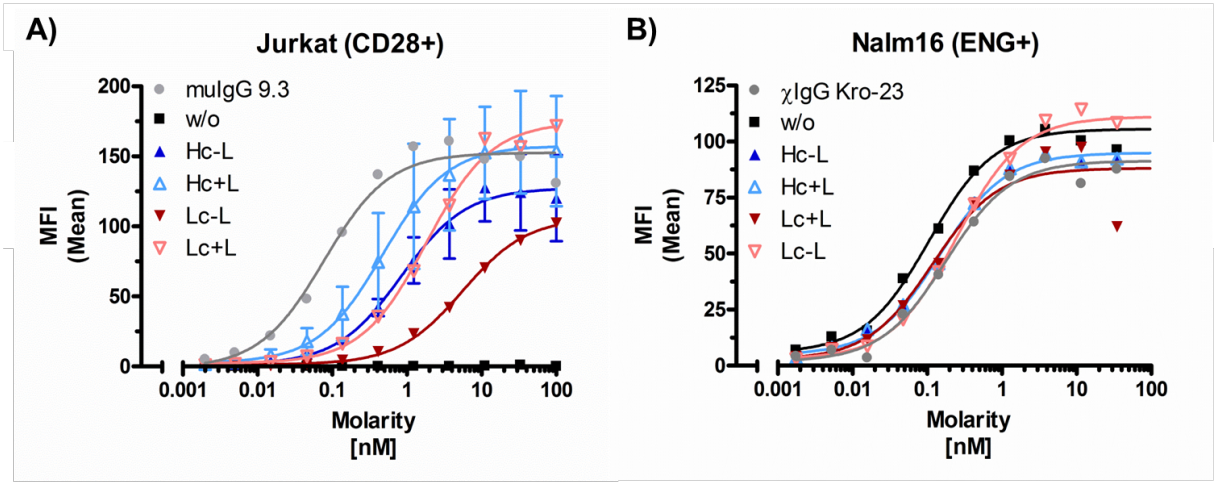

	EC_{50} [nM]
muIgG 9.3	0.08
muKro-23 w/o	-
muKro-23xmu9.3 (Hc+L)	0.48
muKro-23xmu9.3 (Hc-L)	0.84
muKro-23xmu9.3 (Lc+L)	1.83
muKro-23xmu9.3 (Lc-L)	5.56

	EC_{50} [nM]
χIgG Kro-23	0.18
muKro-23 w/o	0.11
muKro-23xmu9.3 (Hc+L)	0.15
muKro-23xmu9.3 (Hc-L)	0.15
muKro-23xmu9.3 (Lc+L)	0.12
muKro-23xmu9.3 (Lc-L)	0.25

Figure 7: Antigen binding of different IgG(scFv)$_2$ endoglinxCD28 formats assessed by flow cytometry. Binding to **A)** CD28 expressed on Jurkat cells with muIgG 9.3 being added as control. Mean ± SD, n≥3. **B)** Binding to endoglin on Nalm16 cells with chimeric IgG Kro-23 being included as a control. Mean values of one representative of 3 independend experiemtns is shown. Format named according to Figure 6 B.

The IgG-like antibody lacking CD28 binding (w/o) did not induce [methyl-3H] thymidine incorporation in PBMCs. Surprisingly, nearly all constructs induced a weak but clearly detectable activation at high molarity in the absence of a CD3 stimulus (Figure 8 A). In comparison to the Lc-L format, the mouse IgG 9.3 and the IgG(ScFv)$_2$ muKro-23xmu9.3 Hc-L, Hc+L, and Lc+L formats induced minimal proliferation of PBMCs starting at a molarity of more than 0.1 nM.

In the presence of a TAA-xCD3 binding bispecific antibody, a marginal increase of T cell proliferation was observed, as seen in Figure 8 B. The IgG(ScFv)$_2$ muKro-23xmu9.3 Lc-L did not present any stimulating activity, while the other variants induced proliferation at higher molarity. The IgG(ScFv)$_2$ muKro-23xmu9.3 Hc-L format provided the highest immunostimulatory activity compared to the Lc+L and Hc+L formats.

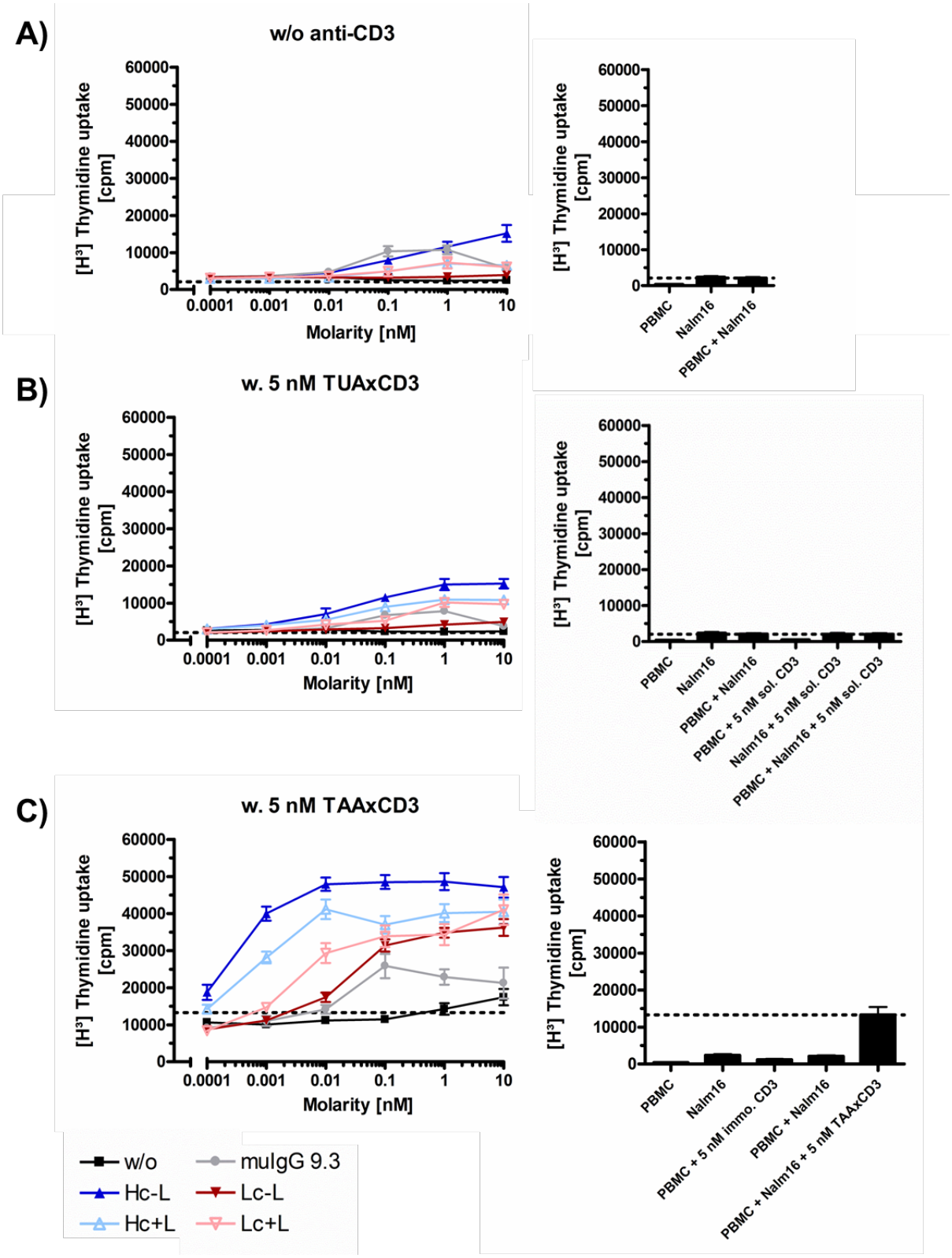

Figure 8: Proliferation of PBMCs in the presence of different endoglinxCD28 formats. A total of 100.000 γ-irradiated Nalm16 cells/well and 250.000 PBMC cells/well were incubated for 48 h with muKro-22xmu9.3 antibodies in different formats and concentrations. Cells were incubated in the presence of either **A)** no CD3 stimulus, **B)** 5 nM TAA-xCD3 antibody or **C)** 5 nM TAAxCD3 antibody and then pulsed with [methyl-^{3}H]-thymidine for 17 h. Mean ± SD, n≥3 for three individual donors. Formats are named according toFigure 6 B.

If a TAA binding bispecific antibody was used, induction of T cell proliferation by the various endoglinxCD28 constructs was detectable (Figure 8 C). TAAxCD3 incubation resulted in a minimal level of proliferation of PBMCs selectively in the presence of Nalm16. CD28-costimulation of IgG(ScFv)$_2$ muKro-23xmu9.3 enhanced the initial response induced by TAAxCD3 with format-dependent differences. In general, the Hc format provided a stronger stimulatory potential in comparison to the Lc format. Fusing the scFv on the heavy chain led to an enhanced proliferation at 10-fold lower molarity compared to light chain fused scFv.

The introduction of a linker, between the IgG backbone and the fused scFv, further modulated the stimulatory activity of the anti-CD28 antibodies. In the Lc format, the introduced linker (Lc+L) induced proliferation in 10-fold lower molarity compared to the format without a linker (Lc-L) with the maximal level of induced proliferation being consistent for both variants. Surprisingly, in the heavy chain formats, no difference was visible in regard to the dose-dependent induction of proliferation. However, the maximal level of induced proliferation was higher for the Hc-L format than for the Hc+L format.

Taken together, the differences in the immunostimulation capacity of the different antibody formats depends on the location of the linked anti-CD28 scFv and the addition of a linker. In correlation with the affinity of the assessed formats, heavy chain-linked scFv induced a strong proliferative response in co-incubation with an immobilized anti-CD3 stimulus, with Hc-L inducing the highest maximal level. However, IgG(ScFv)$_2$ muKro-23xmu9.3 Lc-L was the only variant that indicated a complete lack of off-target activation, which resulted in its selection for further improvements.

2.1.2 Comparison of different endoglin binding antibodies in the LC-L format

The comparison between various bispecific formats in the previous chapter let to the identification of IgG(ScFv)$_2$ muKro-23xmu9.3 Lc-L with the lowest background in the absence of CD3 stimulation. The previous data demonstrated the possibility of modulating the biochemical properties of a bispecific antibody by the selection of its format. Soos et al. demonstrated the varying biochemical properties of antibodies could also differ due to binding to different epitopes on the same target [241].

Thus, a panel of three different endoglin binding clones was selected to validate the effect of varying target epitopes and affinity on the immunomodulating characteristics of the Lc-L format. The selected panel of endoglin binding clones consists of Kro-10, Kro-22, and Kro-23, that were described in the work of Karolin Schwartz [237].

Graphical illustration are shown in Figure 9 A and B. Purification was performed *via* affinity chromatography, followed by preparative size exclusion to eliminate all aggregates. SDS-Page (Figure 9 C) and size exclusion (Figure 9 D) was conducted to confirm protein purity and integrity. The results obtained for the antibody variants using Kro-10 and Kro-22 are similar to the data previously described for the Kro-23 variant in 2.1.1

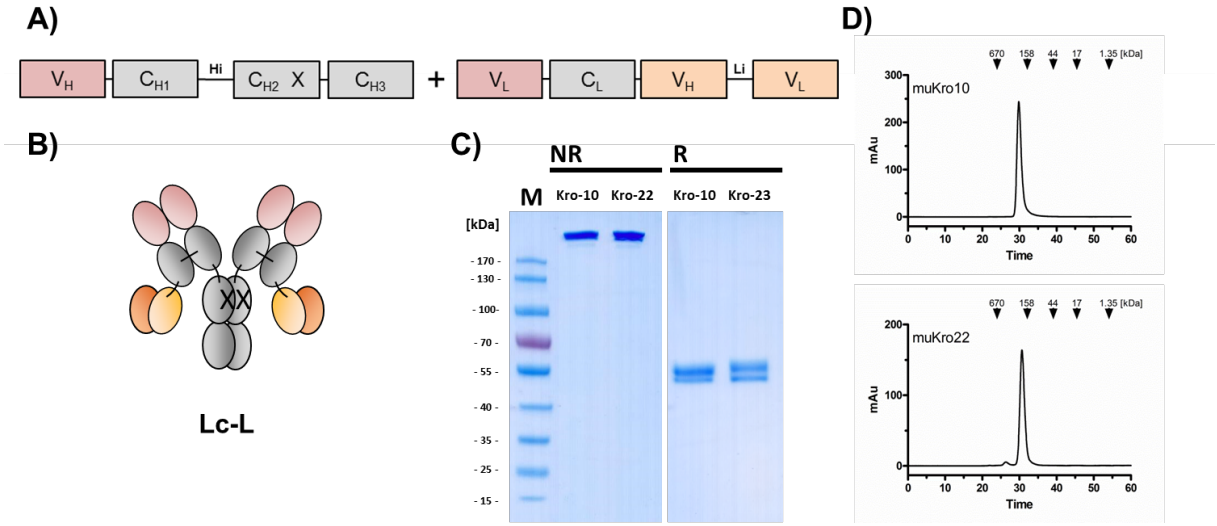

Figure 9: Design and biochemical characterization of different endoglinxCD28 variants in the Lc-L format. A) Illustration of the genotype of different endoglinx9.3 IgG(scFv)$_2$ Lc-L variants with hinge (Hi) and glycine-serin linker (Li) consisting out of (Gly-Gly-Gly-Ser)$_3$ and their **B)** graphical illustration. **C)** SDS-Page analysis (10 % PAA, 2 µg/lane) of purified antibodies with muKro-10 and muKro-22 clones under non-reducing (NR) and reducing (R) conditions. **D)** Analytical size exclusion chromatography with standard proteins and their corresponding molecular masses indicated with arrows. The format is named according to Figure 6 B.

The half-maximum binding was assessed by binding to CD28 expressing Jurkat (Figure 10 A) and endoglin-expressing Nalm16 (Figure 10 B) using flow cytometry.

The binding towards endoglin matches previous results with the parental antibodies. IgG(scFv)$_2$ with Kro-22 showed the lowest EC_{50} of 0.45 nM when being compared to Kro-23 or Kro-10 (Figure 10 B). Differences in the binding were not only detectable when comparing the half-maximum binding of the analyzed clones. Kro-23 showed the highest EC_{50} and also a 1.5-fold decrease in maximal bound protein. Unexpectedly, exchanging Kro-23 with either Kro-22 or Kro-10 in the Lc-L format proved to affect the CD28-binding as well. Using the clone Kro-23 together with the scFv 9.3 led to a decrease of affinity towards CD28 (Figure 10 A), when being compared to the other anti-endoglin binding clones.

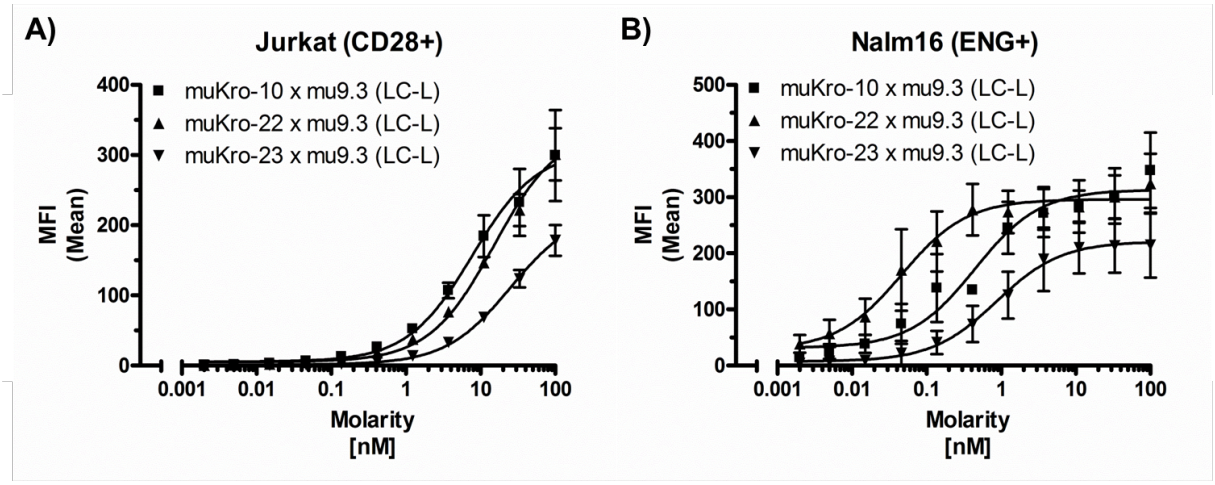

	EC_{50} [nM]
muKro-10xmu9.3 (LC-L)	7.73
muKro-22xmu9.3 (LC-L)	15.16
muKro-23xmu9.3 (LC-L)	25.14

	EC_{50} [nM]
muKro-10xmu9.3 (LC-L)	0.45
muKro-22xmu9.3 (LC-L)	0.046
muKro-23xmu9.3 (LC-L)	0.86

Figure 10: Antigen binding of IgG(scFv)$_2$ endoglinxCD28 variants in Lc-L format assessed by flow cytometry. Antigen binding of **A)** CD28 on Jurkat cells and **B)** endoglin on Nalm16 cells. Mean ± SD, n≥2.

Antibodies with similar EC_{50} values can have a difference in their kinetic rate constants k_A and k_D [242], for their ratio of both is defined as the equilibrium binding constant K_D. In addition to their effect on the affinity of an antibody, single amino acid exchanges can also have an impact on the specific kinetics of the antibody to antigen interaction [243]. Thus, surface plasmon resonance experiments were performed to determine the rate constants k_A and k_D and to calculate the equilibrium binding constant K_D for immobilized IgG(scFv)$_2$ muKro-10, muKro-22, and muKro-23 with soluble endoglin (Figure 11). In comparison, the association constant k_a varied between all clones analyzed. The highest association of endoglin was found for muKro-10 with a k_a value of 65050 1/Ms compared to muKro-22 (k_a of 57375 1/Ms) and muKro-23 (k_a of 58200 1/Ms).

The slowest dissociation of endoglin was identified for muKro-22 with a k_d value of 0.00008 1/s, compared to muKro-10 (k_a of 0.003 1/s) and muKro-23 (k_a of 0.001 1/s).

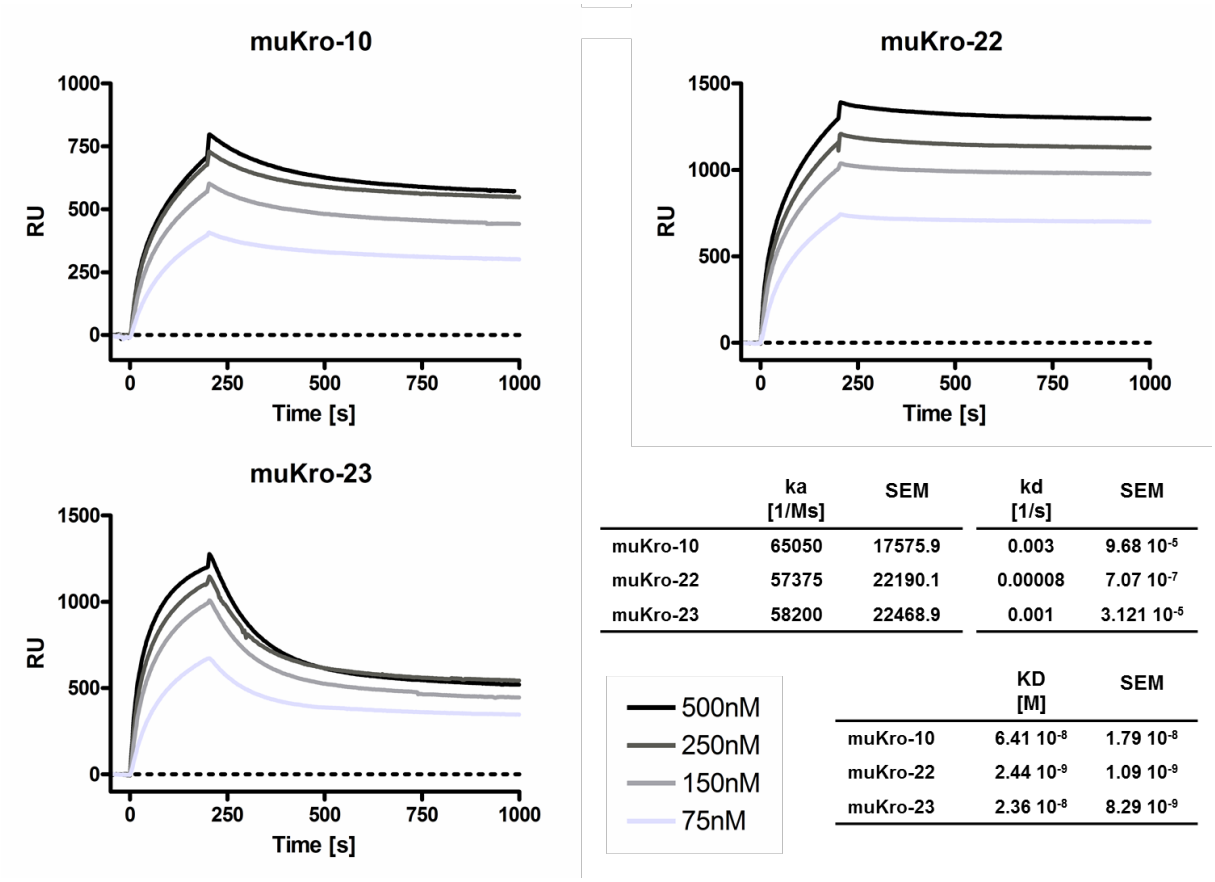

	ka [1/Ms]	SEM	kd [1/s]	SEM
muKro-10	65050	17575.9	0.003	$9.68\ 10^{-5}$
muKro-22	57375	22190.1	0.00008	$7.07\ 10^{-7}$
muKro-23	58200	22468.9	0.001	$3.121\ 10^{-5}$

	KD [M]	SEM
muKro-10	$6.41\ 10^{-8}$	$1.79\ 10^{-8}$
muKro-22	$2.44\ 10^{-9}$	$1.09\ 10^{-9}$
muKro-23	$2.36\ 10^{-8}$	$8.29\ 10^{-9}$

Figure 11: Kinetic of the binding of soluble endoglin to immobilized various anti-endoglin clones. Binding of muKro-10, muKro-22, and muKro-23 to human endoglin was analyzed by surface plasmon resonance with 10 µg/ml immobilized endoglinxCD28 antibody in the IgG(scFv)$_2$ Lc-L format. Binding was analyzed with endoglin concentrations between 500 nM and 75 nm with a flow of 2 µl/min at RT. Kinetic constants were calculated using Biacore X evaluation software. Dotted line represents the baseline.

In summary, the results of the surface plasmon analysis resemble the results obtained *via* flow cytometry with Kro-22 exhibiting not only the lowest EC_{50} but also the lowest K_D value.

Target cell-restricted activation of T cells by different anti-endoglin antibodies was assessed in the presence of an immobilized anti-CD3 stimulus *via* [methyl-3H] thymidine incorporation (Figure 12). All experiments were performed according to 2.1.1. In line with the previous results, all clones demonstrated a lack of activation of resting T cells. Upon initial activation with a TAAxCD3 antibody, all antibodies induced a dose-dependent proliferation with a maximal 5-fold increased [methyl-3H] thymidine incorporation compared to TAAxCD3 alone.

However, comparing the EC_{50}, Kro-23 demonstrated a substantial higher EC_{50} of 0.338 nM compared to muKro-10 (EC_{50} of 0.0038 nM) and muKro-22 (EC_{50} of 0.0044 nM). These results indicate a superior induction of proliferation at approximately 100-fold lower molarity for the clones muKro-10 and muKro-22 compared to muKro-23. In addition, these results resemble the affinity of the antibodies used.

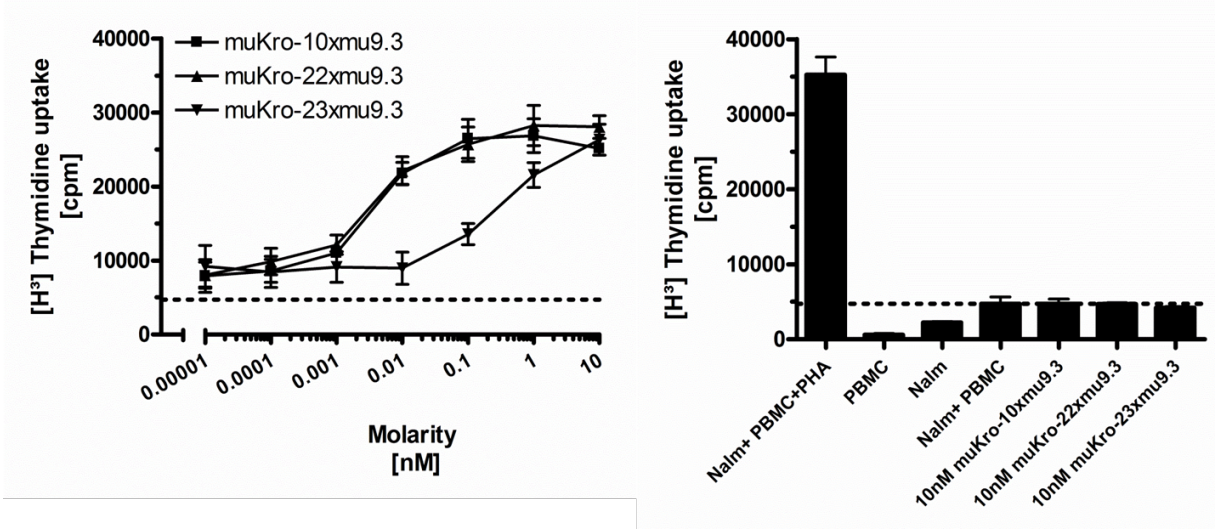

Figure 12: Proliferation of PBMCs in the presence of different endoglin binding clones in Lc-L format. A total of 100.000 Nalm16 cells/well together with 250.000 PBMC cells/well were incubated for 48 h with different antibody concentrations. Cells were incubated in the presence of 5 nM of TAAxCD3 antibody and then pulsed with [methyl-^{3}H]-thymidine for 17 h. Mean ± SD, n≥3 for three individual donors.

In summary, all molecules demonstrated a selective induction of T cell proliferation in combination with TAAxCD3. The antibody muKro-22 was selected for further analysis. A tumor cell lysis assay was performed for the verification of enhancing TAAxCD3-mediated tumor cell killing in co-treatment with IgG(scFv)$_2$ Lc-L muKro-22x9.3, using the xCelligence system. The results are presented in Figure 13.

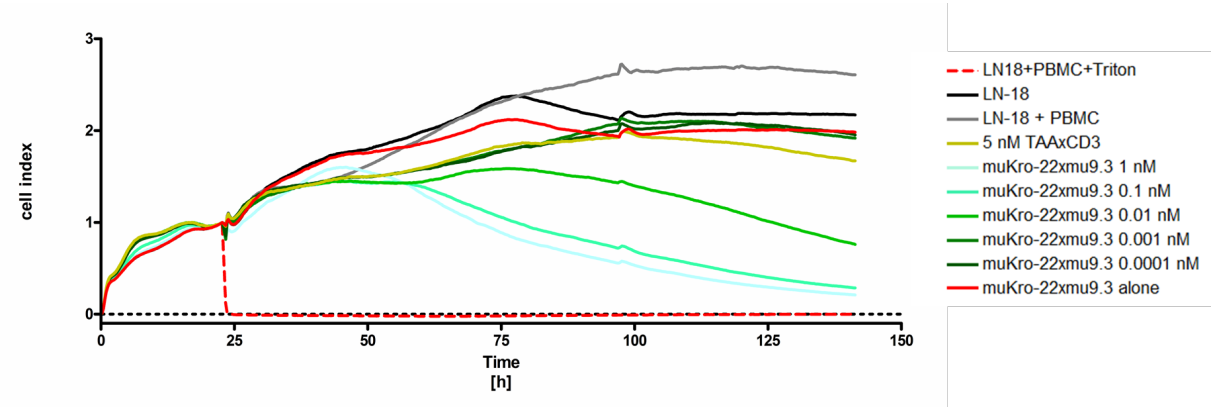

Figure 13: Tumor cell lysis induced of TAAxCD3 and IgG(scFv)$_2$ Lc-L muKro22xmu9.3 on LN-18 cells. A total of 20.000 LN-18 cells were seeded per well. After a 24 h preincubation 20.000 PBMCs/well were added and treated with eiter 5 nM of TAAxCD3 (yellow), 5 nM IgG(scFv)$_2$ Lc-L muKro22xmu9.3 (red, solid line), or a combination of 5 nM TAAxCD3 with a titration of IgG(scFv)$_2$ Lc-L muKro22xmu9.3 (green). Lysed cells were analyzed by the xCelligence system. One representative experiment out of two.

At molarity of 5 nM, the TAAxCD3 antibody-induced limited lysis of LN-18 cells. However, the treatment in the combination of 5 nM TAAxCD3 and IgG(scFv)$_2$ Lc-L muKro-22x9.3 significantly increased the lysis of LN-18 cells in a dose-dependent manner, starting at a molarity of 0.01 nM. The maximally induced tumor cell lysis was identified at a molarity of 0.1 nM or higher

This data are in agreement with the [methyl-3H] thymidine incorporation experiments, demonstrating the selective immunostimulating properties of IgG(scFv)$_2$ Lc-L muKro-22x9.3 together with an induction of an enhanced anti-tumor response of a TAAxCD3 antibody.

2.1.3 Comparison of different CD28 binding antibodies in the IgG(scFv)$_2$ LC-L format

Comparing different clones of endoglin binding antibodies in the IgG(scFv)$_2$ Lc-L format in 2.1.2 demonstrated the effect of affinity and epitope on the immunomodulating properties of a bispecific antibody. To compare 9.3 with other anti-CD28 clones, TGN1412 and 15E9 were selected. 15E9 was first described in 1999 as an agonistic anti-CD28 antibody [253] and TGN1412 was originally described as a superagonistic antibody targeting CD28 by activating T cells without a primary stimulation [123]. Similar to 9.3, both clones were originally generated *via* hybridoma technology and TGN1412 is the humanized variant of the clone 5.11A1. All novel CD28 antibodies were cloned into the scFv format and linked on the light chain (Figure 14 A + B), as described in 2.1.1. Antibodies were produced in the IgG(scFv)$_2$ Lc-L format using muKro-22 as targeting antibody.

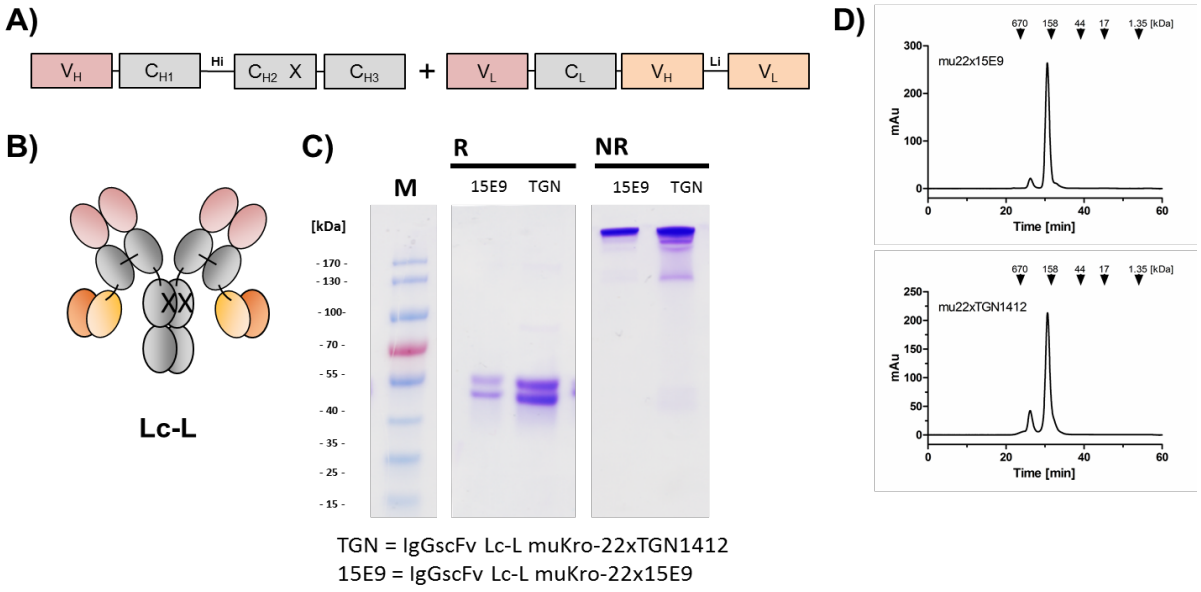

Figure 14: Design and biochemical characterization of different muendoglinxmu9.3 variants in Lc-L format. A) Illustration of the genotype of different muCD105xmu9.3 IgG(scFv)$_2$ variants with hinge (Hi) and glycine-serin linker (Li) consisting out of (Gly-Gly-Gly-Ser)$_3$ and their respective **B)** graphical illustration. **C)** SDS-Page analysis (10 % PAA, 2 µg/lane) of purified antibodies with muKro-10 and muKro-22 clones under non-reducing (NR) and reducing (R) conditions. **D)** Analytical size exclusion chromatography with standard proteins and their corresponding molecular masses indicated with arrows. Format named according toFigure 6 B.

Following the verification of protein purity and integrity, binding was assessed *via* flow cytometry experiments (Figure 15). Exchanging the CD28 specific clone 9.3 with TGN1412 or 15E9 did not effect binding to endoglin on Nalm16 cells (Figure 15 B). Flow cytometry data revealed similar EC_{50} values when comparing the novel molecules with the parental antibody. The binding to CD28, however, showed clone-specific differences (Figure 15 A) with 9.3 demonstrating higher affinity than TGN1412 and 15E9. Saturation of both clones was not reached at a concentration of 100 nM and therefore, the EC_{50} value could not be adequately determined. Nonetheless, TGN1412 showed a higher affinity towards CD28 compared to 15E9.

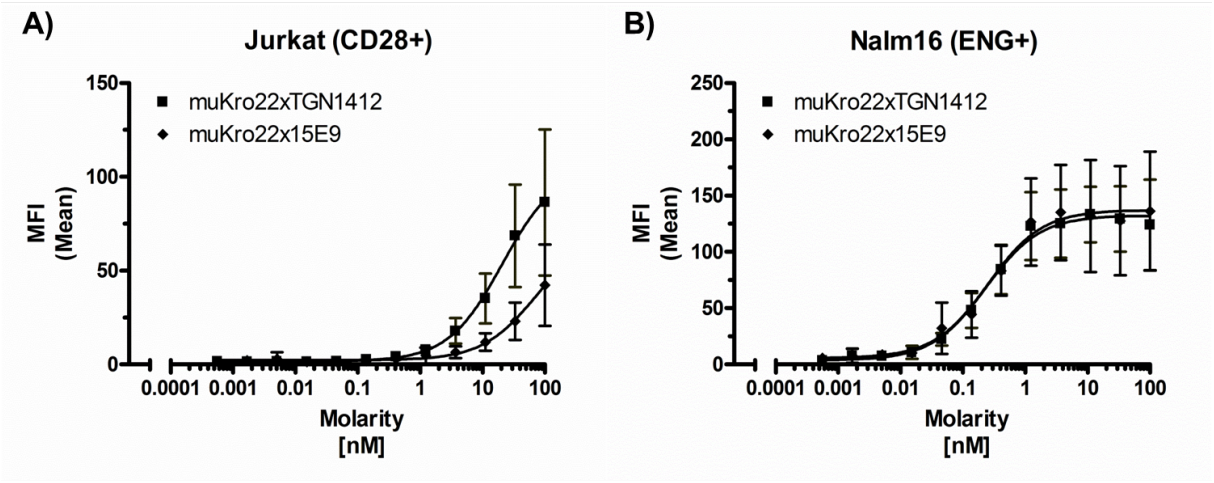

	EC_{50} [nM]
muKro-22xTGN1412	20.66
muKro-22x15E9	72.38

	EC_{50} [nM]
muKro-22xTGN1412	0.23
muKro-22x15E9	0.25

Figure 15: Antigen binding of IgG(scFv)$_2$ endoglinxCD28 variants in Lc-L format assessed by flow cytometry. Antigen binding to cell surface-expressed **A)** CD28 on Jurkat cells and **B)** endoglin on Nalm16 cells. The binding was analyzed by flow cytometry. Mean ± SD, n≥2.

Induction of proliferation of the three different CD28 binding clones was validated *via* [methyl-3H] thymidine uptake experiments Figure 16. In the presence of an immobilized CD3 stimulation, all clones showed a dose-dependent induction of proliferation with the clone 9.3 and TGN1412 inducing proliferation in a 10-fold lower antibody concentration than 15E4 (Figure 16 A). TGN1412 induced strong proliferation on resting PBMCs (Figure 16 C) and in the presence of LN-18 (Figure 16 B), which was not seen for 9.3 and 15E4. TGN1412 demonstrated to have the same superagonistic features as described in the IgG format [107].

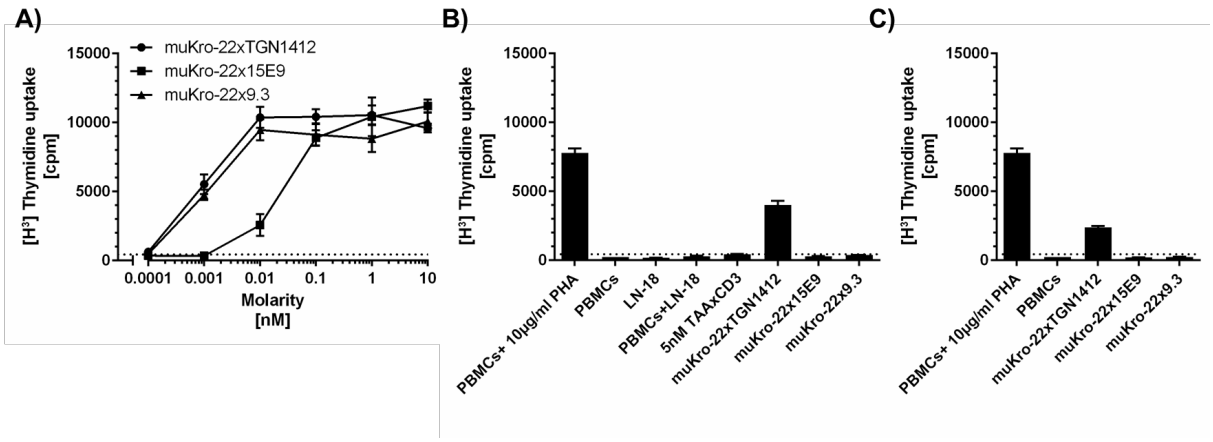

Figure 16: Proliferation of PBMCs in presence of different CD28 binding clones in Lc-L format. A total of 50,000 LN-18 cells/well, together with 250,000 PBMC cells/well were incubated for 48 h with different antibody concentrations. Antibodies were bispecific endoglinxCD28 antibodies in Lc-L format. **A)** Cells were incubated in presence of 5 nM of immobilized anti-CD3 stimulus and then pulsed with [methyl-^{3}H]-thymidine for 17 h with respective controls with **B)** or **C)** without LN-18. Mean ± SD, n≥3 for three individual Donors.

Since 9.3 did prove to refrain from any superagonistic properties while obtaining decisive target-cell specific proliferative effect on T cells, it was selected for further development of a competent stimulatory antibody.

2.1.4 Humanisation of 9.3

The formation of neutralizing and non-neutralizing antibodies against a therapeutic antibody can render treatment ineffective [244]. Several humanization strategies were developed in recent years to avoid the generation of HAMAs. These include exchanging the mouse variable regions with human constant backbone sequences or crafting the mouse on homolog human framework sequences. The anti-CD28 antibody 9.3 was humanized via CDR crafting, and the resulting variants were characterized in the work of Yacine Mahringer [245]. The affinity of the humanized antibody was similar to the parental one.

As a result, the variant hu9.3-8 of was selected for its similar induction of proliferation in the presence of a TAAxCD3 when compared to the parental mu9.3, as seen in Figure 17.

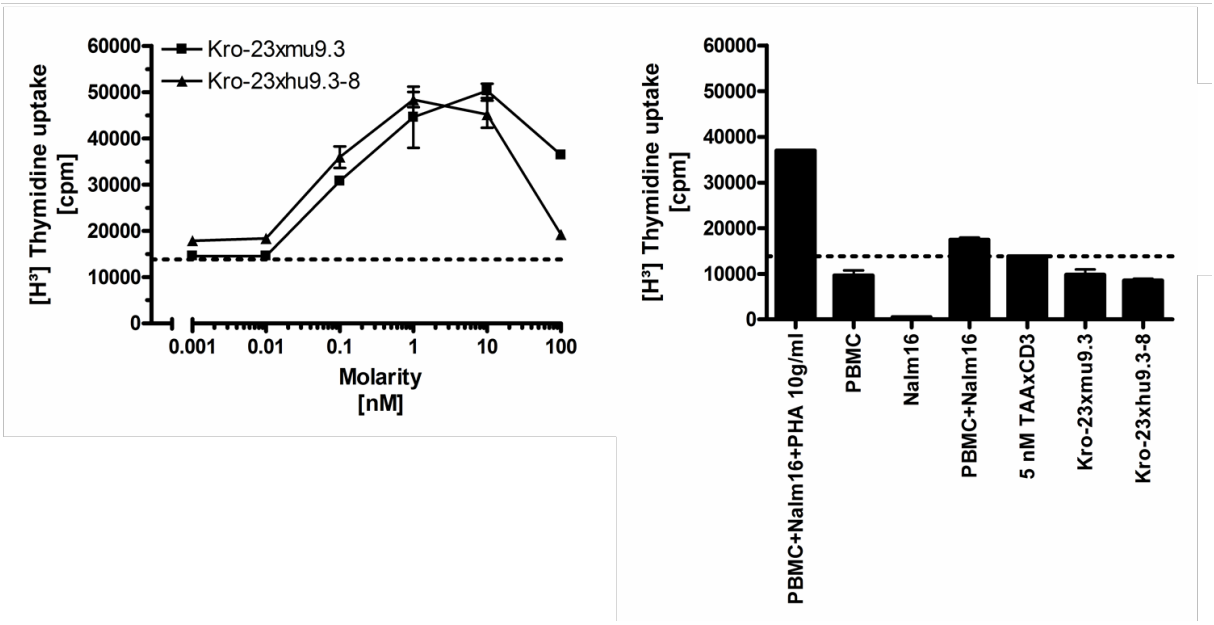

Figure 17: Proliferation of PBMCs in the presence of different endoglin binding clones in the Lc-L format. A total of 100.000 Nalm16 cells/well together with 250000 PBMC cells/well were incubated for 48 h with different antibody concentrations. All antibodies were bispecific endoglinxCD28 antibodies in the Lc-L format. Cells were incubated in the presence of 5 nM of TAAxCD3 stimulus and then pulsed with [methyl-^{3}H]-thymidine for 17 h. Mean ± SD, n≥3 for three individual donors. Data generated in cooperation with Yacine Mahringer.

2.1.5 Humanisation of Kro-22

Following the humanization of 9.3, endoglin binding clone Kro-22 was humanized via CDR crafting. Alternative human germline genes were selected *in silico* sharing the same canonical structure and high sequence homology [246] with the parental sequence while avoiding sequence specific unusual sequence motifs such as glycosylation sites. A total of 5 humanizations were performed for V_H and V_L respectively. Successful humanization was assessed by calculating the T20 score [247] for the most promising candidates (Table 1). Antibody framework sequences with a T20 score higher than 80 are considered as human-like and with scores above 86.6 for all sequences the humanization of the V_H and V_L was successful.

Table 1 Humanness score of different Kro-22 variants. Sequences for heavy and light variable sequences were analyzed by using the T20-score [247]. Framework sequences with a score above 80 are considered human-like, while framework only sequences that score above 85 are considered human-like.

Clone	T20-score Framework	T20-score Framework + CDR
V_H muKro-22	69.8	68.6
V_H huKro-22.2	87.4	81.2
V_H huKro-22.3	86.6	81.0
V_H huKro-22.4	86.8	79.2
V_L muKro-22	60.9	52.6
V_L huKro-22.2.2	98.0	94.2
V_L huKro-22.4	91.3	81.7
V_L huKro-22.6	95.3	80.5

The generated sequences were selected for production in the bispecific IgG(ScFv)$_2$ Lc-L format. Preferences in the pairing of different V_H with V_L sequences are described by Jayaram *et al.* [248]. Such preferred pairings are more likely to be stable which could result in longer shelf life and being less susceptible to aggregation or denaturation. In order to generate a more stable antibody, three selected V_H sequences were paired with a total of three V_L sequences, which resulted in 9 different antibodies variants as depicted in Figure 18 A and B.

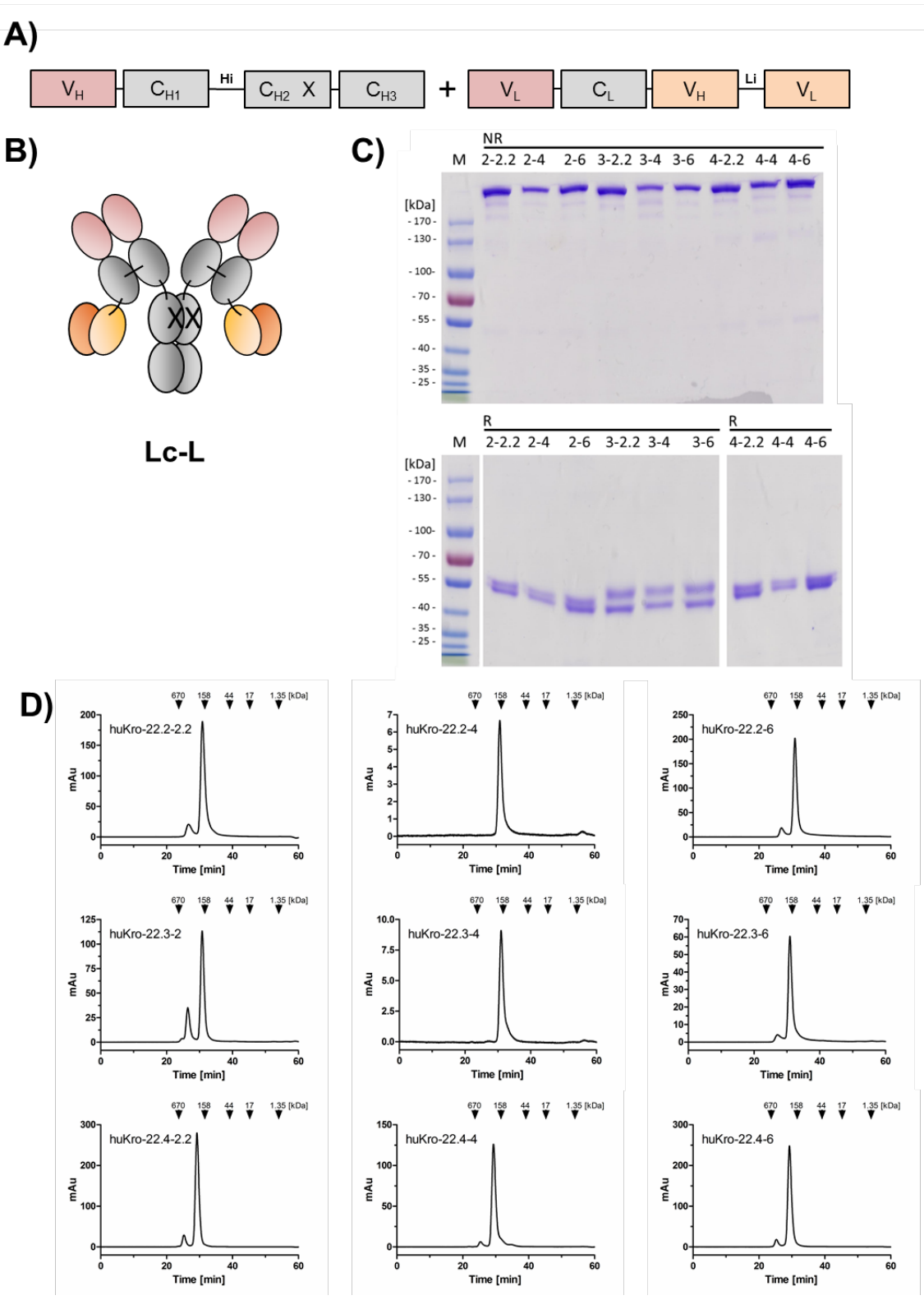

Figure 18: Design and biochemical characterization of different humanized Kro-22 variants in IgG(scFv)$_2$ Lc-L format. A) Illustration of the genotype of different huendoglinxmu9.3 IgG(scFv)$_2$ Lc-L variants with hinge (Hi) and glycine-serin linker (Li) consisting out of (Gly-Gly-Gly-Ser)$_3$ and their respective **B)** graphical illustration. **C)** SDS-Page analysis (10 % PAA, 2 µg/lane) of purified antibodies with huKro-22 variants under non-reducing (NR) and reducing (R) conditions. **D)** Analytical size exclusion chromatography with standard proteins and their corresponding molecular masses indicated with arrows. Format named according toFigure 6 B.

All proteins proved to be intact and did not contain a significant amount of aggregates. Binding was assessed on CD28 expressing Jurkat (Figure 19 A) and endoglin expressing Nalm16 (Figure 19 B) cells by the use of flow cytometry experiments. Unfortunately, not the variants huKro-22.2-4 and huKro22.3-4 were not produced in a significant amount and where not included in further experiments. Half-maximum binding of all variants was similar to the parental antibody. This was demonstrated for the binding of the scFv to CD28 but also of the endoglin. Nonetheless, EC_{50} values for binding to endoglin were nearly 10-fold lower for all humanized variants as compared to the parental mouse version. Varying expression levels of Nalm16 cells might be the reason for variations of the EC_{50}.

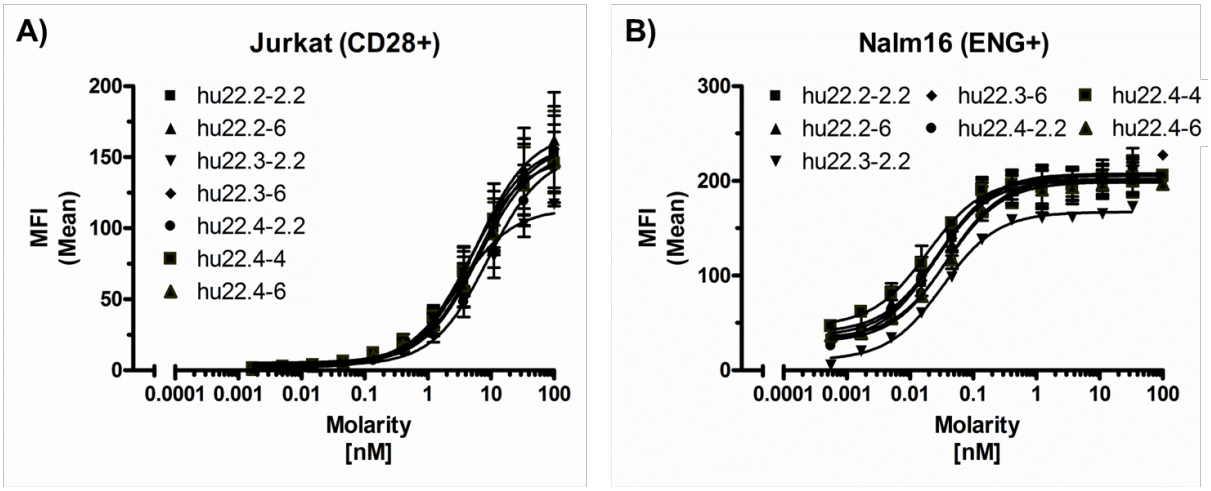

	EC_{50} [nM]
huKro-22.2-2.2xhu9.3-8	6.25
huKro-22.2-6xhu9.3-8	5.71
huKro-22.3-2.2xhu9.3-8	3.01
huKro-22.3-6xhu9.3-8	5.26
huKro-22.4-2.2xhu9.3-8	9.02
huKro-22.4-4xhu9.3-8	4.46
huKro-22.4-6xhu9.3-8	6.36

	EC_{50} [nM]
huKro-22.2-2.2xhu9.3-8	0.025
huKro-22.2-6xhu9.3-8	0.029
huKro-22.3-2.2xhu9.3-8	0.033
huKro-22.3-6xhu9.3-8	0.028
huKro-22.4-2.2xhu9.3-8	0.038
huKro-22.4-4xhu9.3-8	0.019
huKro-22.4-6xhu9.3-8	0.039

Figure 19: Antigen binding of humanized Kro-22 clones in IgG(scFv)$_2$ endoglinxCD28 Lc-L format. Antigen binding to cell surface-expressed **A)** CD28 on Jurkat cells and **B)** endoglin on Nalm16 cells. The binding was analyzed by flow cytometry. EC_{50} values were calculated using the Prism software. Mean ± SD, n≥2.

Previous flow cytometry-based binding analysis demonstrated a high affinity towards cell-bound endoglin of all humanized antibody clones. Following this analysis, the binding kinetic of the humanized clones with soluble endoglin was assessed by surface plasmon resonance analysis. For the lack of a sufficient production, not all clones were included in this analysis shown in Figure 20.

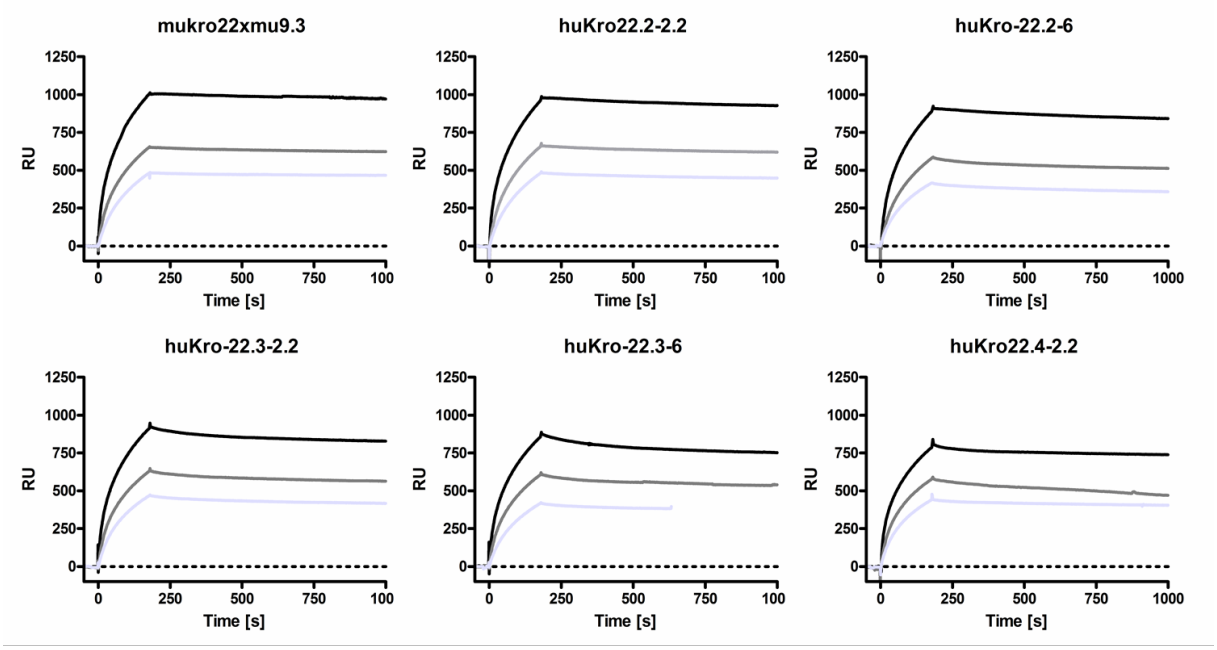

	ka [1/Ms]	SEM	kd [1/s]	SEM	KD [M]	SEM
muKro22	100225	22190	$4.78\ 10^{-5}$	$8.40\ 10^{-6}$	$6.99\ 10^{-10}$	$2.46\ 10^{-10}$
huKro22.2-2.2	50548	23987	$5.74\ 10^{-5}$	$3.55\ 10^{-6}$	$7.11\ 10^{-9}$	$5.91\ 10^{-9}$
huKro22.2-6	92600	34423	$1.08\ 10^{-5}$	$7.85\ 10^{-6}$	$1.57\ 10^{-9}$	$3.74\ 10^{-10}$
huKro22.3-2.2	54238	23949	$2.80\ 10^{-5}$	$1.38\ 10^{-5}$	$3.91\ 10^{-8}$	$3.43\ 10^{-8}$
huKro-22.3-6	88300	31380	$1.83\ 10^{-5}$	$2.15\ 10^{-5}$	$3.37\ 10^{-9}$	$1.38\ 10^{-9}$
huKro-22.4-2.2	104500	38680	$1.25\ 10^{-5}$	3.0110^{-5}	$1.63\ 10^{-9}$	$4.00\ 10^{-10}$

Figure 20: Kinetic of the binding of soluble endoglin on immobilized humanized variants of muKro-22. Binding to human endoglin was analyzed by surface plasmon resonance with 10 µg/ml immobilized endoglinxCD28 antibody in $IgG(scFv)_2$ Lc-L. Binding was analyzed with endoglin concentrations between 300 nM and 50 nm with a flow of 2 µl/min at RT. Kinetic constants were calculated using Biacore X evaluation software. Dotted line represents the baseline.

The association constant k_a for the interaction of soluble endoglin towards immobilized antigen was in a range of 54238 1/Ms to 104500 1/Ms for all humanized variants, with 100225 for the mouse parental clone muKro-22. In addition, dissociation of all humanized clones was similar to the muKro-22 with a dissociation constant k_d ranging from 1.08 1/s to 5.74 1/s. The results obtained for k_a and k_d were used in the calculation of the K_D values resulting in values in similar ranges compared to the previously determined EC_{50} values in flow cytometry (Figure 19). Taken together, the detailed analysis of the binding to endoglin indicated no significant difference between the humanized clones to the parental antibody.

The thermal stability is an important indicator of the overall stability of an antibody. Generating stable antibodies is, an essential goal in the development of antibody-based therapeutics. Especially the physical stability of scFv fragment is shown to have multiple effects including but not being limited to protein stability and formation of aggregates [250, 251]. Thus, screening methods in the identification of novel antibody clones were developed based on the thermal stability [252]. A thermal stability assay quantifies the change in the thermal denaturation temperature of a protein. Stepwise increasing the temperature results in a partial unfolding of a protein which is enabling a dye of staining otherwise unaccessible amino acids. Thermal stability analysis of the humanized IgG(scFv)$_2$ Lc-L variants together with the parental antibody are shown in Figure 21.

The first derivate (Figure 21 B) was calculated of the raw data (Figure 21 A) to asses the melting point for each antibody. A comparison between the parental antibody with its humanized variants resulted in similar melting points with a range of 2°C. No preferential V_H/V_L pairing was identified, which concludes no effect on the stability of the humanized variants of muKro-22 following CDR grafting.

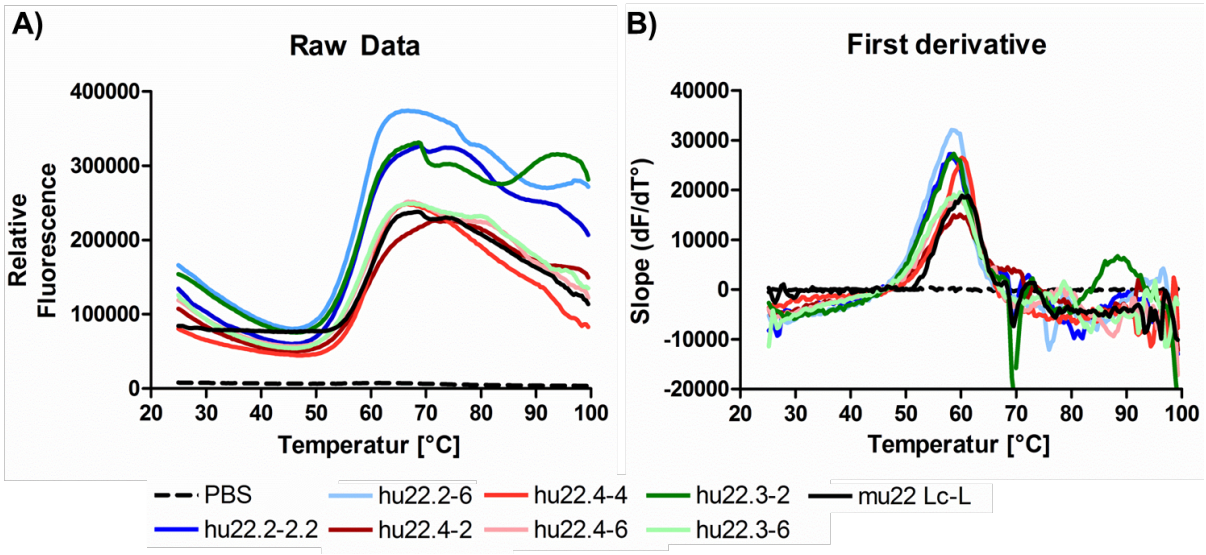

Figure 21: Thermal Stability of Humanized Kro-22 variants in Lc-L format. Molecular stability of the humanized Kro-22 clones was assessed by **A)** differential scanning fluorimetry. **B)** The melting temperature (T_m) was determined by visual interpretation of the calculated first derivative of the raw data.

Contrary to the expected results, the initial analysis demonstrated no significant differences when comparing the humanized variants of Kro-22 regarding their biochemical properties. As a next step, immunomodulating properties were to be assessed via the potential induction of proliferation on PBMCs (Figure 22). The proliferation of resting PBMCs was not induced by any of the humanized antibodies without the presence of TAAxCD3 but in the presence of Nalm16 (Figure 22 B).

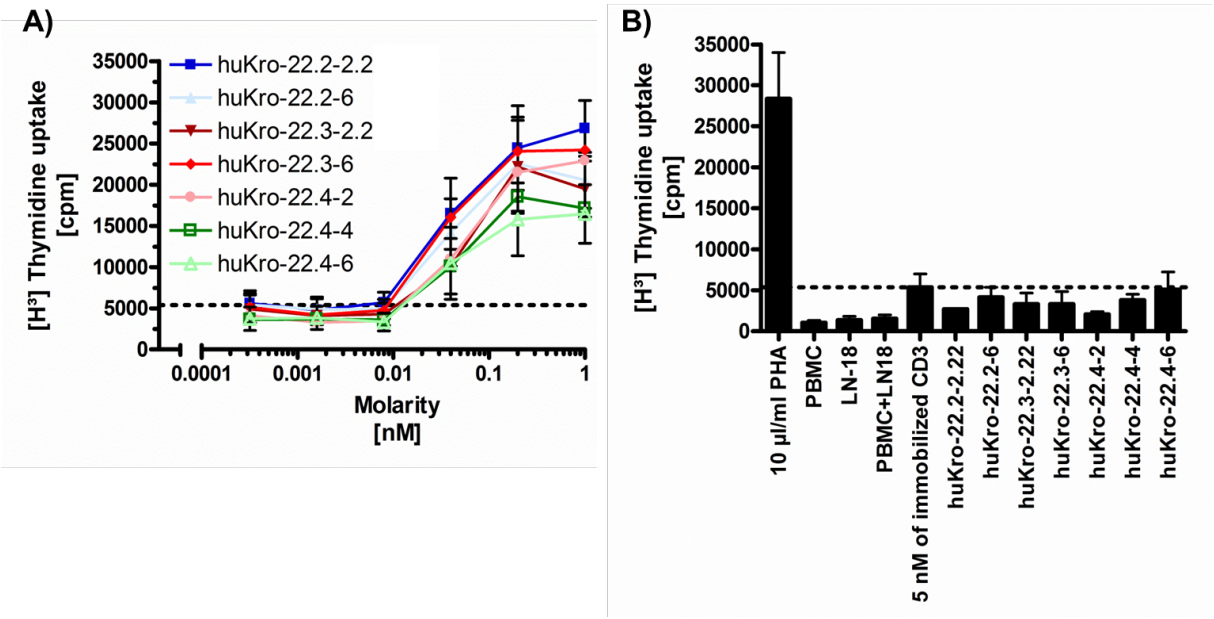

Figure 22: Proliferation of PBMCs in the presence of different endoglin binding clones in Lc-L format. A total of 30,000 LN-18 cells/well, together with 250,000 PBMC cells/well, were incubated for 48 h. Antibodies were bispecific endoglinxCD28 antibodies in Lc-L format. Cells were incubated in presence of 5 nM of an immobilized CD3 stimulus with **A)** different antibody concentrations or **B)** without anti-CD3 stimulus with 5 nM. In addition, cells were pulsed with [methyl-^{3}H]-thymidine for 17 h. Mean ± SD, n≥3 for three individual Donors.

Upon initial activation of PBMCs *via* a TAAxCD3 antibody (Figure 22 A), all humanized variants of muKro-22 induced a dose-dependent proliferation on T cells starting at a molarity of 0.01 nM. [methyl-3H] thymidine incorporation increased to a maximum level of 3- to 5-fold higher compared to a sole stimulation by TAAxCD3 (dotted line). This data indicates a target cell-specific T cell activation for all humanized variants according to the previously obtained results. However, IgG(scFv)$_2$ Lc-L huKro-22.2-2xhu9.3-8 demonstrated to induce the most substantial level of proliferation at a molarity of 1 nM.

In addition to their potential to specifically inducing T cell proliferation, the humanized variants were analyzed with respect to their potential to stimulate a TAAxCD3-mediated tumor cell killing *via* the use of xCelligence assay (Figure 23). All IgG(scFv)$_2$ Lc-L huKro-22 variants enhanced the TAAxCD3-mediated lysis of LN-18 cells. The results of the xCelligence assay resemble previous data with no significant difference between each humanized variant of Kro-22 and its parental antibody.

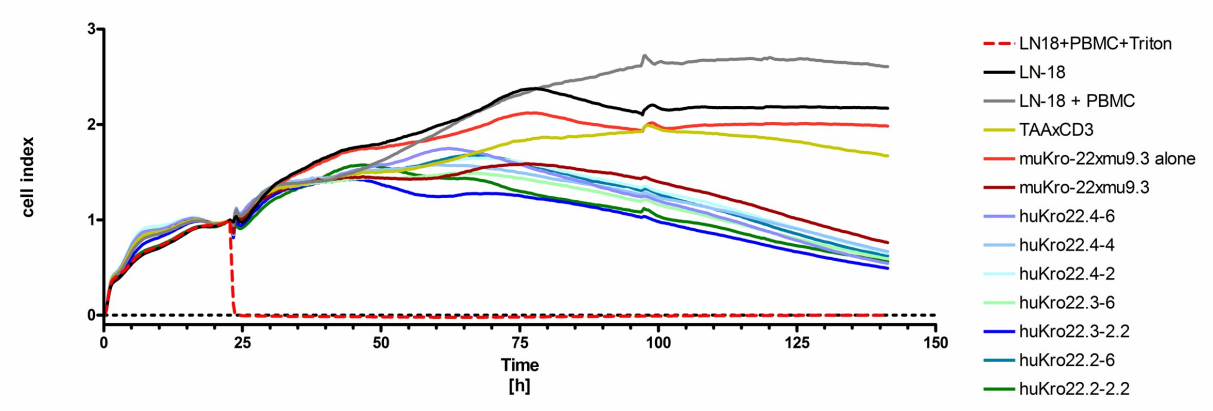

Figure 23: Tumor cell lysis induced of TAAxCD3 and IgG(scFv)$_2$ Lc-L huKro22 varaints on LN-18 cells. A total of 20.000 LN-18 cells were seeded per well. After a 24 h preincubation 20.000 PBMCs/well were added and treated with eiter 5 nM of TAAxCD3 (yellow), 5 nM IgG(scFv)$_2$ Lc-L muKro22xmu9.3 (red, solid line), or a combination of 5 nM TAAxCD3 with a 0.01 nM IgG(scFv)$_2$ Lc-L humanized Kro22 variants (blue). Lysed cells were analyzed by the xCelligence system. Results represent mean values of triplicates with one representative experiment out of two shown.

Overall completing the characterization of all humanized variants of Kro-22 let to the conclusion that there are no striking differences regarding the biochemical and immunomodulating characteristics. However, the comparison let to the identification of IgG(scFv)$_2$ Lc-L huKro-22.2-2xhu9.3-8 as the most promising clone with respect to a low tendency for aggregation and overall better producibility.

2.2 Development of the endoglinx4-1BB bispecific antibody

2.2.1 Antibody Generation

The 4-1BB binding antibodies were obtained *via* hybridoma generation as well as phage display technology. The phage display derived antibodies were generated in cooperation with the lab of Stefan Dübel at the Departement of Biotechnology, Technical University of Braunschweig. All generated clones are listed in Table 2 together with their respective isotype. Julian Weischedel performed the initial characterization of the phage display derived antibodies [254]. Antibodies with sufficient producibility were selected for further characterization and their supernatants were purified *via* protein A affinity chromatography. Purity and integrity were analyzed by SDS-Page and size exclusion chromatography and the results for the IgG antibodies are shown in Figure 24. The SDS-Page analysis resulted in the expected bands at approximately 180 kDa for the whole IgG under non-reducing conditions and 28 kDa for the LC and 50 kDa for the HC under reducing conditions respectively.

Table 2: List of 4-1BB binding antibodies. The antibodies were derived either by hybridoma generation (Hybridoma) or phage display technology (Phage). Isotype of the hybridoma derived antibodies is stated.

Phage	Hybridoma	Isotype
TIM5-A3	TIM1	IgG1κ
TIM5-A8	TIM7-F10	IgG2bκ
TIM5-B5	TIM9-C2	-
TIM5-B12	TIM9-F9	-
TIM5-C2	TIM9-G6	IgG1κ
TIM5-C3	TIM10-B1	IgG2aκ
TIM5-C5	TIM10-F4	IgG1κ
TIM5-D6	TIM11-A8	IgG2aκ
TIM5-E4	TIM11-B3	IgG1κ
TIM5-E11	TIM11-C1.1	IgG2aκ
TIM5-G8	TIM11-D4	IgG2aκ
TIM5-H11		
SH1689-B12		
SH1689-C3		
SH1689-E12		

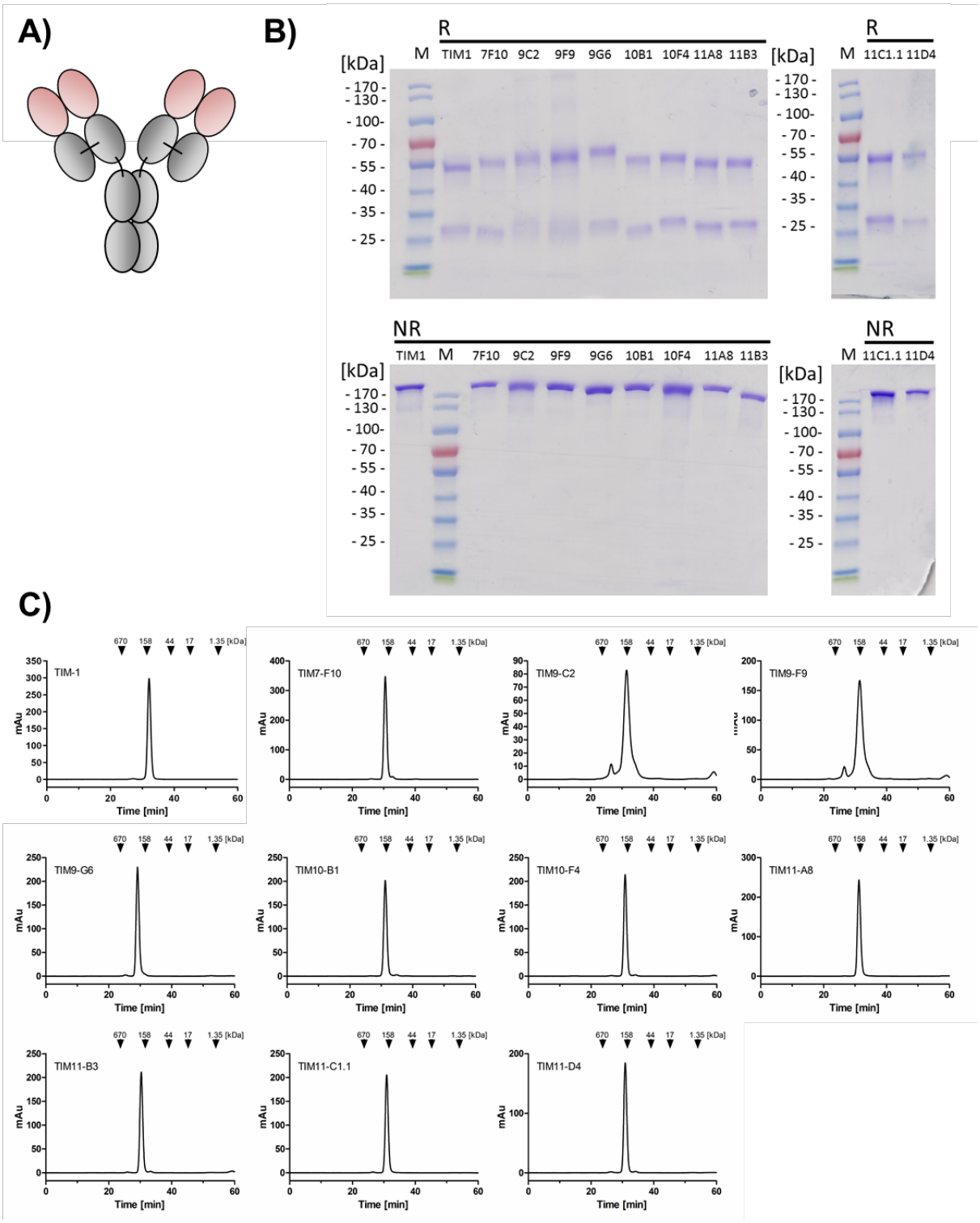

Figure 24: Design and biochemical characterization of different anti-4-1BB IgG clones generated by hybridoma technology. A) Graphical illustration of the anti-4-1BB clones and their **B)** SDS-Page analysis (10 % PAA, 2 µg/lane) under non-reducing (NR) and reducing (R) conditions. Names of the clones were abbreviated for clarification. **C)** Analytical size exclusion chromatography with standard proteins, corresponding molecular masses are indicated by arrows.

The majority of IgGs lacked the presence of any visible aggregates upon analytical size exclusion. However, the results for TIM9-C2 and TIM9-F9 showed the presence of high- and low-molecular-weight aggregates, which were not detectable upon SDS-Page analysis. Nonetheless, all clones were selected for further characterization.

2.2.2 Characterization of anti-4-1BB antibodies

Evaluation of the binding properties of the different hybridoma generated antibodies was done by flow cytometry in three independent experiments, each represented by a single graph (Figure 25). All molecules showed concentration-dependent binding to cell surface-expressed 4-1BB on stably transfected SP2/0 cells with EC_{50} values ranging from 0.07 nM for TIM10-F4 to 54.21 nM for TIM9-C2.

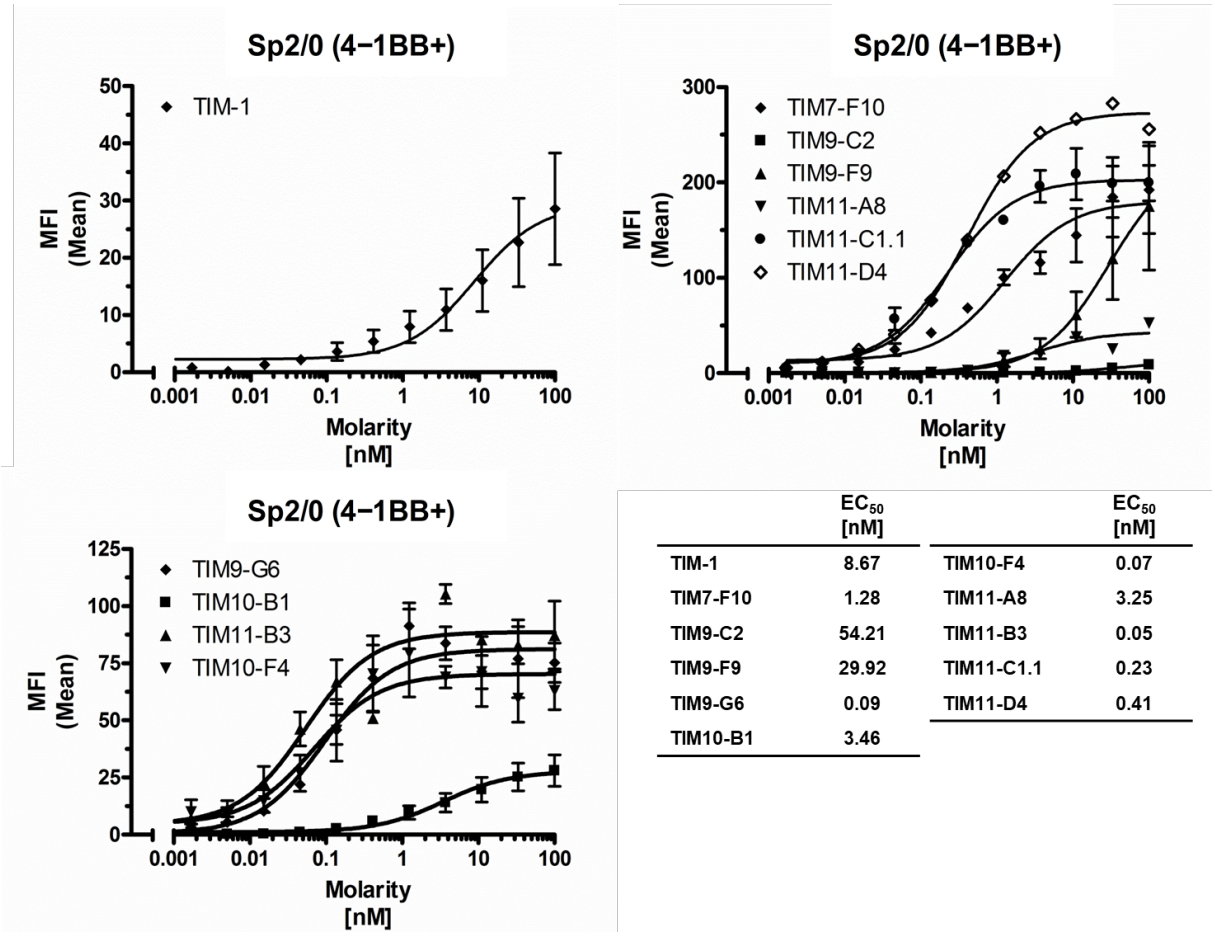

	EC_{50} [nM]		EC_{50} [nM]
TIM-1	8.67	TIM10-F4	0.07
TIM7-F10	1.28	TIM11-A8	3.25
TIM9-C2	54.21	TIM11-B3	0.05
TIM9-F9	29.92	TIM11-C1.1	0.23
TIM9-G6	0.09	TIM11-D4	0.41
TIM10-B1	3.46		

Figure 25: Binding of hybridoma derived antibodies to cell-bound 4-1BB. Binding was analyzed by flow cytometry in three indipendent experiments, each represented by one graph. EC_{50} values were calculated using the Prism software. Mean ± SD, n≥3.

However, a precise determination of the half-maximum binding was not possible for the clones TIM9-C2 and TIM9-F9 for saturation was not reached at 100 nM. Also, it must be pointed out that the clones TIM9-C2, TIM10-B1, and TIM11-A8 did show a substantial lower plateau level questioning their specific binding to 4-1BB. Comparable binding curves were determined for the phage display derived antibodies by Julian Weischedel [254], and their respective half-maximum binding concentrations are listed in Table 3 together with the EC_{50} values determined for hybridoma generated antibodies.

Table 3 List of anti-4-1BB binding clones. The clones were derived by either hybridoma generation (Hybridoma) or phage display technology (Phage). The half-maximum binding was assessed by flow cytometry. Phage display derived antibodies were analyzed in the work of Julian Weischedel [254].

Hybridoma	**EC_{50} [nM]**	**Phage**	**EC_{50} [nM]**
TIM1	8.67	TIM5-A3	0.26
TIM7-F10	1.28	TIM5-A8	1.25
TIM9-C2	54.21	TIM5-B5	0.88
TIM9-F9	29.92	TIM5-B12	0.18
TIM9-G6	0.09	TIM5-C2	0.25
TIM10-B1	3.46	TIM5-C3	0.46
TIM10-F4	0.07	TIM5-C5	0.88
TIM11-A8	3.25	TIM5-D6	0.65
TIM11-B3	0.05	TIM5-E4	0.56
TIM11-C1.1	0.23	TIM5-E11	0.67
TIM11-D4	0.41	TIM5-G8	0.46
		TIM5-H11	1.62
		SH1689-B12	0.45
		SH1689-C3	0.37
		SH1689-E12	0.24

Epitope characterization of hybridoma generated antibodies was assessed by ELISA experiments, as depicted in Figure 26. The binding towards complete 4-1BB-Fc fusion protein was compared with truncated versions lacking cysteine-rich regions as depicted in Figure 26 A. The integrity of the fusion proteins was assessed via SDS-Page (Data not shown). No binding was detected towards ΔCys1-2 4-1BB-Fc for any of the clones. These results question the integrity of ΔCys1-2 4-1BB-Fc. Nonetheless, the epitope characterization led to the identification of three groups. The first one consists of TIM-1, TIM9-G6, TIM10-F4, TIM11-B3, TIM11-D4, and TIM11-C1.1. Besides the binding to ΔCys3-4 4-1BB-Fc they bound the intact 4-1BB-Fc fusion protein, which indicates a binding towards either Cys1 or Cys2 of 4-1BB. The results of the clones TIM10-B1 and TIM11-A8 indicate binding towards Cys4, assuming not fully functional ΔCys1-2 4-1BB-Fc. TIM7-F10 and TIM9-F9 demonstrated no binding to any of the 4-1BB fusion protein variants. Diminished binding of TIM7-F10 and TIM9-F9 to the fusion protein correlates to the results of flow cytometry experiments (Figure 25).

Results of the epitope characterization are summarized in Table 4 together with the data for the phage display generated antibodies analyzed in the work of Julian Weischedel [254]. Taken together, the results obtained with the hybridoma derived antibodies in this work demonstrated a tendency of binding to Cys1 of 4-1BB, while the epitopes of the phage display derived antibodies are distributed across all Cys domains of 4-1BB.

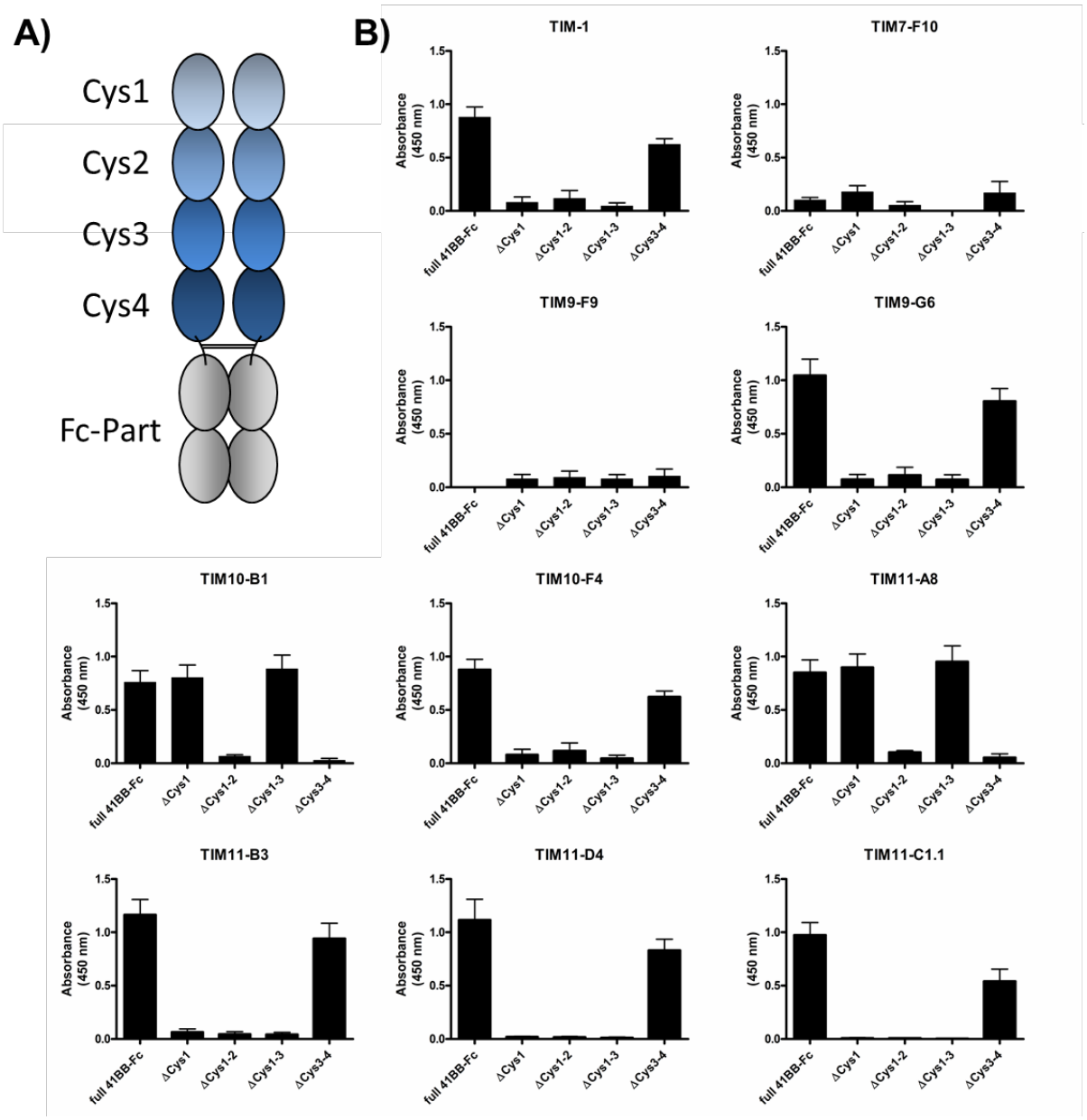

Figure 26: Epitope characterization of hybridoma derived 4-1BB specific antibodies. Binding was assessed by enzyme-linked immunesorbent assay (ELISA) experiments towards truncated 4-1BB fusion proteins. **A)** Graphical illustration of the complete 4-1BB fusion protein with cysteine rich domains (Cys) and Fc-part indicated. **B)** Binding towards 1 µg/ml complete immobilized fusion protein or a truncated vairant. Experiments were performed in cooperation with Julian Weischedel. Mean ± SD, n≥3.

Table 4 List of anti-4-1BB binding clones and their respective epitope. The clones were derived by either hybridoma generation (Hybridoma) or phage display technology (Phage). Epitope characterization was done by ELISA study using truncated 4-1BB-Fc fusion proteins (Figure 26). Phage display derived antibodies were analyzed in the work of Julian Weischedel [254].

Hybridoma	estimated epitope	Phage	estimated Epitope
TIM1	1	TIM5-A3	1
TIM7-F10	-	TIM5-A8	2+3
TIM9-C2	4	TIM5-B5	2+3
TIM9-F9	-	TIM5-B12	3
TIM9-G6	1	TIM5-C2	2+3
TIM10-B1	4	TIM5-C3	1
TIM10-F4	1	TIM5-C5	2
TIM11-A8	1	TIM5-D6	1
TIM11-B3	1	TIM5-E4	2
TIM11-C1.1	1	TIM5-E11	2+3
TIM11-D4	1	TIM5-G8	1
		TIM5-H11	2
		SH1689-B12	3
		SH1689-C3	1
		SH1689-E12	3

As a next step, the 4-1BB binding clones were analyzed for their *in vitro* potential to induce activation of cell-bound 4-1BB-receptor, and the results are depicted in Figure 27. To this end, a NF-κB luciferase reporter assay was performed, which included a 4-1BB expressing Jurkat reporter cell line. Immobilization of 4-1BB targeting antibodies is known to be required for receptor activation [259, 260]. Therefore, the assay was performed in the presence or absence of FcγRIIB (CD32B) expressing CHO cells to ensure cross-linking of the 4-1BB receptor on the cell surface. Cross-linked 4-1BB receptor leads to the NF-κB mediated expression of a receptor luciferase. Thus, the level of luminescence directly correlates with the activation of 4-1BB. Previous studies have described the mouse IgG1κ 4B4-1 as an agonistic antibody [222]. Therefore, this antibody was included as a positive control together with an scFv-Fc antibody not binding 4-1BB (Ctrl Ab). Similar to the cellular background (cells), the Ctrl Ab had no detectable effect (Figure 27).

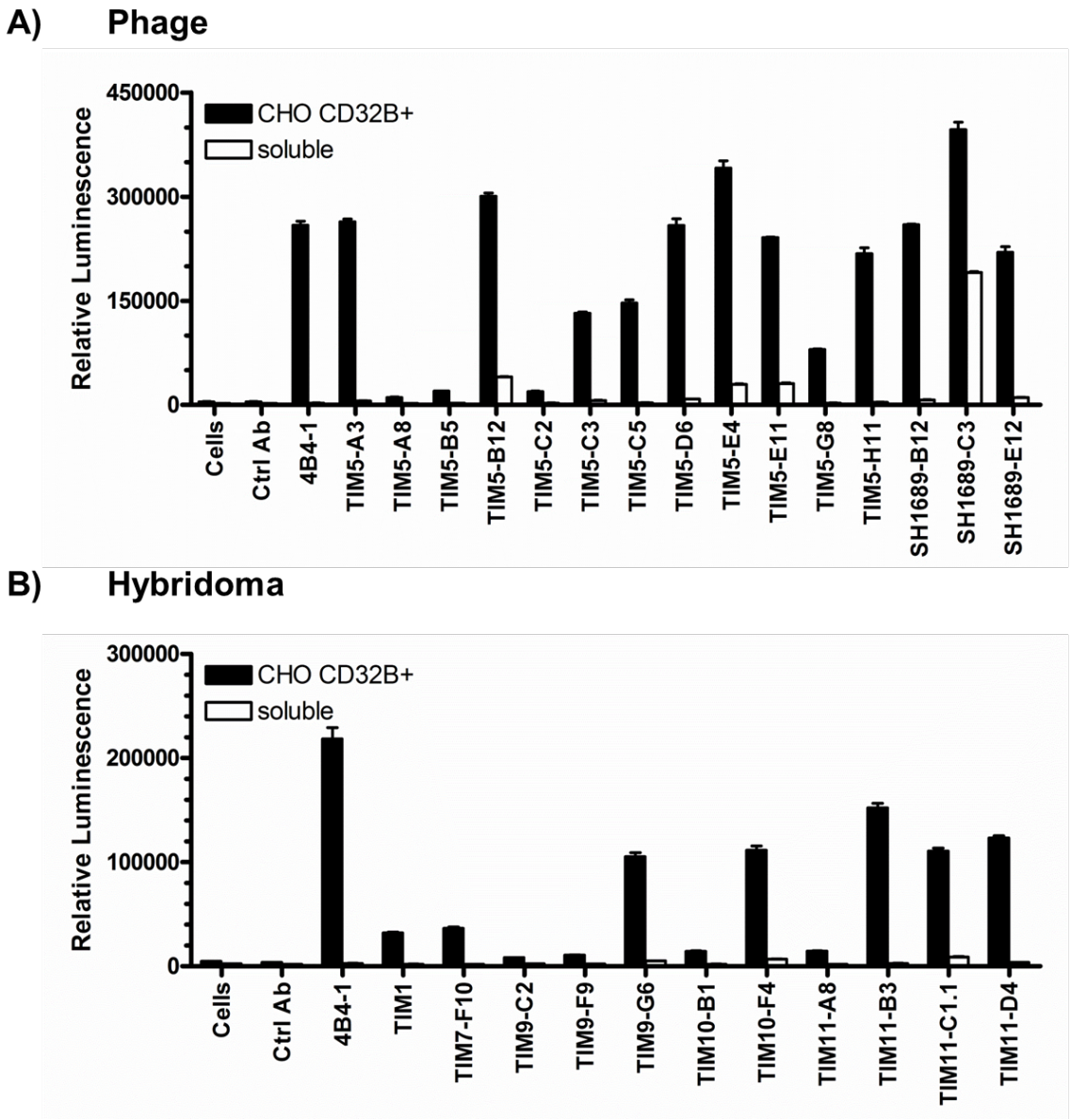

Figure 27: Determination of 4-1BB agonism of different antibody clones. 4-1BB expressing Jurkat effector cells were stimulated for 6 h with 10µg/ml of **A)** phage display derived (Phage) antibodies in scFv-Fc format or **B)** hybridoma derived (Hybridoma) IgG antibodies. Antibodies were crosslinked on CD32b expressing CHO cells (black) or added soluble to the assay (white). Agonistic IgG 4B4-1 and an unspecific IgG antibody (Ctrl Ab) were added as a control. Data generated in cooperation with Julian Weischedel.

The clone 4B4-1 induced a strong level of luminescence when cross-linked on CHO FcγRIIb cells but not in soluble co-cultivation. Of all antibodies assessed, the only antibody inducing luminescence without the presence of FcγRIIB expressing CHO was SH1689-C3. Hybridoma derived clones induced an overall 2-3 times lower luminescence in comparison to the phage display derived antibodies.

The hybridoma derived clones TIM9-C2, TIM10-B1, and TIM11-A8 lack an agonistic effect. These results are in accordance with the previous analysis and can be explained by their inferior binding to 4-1BB. Surprisingly, the presence of aggregates did not induce unspecific 4-1BB activation of TIM9-C2 and TIM9-F9.

In this experiment, 4-1BB targeted agonism was defined at an induced luminescence of at least 50,000 counts. By this definition, 17 clones were identified as agonistic antibodies and these are listed in Table 5. Isotype of the hybridoma derived antibodies did not predict nor limit agonistic properties of the hybridoma derived antibodies. The epitope of 13 was either located in Cys1 or Cys2 domain of 4-1BB.

Table 5: List of identified agonistic anti-4-1BB binding clones. The function was assessed by luciferase reporter assay (Figure 27). Antibodies are either hybridoma generation (Hybridoma) or phage display technology (Phage) derived.

Hybridoma	Phage
TIM9-G6	SH1689-B12
TIM10-F4	SH1689-C3
TIM11-B3	SH1689-E12
TIM11-C1.1	TIM5-A3
TIM11-D4	TIM5-B12
	TIM5-C3
	TIM5-C5
	TIM5-D6
	TIM5-E4
	TIM5-E11
	TIM5-G8
	TIM5-H11

2.2.3 Generation of bispecific 4-1BB binding clones in the Hc+L format.

Nearly all agonistic antibody clones previously identified required to cross-linking via FcγRIIB in order to induce a 4-1BB activation. The requirement of cross-linking was previously described in the literature [141, 143]. All agonistic antibodies identified were selected for the use in the IgG(scFv)$_2$ Hc+L format and endoglin was used as target antigen. The addition of a linker was expected to increase the flexibility of the scFv, resulting in a higher probability of maintaining the agonistic properties of the 4-1BB clones identified in previous experiments (Table 5). For the design of bispecific antibodies, phage display derived antibodies were selected as for the sequencing of the hybridoma generated agonists were not finished at the time of the experiments. The cloning of TIM5-E4 in the IgG(scFv)$_2$ Hc+L did fail and therefore, this clone was cloned and produced in IgG(scFv)$_2$ Hc-L format. Protein integrity was validated via SDS-Page (Figure 28 C) and SEC (Figure 28 D). The results of the biochemical analysis led to results similar to those described in 2.1.1.

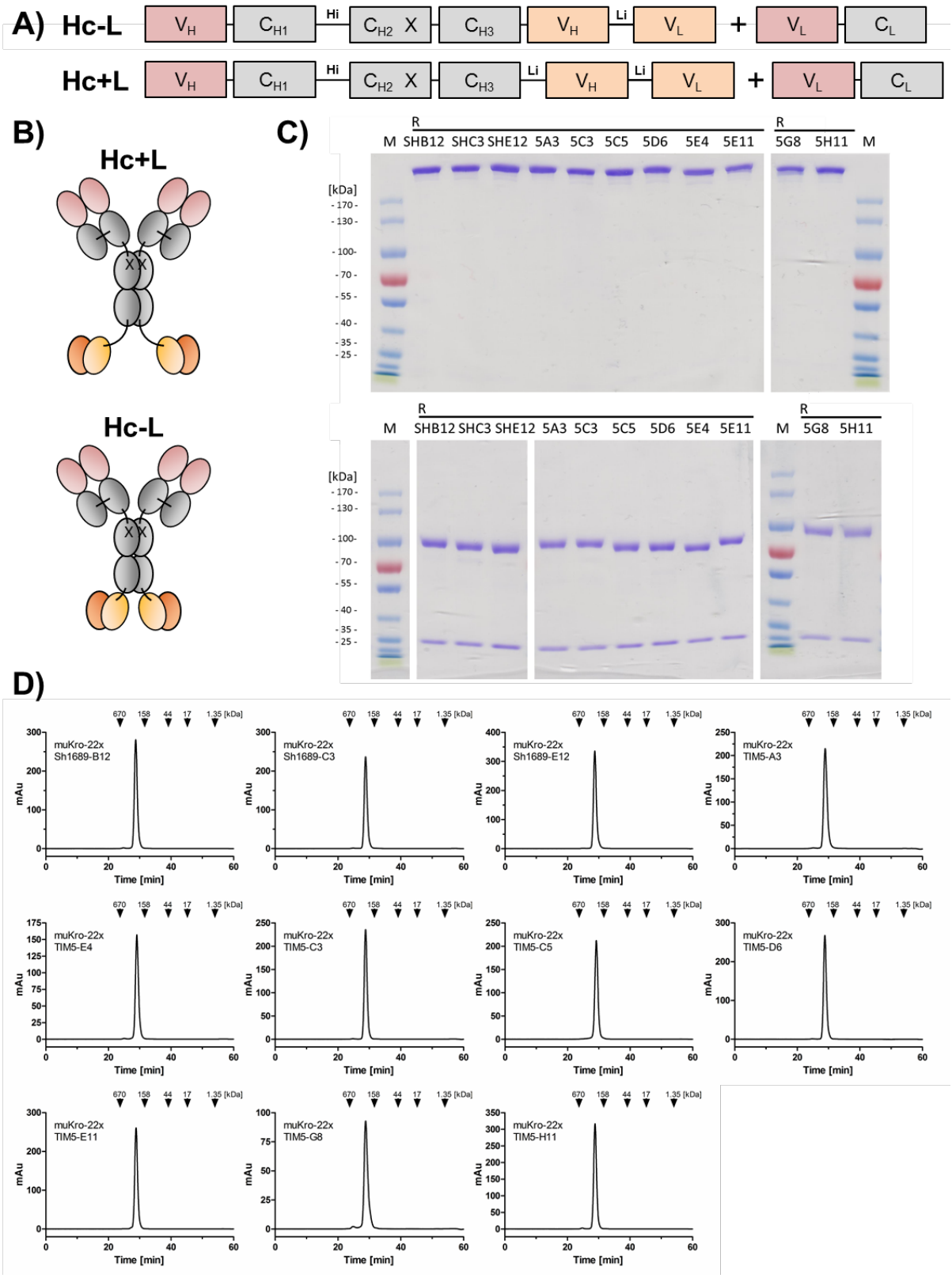

Figure 28: Design and biochemical characterization of different endoglinx4-1BB variants in the Hc+L format. A) Illustration of the genotype of different endoglinxmu9.3 IgG(scFv)$_2$ variants with hinge (Hi) and glycine-serin linker (Li) and the respective **B)** graphical illustration. **C)** SDS-Page analysis (10 % PAA, 2 µg/lane) of purified antibodies under non-reducing (NR) and reducing (R) conditions. **D)** Analytical size exclusion chromatography with standard proteins and their corresponding molecular masses indicated with arrows. Format named according to Figure 6 B.

Binding to cell-bound 4-1BB and endoglin was assessed by flow cytometry. Bispecific antibodies bound to 4-1BB with a half-maximum binding of 0.87 nM to 27.12 nM (Figure 29 A). Comparing the EC_{50} values to that depicted in Table 3 demonstrated an increase of up to 10-fold for nearly all selected clones in the scFv-Fc format, excluding TIM5-E11 (28.8-fold increase) and TIM5-G8 (58.9-fold increase).

In contrast to the binding to 4-1BB, the evaluation of the binding to endoglin showed a half-maximum binding of around 0.06 nM for all clones (Figure 29 B), resembling earlier described antibodies containing the mouse clone Kro-22.

In summary, these results demonstrated a loss of affinity for all 4-1BB specific clones upon re-formatting into the IgG(scFv)$_2$ HC+L format while the affinity of the mouse Kro-22 antibody remained intact in all antibodies.

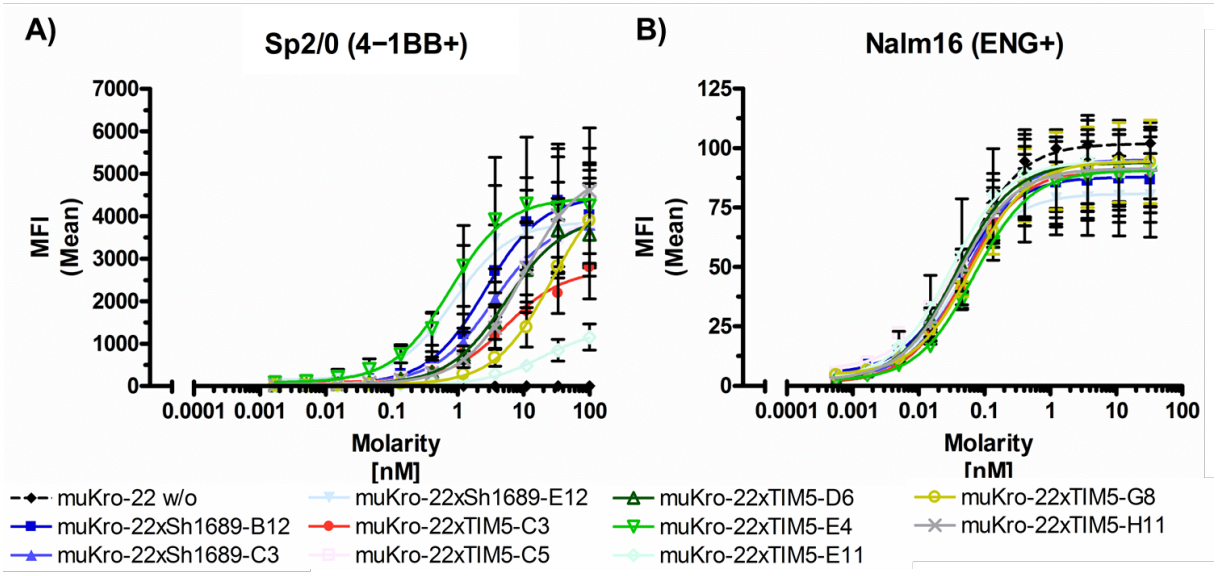

	EC_{50} [nM]
muKro22 w/o	-
muKro22xSH1689-B12	2.64
muKro22xSH1689-E12	0.87
muKro22xSH1689-C3	3.44
muKro22xTIM5-C3	5.40
muKro22xTIM5-C5	5.27
muKro22xTIM5-D6	5.45
muKro22xTIM5-E4	0.77
muKro22xTIM5-E11	19.30
muKro22xTIM5-G8	27.12
muKro22xTIM5-H11	9.48

	EC_{50} [nM]
muKro22 w/o	0.05
muKro22xSH1689-B12	0.04
muKro22xSH1689-E12	0.04
muKro22xSH1689-C3	0.05
muKro22xTIM5-C3	0.05
muKro22xTIM5-C5	0.04
muKro22xTIM5-D6	0.04
muKro22xTIM5-E4	0.07
muKro22xTIM5-E11	0.03
muKro22xTIM5-G8	0.06
muKro22xTIM5-H11	0.04

Figure 29: Antigen binding of IgG(scFv)$_2$ endoglinx4-1BB variants in Hc+L format. Antigen binding of cell surface-expressed **A)** 4-1BB on transfected Sp2/0 cells and **B)** endoglin on Nalm16 cells. The binding was analyzed by flow cytometry. Mean ± SD, n≥3. Format named according to Figure 6 B

Changing the format might not only affect the binding towards its antigen but might also alter the agonistic characteristics of a clone. The potential capabilities of the bispecific antibodies to activate cell-bound 4-1BB was again analyzed using of the NF-κB luciferase reporter assay (Figure 30). The antigen-dependent agonism was assessed by exchanging FcγRIIB expressing CHO, which were used in previous experiments (Figure 30), with endoglin expressing LN-18 cells. Immobilization of the bispecific antibodies towards LN-18 was assumed to result in a cross-linking of 4-1BB and its activation. Successful clustering of the 4-1BB receptor on the surface of the Jurkat cells is induces NF-kB mediated expression of luciferase, which can be detected by an increased level of luminescence.

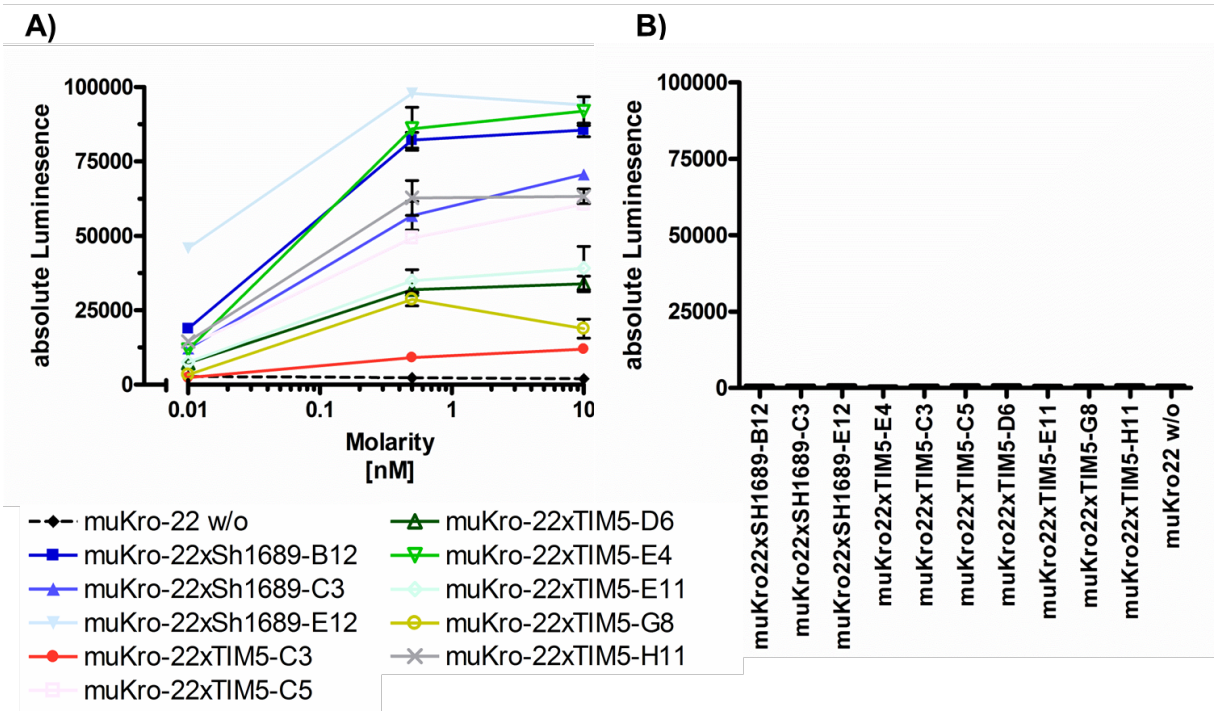

Figure 30: 4-1BB agonism of different antibody clones in IgG(scFv)$_2$ Hc+L format. 4-1BB expressing Jurkat effector cells were stimulated for 6 h with a titration of phage display derived antibodies in IgG(scFv)$_2$ Hc+L format. Antibodies were **A)** immobilized via their binding to LN-18 cells or added **B)** soluble with 10 nM to the assay. Format named according to Figure 6 B.

The Kro-22 IgG (w/o) was used as a control for it is lacking a 4-1BB binding moiety. No induction of luminescence could be observed for any of the clones without the presence of LN-18 cells (Figure 30 B). These results are consistent with the previously acquired results obtained with the scFv-Fc format (Figure 27). All bispecific antibodies, except the control antibody w/o, showed a dose-dependent induction of luminescence when being immobilized on LN-18 cell at concentrations as low as 0.01 nM (Figure 30 A). However, differences in the maximally induced luminescence were detectable. The SH1689-B12, SH1689-C3, SH1689-E12, and TIM5-E4 induced the highest level of 4-1BB activation with a luminescence of up to 9-fold higher compared to the weakest induction by TIM5-C3 and TIM5-G8. These results are consistent with the previous results obtained with the scFv-Fc format (Figure 27). In addition, the extent of 4-1BB activation correlates with the affinity of the analyzed antibodies. These findings demonstrate that all agonistic 4-1BB antibodies facilitate an endoglin dependent activation of the 4-1BB pathway.

To investigate whether the bispecific 4-1BB antibodies can be used for an effective stimulation of human T cells, a culture assay including such cells and endoglin expressing LN-18 cells was developed. Human T cells were stimulated via an immobilized anti-CD3 stimulus in the presence of bispecific 4-1BB antibodies were added. The clones SH1689-B12 , SH1689-C3, SH1689-E12, and TIM5-E4 demonstrated the strongest activation of 4-1BB in the initial assessment *via* luciferase reporter assay (Figure 30) and were selected for this type of analysis.

Without the presence of the anti-CD3 stimulus, no proliferation was detected (Figure 31 B). However, all bispecific antibodies selected for this assay regained agonism in a dose-dependent matter in co-incubation with an anti-CD3 stimulus, starting at a concentration of 0.01 nM. In contrast to earlier experiments, SH1689-C3 did demonstrate a 100-fold lower dose-dependent [^{3}H]-thymidine incorporation, and a 0.75-fold lower plateau level.

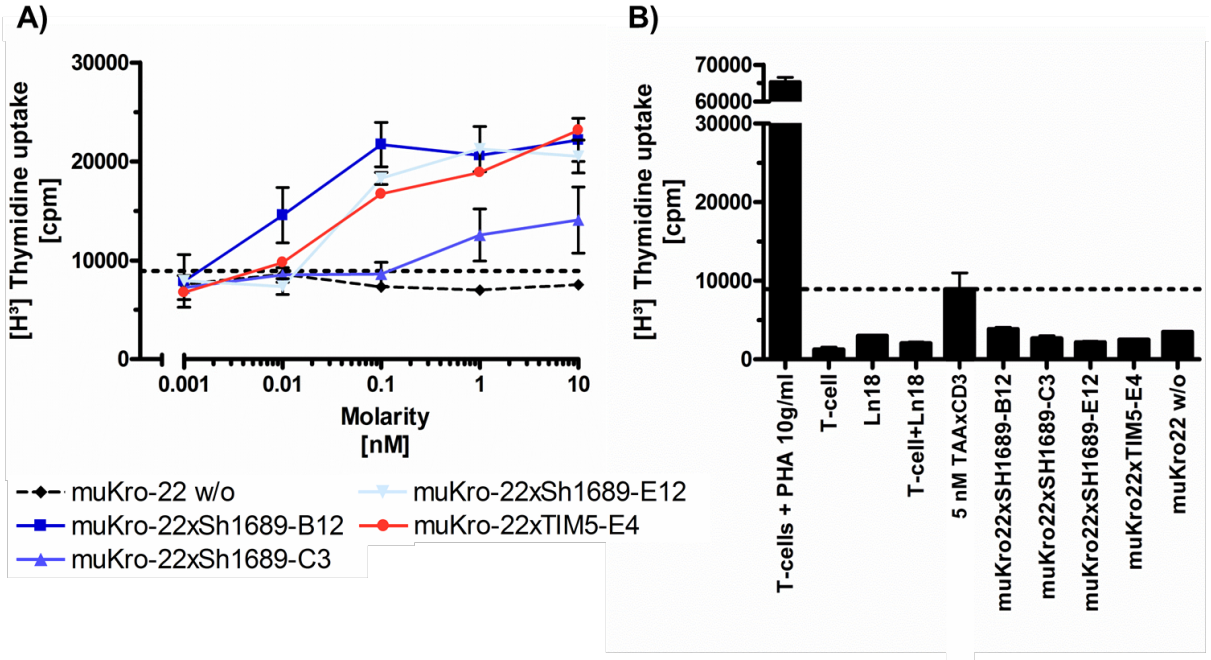

Figure 31: Proliferation of purified T cells in thepresence of different endoglinx4-1BB binding clones in Hc-L format. A total of 30,000 LN-18 cells/well, together with 100;000 purified T cells/well, were incubated for 48 h. Cells and bispecific endoglinx4-1BB antibodies in Hc+L format were incubated in presence of 5 nM of immobilized anti-CD3 stimulus with **A)** different antibody concentrations or **B)** without anti-CD3 stimulus with 10 nM. In addition, cells were pulsed with [methyl-^{3}H]-thymidine for 17 h. Mean ± SD, n≥3 for three individual Donors. Format named according to Figure 6 B.

To summarize these findings, the clones SH1689-B12, SH1689-E12, and TIM5-E4 proved to induce 4-1BB activation not only in a monospecific scFv-Fc format but also in the bispecific IgG(ScFv)$_2$ Hc+L format. This data confirms the necessity of target cell restricted endoglin mediated immobilization to facilitate an effective 4-1BB mediated T cell costimulation.

In addition to their potential of specifically providing T cell costimulation, the bispecific endoglinx4-1BB variants were analyzed in their potential to enhance a TAAxCD3-mediated tumor cell killing using a real-time and long-term xCelligence assay. The results are shown in Figure 32. TIM5-E4, SH1689-B12, and SH1689-E12 were capable of enhancing the TAAxCD3-mediated lysis of LN-18 cells, whereas SH1689-C3 was much weaker, the controls were negative.

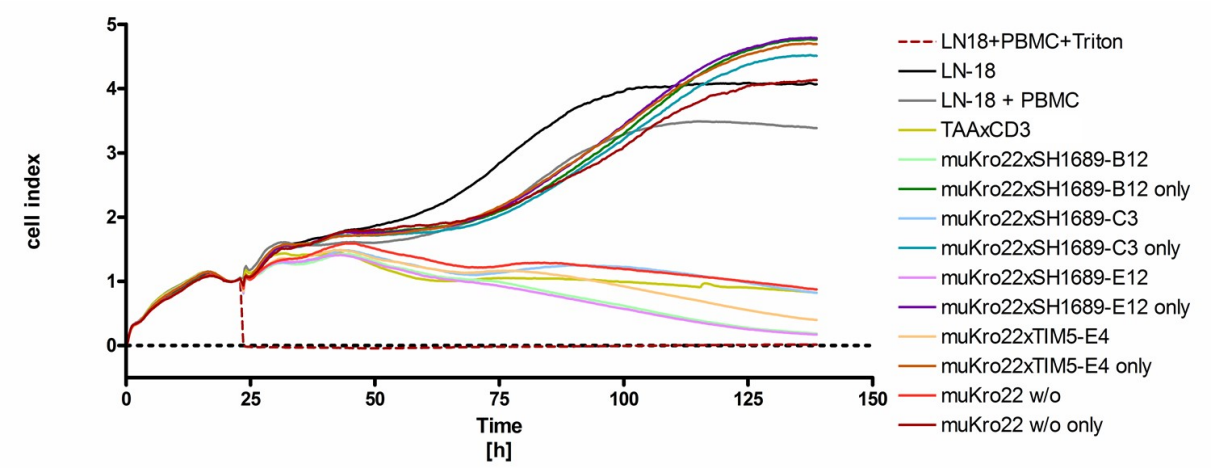

Figure 32: Tumor cell lysis induced of TAAxCD3 and IgG(scFv)$_2$ Lc-L muKro22x4-1BB on LN-18 cells. A total of 20.000 LN-18 cells were seeded per well. After a 24 h preincubation 20.000 PBMCs per well were added and treated with eiter 5 nM of TAAxCD3 (yellow), 5 nM IgG muKro22 (red, solid line), or a combination of 5 nM TAAxCD3 with 5 nM of IgG(scFv)$_2$ Hc+L muKro22x4-1BB. Lysed cells were analyzed by the xCelligence system. One representative experiment out of two with mean values of triplicates are shown.

2.3 Development of endoglinxPD-1 bispecific antibody

2.3.1 Antibody generation

The generation of all PD-1 binding antibodies was performed again via hybridoma generation and phage display technology, and all clones are listed in Table 6 together with their respective isotype.

Table 6: List of PD-1 binding antibodies. Antibody clones were derived by either hybridoma generation (Hybridoma) or phage display technology (Phage).

Phage	Hybridoma	Isotype
TIM4-A6	TIM9-E6	IgG2aκ (or IgG1κ)
TIM4-B12	TIM10-C1	IgG2bκ
TIM4-C7	TIM11-E12	IgG2bκ
TIM4-D8	TIM11-F3.1	IgG2aκ (or IgG1κ)
TIM4-E6	TIM11-H1	IgG2aκ (or IgG1κ)
TIM4-F4		
TIM4-G1		
TIM4-H8		
TIM4-H11		
TIM4-G4		
SH1716-A1		
SH1716-A3		
SH1716-B2		
SH1716-B4		

For an initial characterization, phage display derived antibodies were produced via transiently transfected CHO cells and hybridoma cultures respectively. After purification *via* protein A affinity chromatography, protein purity and integrity were assessed by SDS-Page analysis and analytical size-exclusion chromatography and the results are shown in Figure 33 and Figure 34. Upon purification, the isotype of the hybridoma derived antibodies was determined and the results are stated in Table 6. The results of TIM4-A6, TIM-D8, and TIM-E6 were not clear cut for the presence of a slight background for IgG1κ.

Phage display antibodies were produced in the scFv-Fc format, as depicted in Figure 33 A. The purity of the clones was validated by SDS-Page analysis. The scFv-Fc format comprises a scFv covalently linked with a human Fc-part. Thus, the homodimer has an expected size of approximately 110 kDa. Lanes resembling the expected size in reducing and non-reducing conditions were visible in the SDS-Page analysis in Figure 33 B. secondary bands were visible for some of the clones analyzed, clearly indicating the presence of aggregates.

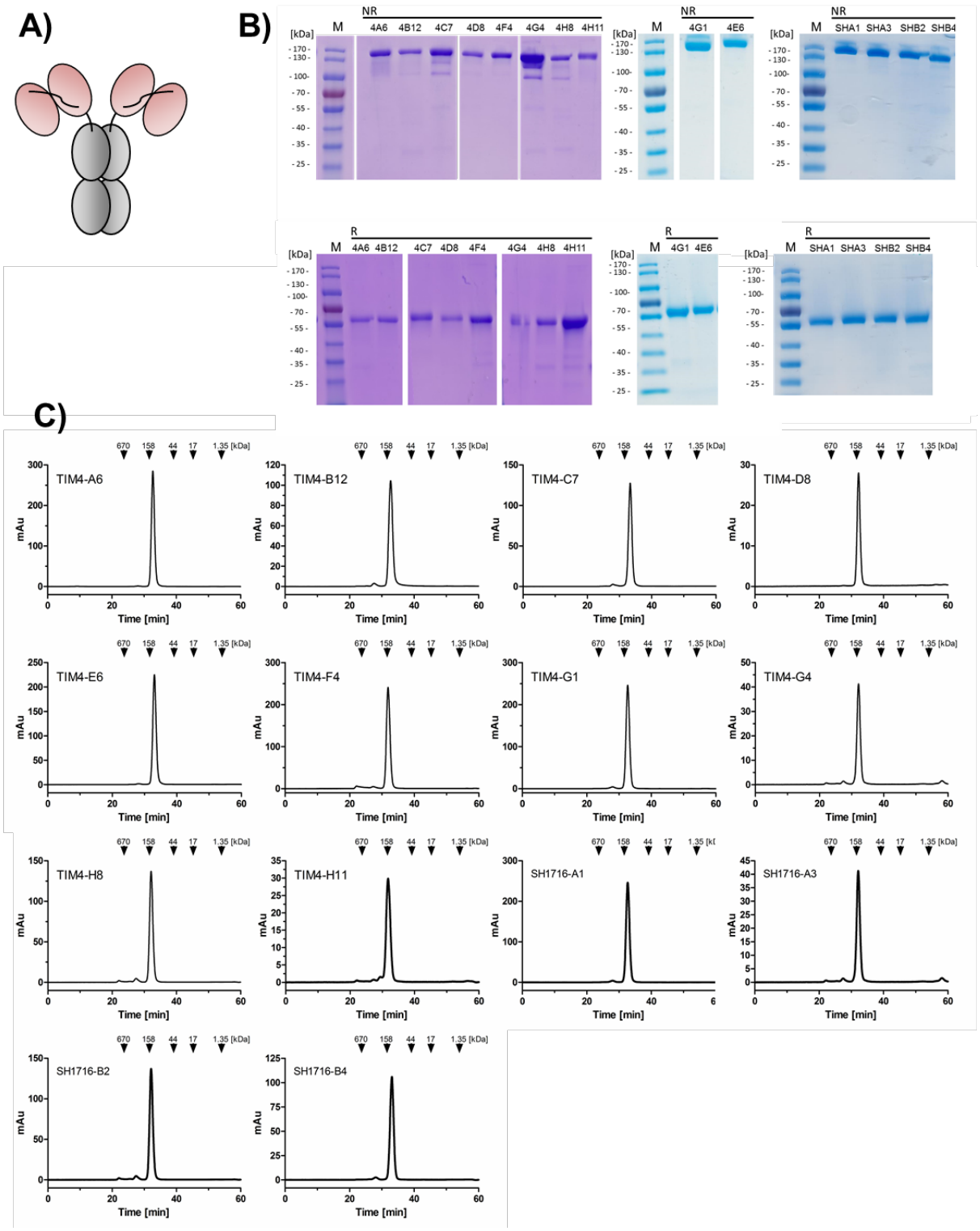

Figure 33: Design and biochemical characterization of different phage display derived PD-1 clones. A) Graphical illustration of the scFv-Fc format. **B)** SDS-Page analysis (10 % PAA, 2 µg/lane) of purified antibodies under non-reducing (NR) and reducing (R) conditions. **C)** Analytical size exclusion chromatography with standard proteins and their corresponding molecular masses indicated with arrows.

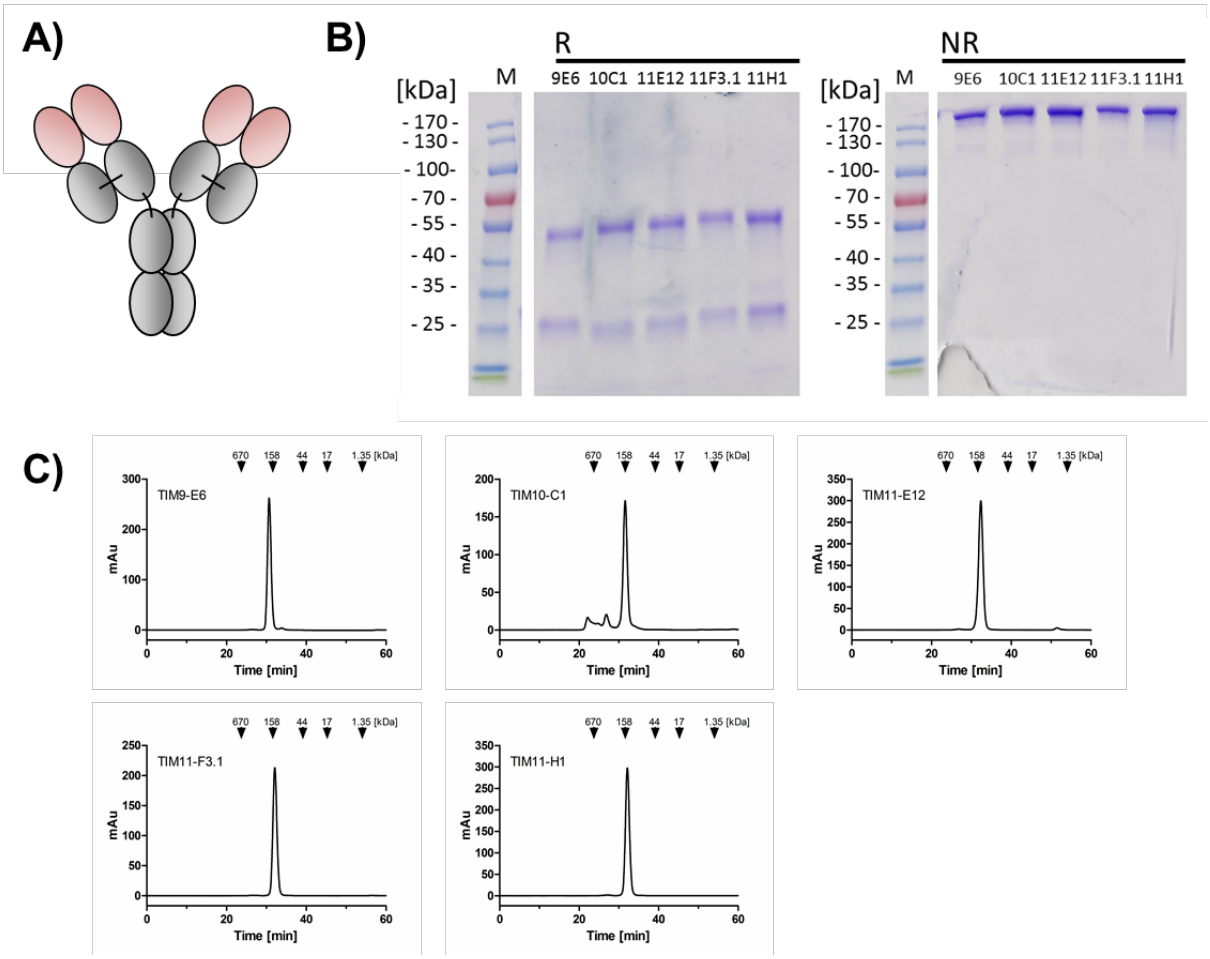

Figure 34: Design and biochemical characterization of different PD-1 clones generated *via* hybridoma generation. A) Graphical illustration of the IgG. **B)** SDS-Page analysis (10 % PAA, 2 µg/lane) of purified antibodies under non-reducing (NR) and reducing (R) conditions. **C)** Analytical size exclusion chromatography with standard proteins and their corresponding molecular masses indicated with arrows.

The results of the SDS-Page correlate with the results of the analytical SEC in Figure 33 C. Overal integrity and purity of all antibodies could be proven by a single peak at the estimated size of about 120 kDa. Nonetheless, similar to SDS-Page analysis, small amounts of high low molecular weight aggregates were visible in the SEC analysis.

The binding of the novel anti-PD-1 antibodies to cell-bound PD-1 was investigated via flow cytometry experiments and the results are depicted in Figure 35. All clones were found to bind to PD-1 expressing SP2/0 cells (Figure 35 A and Figure 35 B). EC_{50} values range in between 0.11 nM to 107.5 nM (Figure 35 C) for cell surface-expressed PD-1. In comparison with the clinical IgG Pembrolizumab (EC_{50} = 1.04 nM) and Nivolumab (EC_{50} = 1.42 nM) (Figure S 1), it became clear that the hybridoma derived antibodies demonstrated similar or higher affinity than the phage display derived antibodies.

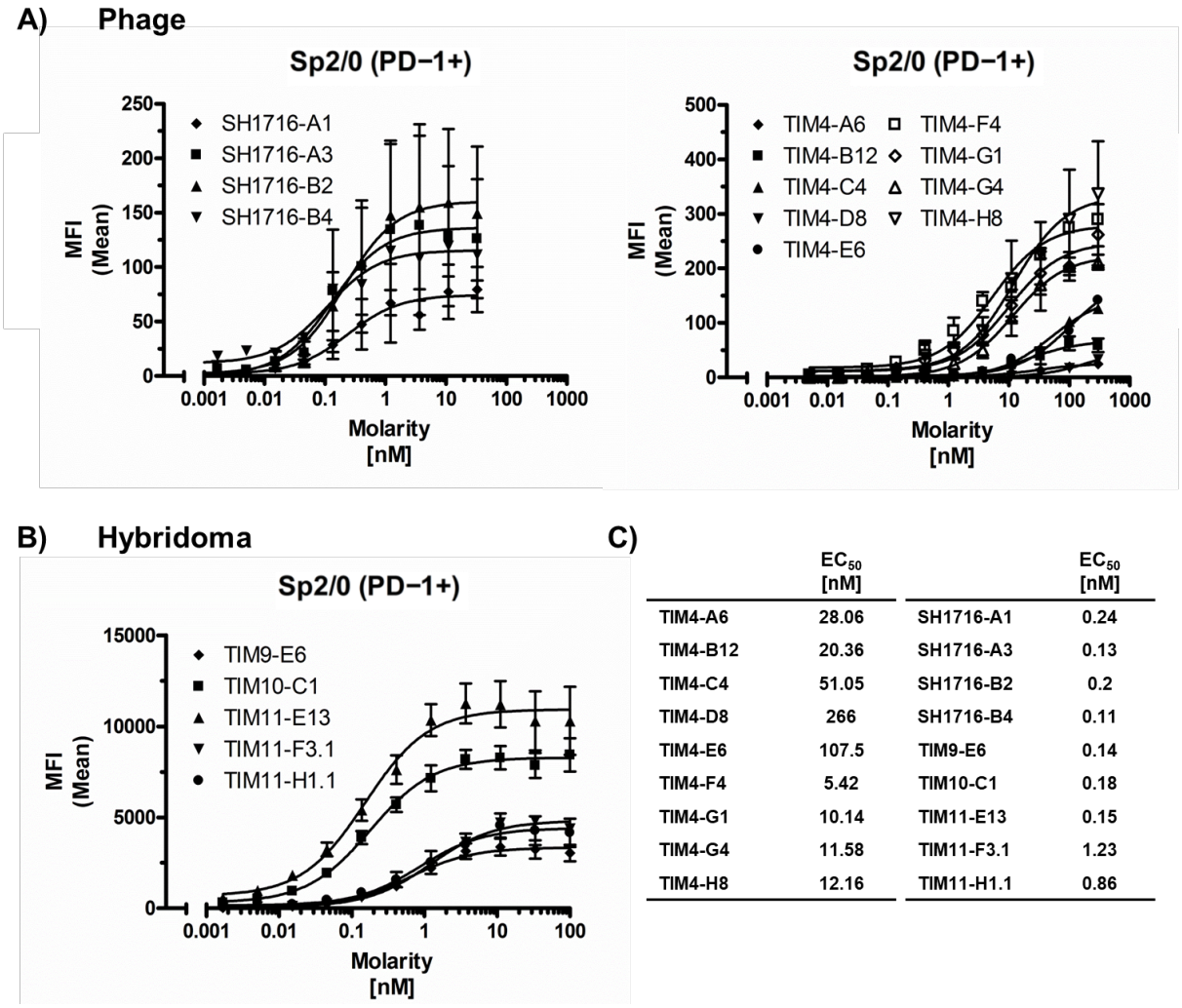

	EC_{50} [nM]		EC_{50} [nM]
TIM4-A6	28.06	SH1716-A1	0.24
TIM4-B12	20.36	SH1716-A3	0.13
TIM4-C4	51.05	SH1716-B2	0.2
TIM4-D8	266	SH1716-B4	0.11
TIM4-E6	107.5	TIM9-E6	0.14
TIM4-F4	5.42	TIM10-C1	0.18
TIM4-G1	10.14	TIM11-E13	0.15
TIM4-G4	11.58	TIM11-F3.1	1.23
TIM4-H8	12.16	TIM11-H1.1	0.86

Figure 35: Binding analysis of different anti-PD-1 IgG antibodies to cell-bound PD-1. Antigen binding of **A)** phagedisplay derived (Phage) and **B)** hybridoma derived (Hybridoma) antibody clones to cell surface-expressed PD-1 transfected Sp2/0 cells. The binding was analyzed by flow cytometry. With their respective **C)** half-maximum binding. Mean ± SD, n≥3.

2.3.2 Functional characterization of anti-PD-1antibodies

Blocking the interaction of the receptor PD-1 with its ligands PD-L1 and PD-L2 are required to diminish the inhibitory effect onto T cells. Evaluation of the functional inhibitory effect of the anti-PD-1 generated antibodies was assessed using a reporter cell assay (Figure 36). A PD-1 expressing Jurkat reporter cell line was co-cultured with a CHO effector cell line expressing either PD-L1 or PD-L2 and a TCR stimulating moiety. Activation of the TCR mediates the expression of a NFAT mediated luciferase in the reporter cell line. Binding of PD-L1 or PD-L2 towards their receptor PD-1 results in the inhibition of the TCR signaling and thus, a diminished induction of NFAT expression. The total level of measured luminescence indicates, therefore, indicates the degree of PD-1 blockade.

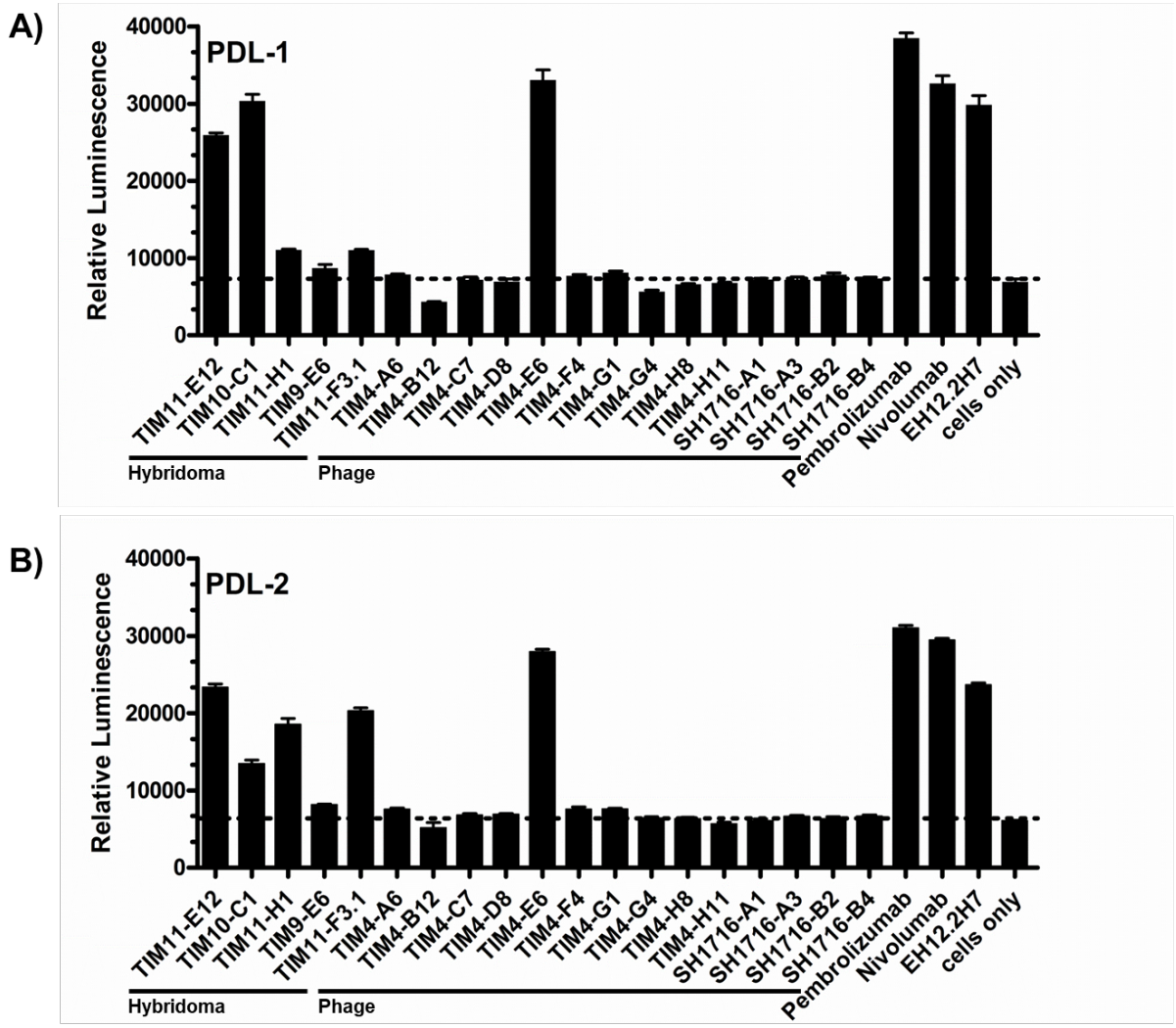

Figure 36: Validation of PD-1 antagonism of different anti-PD-1 clones. PD-1 expressing Jurkat effector cells were stimulated for 6 h with 10 µg/ml of anti-PD-1 antibodies which are either hybridoma derived (Hybridoma) or phage display derived (Phage). Cultivation was performed in presence of either **A)** PD-L1 or **B)** PD-L2 expressing CHO bystander cells. Antagonsitic IgG Nivolumab, Pembrolizumab, EH12.2H7 were added as a control. Data generated in cooperation with Julian Weischedel.

Co-incubation of the reporter cell line in the presence of the effector cell line led to an inhibition of the signal via the ligation of PD-1 with its ligand and was therefore defined as the cellular background (cells only). The anti-PD-1 clones EH12.2H7, Pembrolizumab, and Nivolumab were chosen as controls for they are described as ligand blocking antibodies in the literature [220, 226, 261]. By adding these control antibodies the recovery of luminescence signal in the co-culture of either PD-L1 (Figure 36 A) or PD-L2 (Figure 36 B) expressing effector cells was achieved. Ligand-blocking antibodies were defined by a recovered luminescence value of higher than 10,000. As a result, the functional inhibitory effect of the novel generated antibodies could be assessed for several clones which are listed in Table 7.

Table 7: Antagonistic PD-1 binding antibodies. Antibodies are listed by their capability of blocking the interaction of PD-1 with its ligands PD-L1 and PD-L2

PD-L1 and PD-L2 blocking	exclusive PD-L2 blocking
TIM11-E12	TIM11-H1
TIM10-C1	TIM11-F3.1
TIM4-E6	

As a result of the luciferase reporter assay (Figure 36), the phage display derived clone TIM4-E6 and Pembrolizumab were identified as PD-L1 and PD-L2 blocking antibodies and therefore, these clones were selected for construction of a bispecific endoglinxPD-1 antibody. The PD-L1 and PD-L2 blocking hybridoma antibodies were not yet sequenced at the time of the experiments and could not be selected for a bispecific antibody.

2.3.3 Generation of bispecific endoglinxPD-1 antibodies

For a target cell restricted, rather than systemic PD-1 blockade, bispecific antibodies targeting endoglin and PD-1 were designed to overcome the restrictions of the PD-1 monotherapy in order to prevent systemic side effects. At the time of the experiments, Kro-22 was not yet humanized and therefore, the mouse clone muKro-22 was selected for use. The antibodies TIM4-E6 and Pembrolizumab were selected in the construction of a bispecific antibody. The design of the novel molecules and the results of their biochemical characterization are depicted in Figure 37. Results of the SDS-Page analysis are presented in Figure 37 C together with the analytical size exclusion in Figure 37 D. Under non-reducing conditions, smaller secondary bands were visible in the samples of muKro-22xPembrolizumab. These aggregates were also visible in size exclusion analysis proving the presence of a small amount of high molecular weight aggregates. Nonetheless, these small amounts of aggregates were neglected in further analysis of the bispecific antibodies.

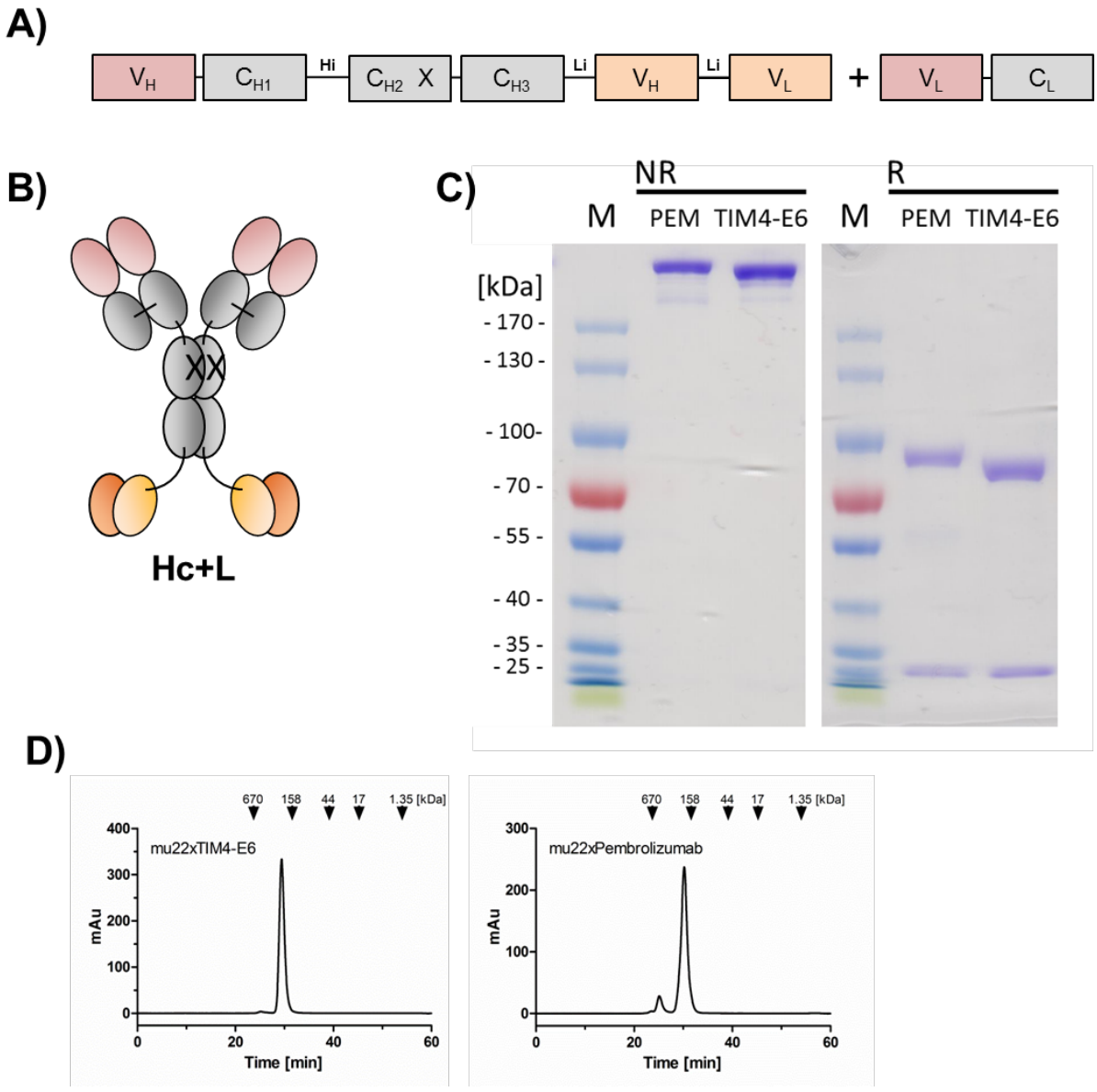

Figure 37: Design and biochemical characterization of different endoglinxPD-1 variants in Hc+L format. A) Illustration of the genotype of different endoglinxPD-1 IgG(scFv)$_2$ variants with hinge (Hi) and glycine-serine linker (Li) consisting out of (Gly-Gly-Gly-Ser)$_3$ and the respective **B)** graphical illustration. **C)** SDS-Page analysis (10 % PAA, 2 µg/lane) of purified antibodies under non-reducing (NR) and reducing (R) conditions. **D)** Analytical size exclusion chromatography with standard proteins and their corresponding molecular masses indicated with arrows. Format named according to Figure 6 B.

After assessing the protein integrity of the bispecific endoglinxPD-1 antibodies, binding towards cellular expressed antigen was analyzed and the results are shown in Figure 38. Half maximum-binding towards endoglin was assessed on Nalm16 cells (Figure 38 B). With an EC_{50} of 0.04 nM and 0.03 nM for the binding towards endoglin of the bispecific antibodies comprising Pembrolizumab or TIM4-E6 with muKro-22. This data resembled previously obtained data with the mouse clone Kro-22.

Binding to PD-1 was analyzed on stably transfected PD-1 expressing Jurkat cells and the results are depicted in Figure 38 A. With an EC_{50} of 17.37 nM, the half-maximum binding of the bispecific muKro-22xTIM4-E6 was 6.2-fold lower when compared to the monospecific scFv-Fc format. Reformatting from IgG into IgG(scFv)$_2$ resulted in a small increased affinity of Pembrolizumab, increasing the EC_{50} from 1.04 nM (Figure S 1)to 0.16 nM (Figure 38 A).

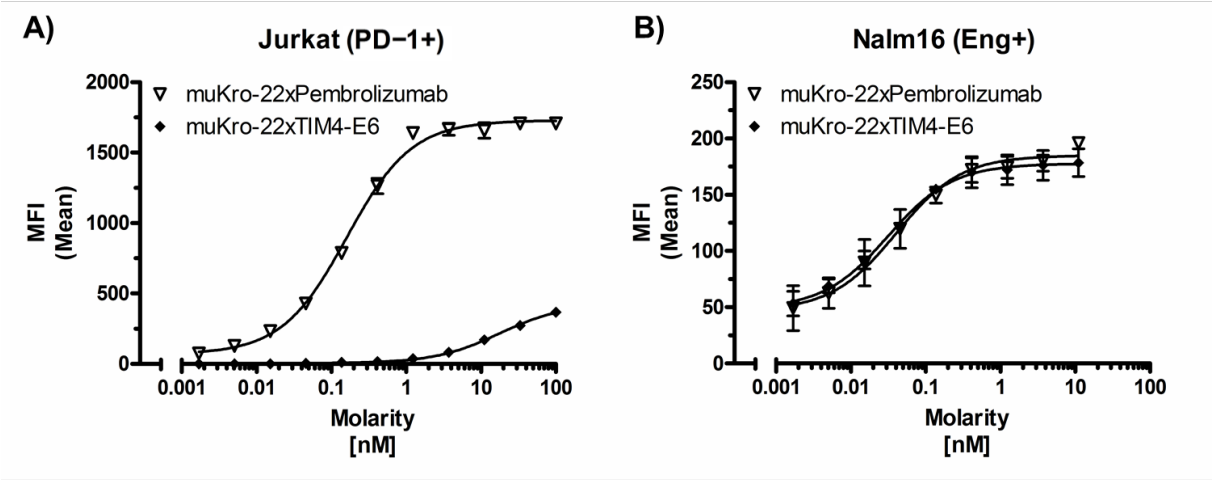

	EC_{50} [nM]
muKro-22xPembrolizumab	0.16
muKro-22xTIM4-E6	17.37

	EC_{50} [nM]
muKro-22xPembrolizumab	0.04
muKro-22xTIM4-E6	0.03

Figure 38: Antigen binding of IgG(scFv)$_2$ endoglinxPD-1 variants in Hc+L format. Antigen binding of cell surface-expressed **A)** PD-1 on transfected Jurkat cells and **B)** endoglin on Nalm16 cells. The binding was analyzed by flow cytometry. Mean ± SD, n≥3. Format named according to Figure 6 B

For functional analysis of the bispecific IgG(scFv)$_2$ format, a luciferase reporter assay was performed and the results a presented in Figure 39. Target cell-specificity analysis was assessed by co-culturing the PD-1 expressing reporter cell line with a PD-L1/endoglin double-positive cell line, LN-18. The two IgG antibodies Pembrolizumab and muKro-22 w/o were used as a control, for they were lacking either endoglin or a PD-1 binding moiety. The initial stimulation of the reporter cell line was archived *via* an immobilized anti-CD3 stimulus (Figure 39 A). Lacking initial TCR stimulation, none of the antibodies appeared to have any effect on the reporter cell line. Both did not induce luminescence (Figure 39 B). Upon initial stimulation with an anti-CD3 stimulus, striking differences between the different variants were visible. Pembrolizumab maintained its PD-1/PD-L1 blocking characteristics not only in the soluble IgG format but also in IgG(scFv)$_2$ format. Thus, indicating a soluble rather than a target-cell specific blockade of the interaction of PD-1 and its ligand.

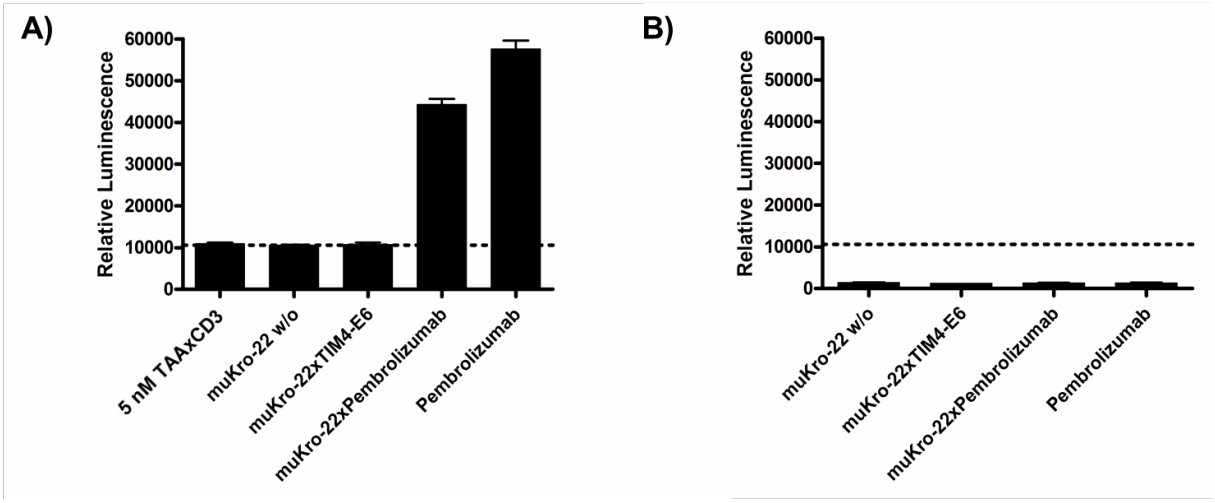

Figure 39: Validation of PD-1 antagonsism of different endoglinxPD-1 clones in IgG(scFv)$_2$ Hc+L format *via* luciferase reporter assay. PD-1 expressing Jurkat effector cells were cultivated for 6 h in the presence of 10 µg/ml of anti-PD-1 antibodies and 30,000 PD-L1 expressing LN-18 bystander cells. Co-culture was performed with **A)** and **B)** without initial stimuation of 5 nM TAAxCD3 antibody. The antagonsitic IgG Pembrolizumab was added as a control as well was the IgG mouse Kro-22 w/o.

When comparing the results of muKro-22xTIM4-E6 with the control IgG muKro-22 w/o, no difference to the PD-1 induced blockade of TAAxCD3 stimulus was present. In the monospecific form, TIM4-E6 blocked the interaction of PD-1 and its ligands. However, it has not lost its blocking function in the bispecific format when it was bound to a target cell.

Nonetheless, the results obtained with the mono- and bispecific variants of Pembrolizumab indicate the general functionality of the assay. A significant lower affinity and a lower plateau-level might contribute to the loss of PD-L1 blockade.

3. Discussion

3.1 General considerations

This thesis presents the study on the generation of novel immunomodulating antibodies directed to the co-stimulatory 4-1BB receptor and co-inhibitory PD-1 receptor. The aim was to restrict the activity of those antibodies as well as that of costimulatory anti-CD28 antibodies to target cells employing bispecific antibodies. A second aim was the selection of a bispecific format that was optimized for this purpose. The exemplary target antigen, selected in this study, was endoglin, because it allows the targeting of tumor vascular cells.

3.2 Development of a bispecific immunomodulating antibody targeting CD28

The selective stimulation of CD28 is one of several attractive strategies for therapeutic T cell stimulation. However, the clinical trial of TGN1412 demonstrated the problematic use of monospecific anti-CD28 superagonists by inducing systemic inflammatory responses in patients [107, 130]. The initial goal of this work was on the identification of an optimal format, to enable a target cell restricted CD28 costimulation with bispecific antibodies.

3.2.1 Evaluation of bispecific antibody formats

A remarkable acceleration in the development of bispecific antibodies came with the development of novel genetic engineering methods, which resulted in the development of an ever-growing number of new bispecific formats [4, 6]. In general, most studies about bispecific antibodies in cancer immunotherapy have only focused on a single format.

In this work, an extensive study was performed on the selection of an optimal format of an endoglinxCD28 bispecific antibody. The format selected was based on the work of Coloma and Morrison [239] in which a scFv of different specificity was fused to the c-terminus of an IgG. By not only fusing the scFv to the heavy and light chain of the IgG but also by the introduction of a linker in between the constant region and the scFv, a total of four different bispecific antibody formats was generated.

The impact of the scFv fusion site on the functionality of a bispecific antibody was initially assessed for IgG(scFv)$_2$ muKro-23x9.3. In general, all variants demonstrated a lower affinity in the binding of the scFv to CD28 than the parental IgG. However, fusing the scFv moiety to the light chain resulted in a more substantial loss of affinity in comparison to the heavy chain-linked variants.

This work demonstrates that varying scFv fusion sides of a tetravalent format can influence the affinity of a bispecific endoglinxCD28 antibody. Besides the selected format, antibody-mediated activation of T cells can correlate with the length of introduced linkers, as demonstrated for a CD19xCD3 diabody [264]. This study is in line with the literature by demonstrating a higher affinity upon the introduction of a linker, which resulted in the Lc-L proving to be the format with the lowest affinity towards CD28 and Hc+L being of highest affinity.

The format-specific variation in the levels of affinity resembled the results of the T cell activation. The diminished affinity led to a limited T cell activation. Limited flexibility and a more distant binding between the two scFv moieties might contribute to the limited activity of the Lc-L format. The limited activity resulted in Lc-L being the only variant with target cell-specific activation exclusively in the presence of the initial stimulation of a TAAxCD3. All other formats demonstrated some T cell activation without an initial T cell stimulation. The Lc-L format was considered superior to the other formats assessed with respect to target cell restricted T cell activation.

In contrast to this study, Crosadale et al. found better performance in a bispecific tetravalent format similar to the Lc+L format used in this work when analyzing an antagonistic antibody targeting insulin-like growth factor receptor type I and epidermal growth factor receptor, [262]. It can be concluded that the antibody efficacy can be mediated by the fusion site of the scFv in a tetravalent format and the use of a linker. However, the activity of the selected format might be depended on the structure and function of the targets of interest and should be assessed individually.

3.2.2 Evaluation of the different endoglin binding antibodies

The next focus was set on identifying an optimal endoglin binding clone for the use in the IgG(scFv)$_2$ Lc-L format. The endoglin binding clone Kro-23 was initially used for assessing the optimal format, and the clones Kro-10 and Kro-22 were selected for further comparison. The chosen clones were generated and described in the thesis of Karolin Schwartz [237]. These clones were selected because of their differences in biochemical characterization, such as affinity, ADCC induction, and immunohistochemistry, while not sharing the same epitope.

Kro-22 demonstrated the highest affinity in the IgG(scFv)$_2$ Lc-L format, which is resembling the results for the parental IgG, as shown by Karolin Schwartz [237]. Further analysis of the binding kinetic towards endoglin demonstrated a similar association of all clones analyzed. However, Kro-22 demonstrated significantly decreased dissociation. The affinity constant K_D is defined as a ratio of k_d/k_a, between the antibody and its antigen. Thus, the superior dissociation of Kro-22 explains its higher affinity to endoglin. Similar to the previous results, target-cell specific T cell activation correlated with the affinity of the different variants Kro-22 and Kro-21.

Higher affinity in the binding towards the tumor-associated antigen is generally a promising aspect in the use of bispecific antibodies for a successful T cell focusing. Hoffmann et al. demonstrated, through the use of a bispecific C19xCD3 antibody, the necessity of a higher affinity when targeting CD19 as opposed to CD3. Increased affinity towards CD19 resulted in a more focused binding of the antibody to the target cell rather than to the T cell [236], consequently turning the surface of the target cell into a T cell activation matrix, rather than “arming” polyclonal T cells. Therefore the biochemical characteristics of the clone Kro-22 were considered superior when compared to the clones Kro-10 and Kro-23.

Besides the identification of Kro-22 as an optimal endoglin binding clone in the IgG(scFv)$_2$ Lc-L format, the extensive focus was set on the comparison of different CD28 binding clones. Two additional clones were selected as an alternative to the initially used 9.3 antibody. The first clone selected was 15E9, an agonistic antibody first described in 1999 [253], and TGN1412 was selected as a second clone. TGN1412 was initially described as a superagonistic antibody activating T cells without the need for a primary TCR stimulation [123, 130].

The scFv of TGN1412 and 15E9 demonstrated a lower affinity in comparison to 9.3. Besides lower affinity, T cell activation of IgG(ScFv)$_2$ Lc-L muKro-22xTGN1412 was identical to IgG(ScFv)$_2$ Lc-L muKro-22x9.3, while IgG(ScFv)$_2$ Lc-L muKro-22x15E9 demonstrated lower T cell activation. Moreover, TGN1412 demonstrated superagonistic characteristics by inducing T cell activation without an initial activation via TAAxCD3 bispecifics regardless of being soluble or immobilized on tumor cells. Superagonsitic T cell activation by TGN1412 may explain its similar immunostimulating capabilities when being compared to 9.3, despite its lower affinity.

In direct comparison with 15E9 and TGN1412, the clone 9.3 demonstrated the most potent target cell-restricted immunomodulating capacity while not inducing superagonistic T cell activation. However, it should be noted that *in vitro* analysis of the CD28 superagonist TGN1412 failed to predict the strong response seen in patients. Extensive studies after the failed clinical trial of TGN1412 discovered a significantly lower expression of CD28 on monkey T cells. Different expression patterns from monkeys to humans attributed to the induction of cytokine storm in humans [130]. High-density PBMC preculture increases the sensitivity of T cell towards anti-CD28 stimulation, revealing a cytokine release by the CD28 superagonist TGN1412 which is resembling the reaction seen in patients [128]. Assessing the effect of the final IgG(ScFv)$_2$ endoglinxCD28 bispecific on high-density precultured T cells might, therefore, be an important indicator for assessing its clinical safety. Humanization of IgG(scFv)$_2$ Lc-L

The process of humanization via CDR-grafting is often associated with minimal alterations in the reconstructed CDR and framework regions of the antibodies [265]. Generally, these changes are considered a major challenge of this technique. The hybridoma derived clone 9.3 was humanized in collaboration with Yacine Mahringer as part of her master thesis [245]. A total of ten humanizations resulted in the identification of hu9.3-8. The variant hu9.3-8 demonstrated no decrease in affinity and immunostimulating capacity compared to its parental antibody.

Surprisingly, while the humanization of 9.3 proved to be more critical, the humanization of Kro-22 resulted in a panel of highly functional antibodies. All of these humanized variants resulted in antibodies with high affinity towards CD28, which could not be distinguished due to their biochemical characterization or function. The selection towards humanized variant huKro22.2-6 was made for its superior production yield together with the smallest percentage of aggregates after protein A purification. This decision was made purely with respect to process development for industrial antibody manufacturing.

3.2.3 Comparison to the literature

In a recent study, Skokos et al. [190] presented two TAAxCD28 costimulatory bispecific antibodies that target either MUC16 or PSMA. When paired with an appropriate TAAxCD3 antibody of another specificity, these bispecific antibodies promoted TAA-direct T cell activation and enhanced the antitumor activity of the TAAxCD3 similar to the bispecific antibodies described in this work. However, there was still undesired activation by the MUC16xCD28 and PSMAxCD28 antibodies in contrast to the Lc-L antibody in this work. The here described bispecific antibody IgG(scFv)$_2$ Lc-L huKro-22.2-6xhu8.9-8 antibody demonstrated a more specific mode of action. Upon its extensive optimization, it was possible to restrict the stimulatory activity of CD28 to target cells and the combination of an initial TAAxCD3 stimulus. In a clinical situation where it is essential to control and limit extensive T cell activation, a more defined mode of action might be preferable.

3.3 Development of a bispecific immunomodulating antibody targeting 4-1BB

Similar to the stimulatory receptor CD28, several studies have highlighted the potential of 4-1BB-mediated costimulation. 4-1BB stimulation is maintaining a long-term functionality of T cells by mediating anti-apoptotic protein expression, T_H1 polarization, increase in memory formation, and T cell survival [135, 137, 139]. However, monospecific antibodies have not moved beyond early clinical trials due to severe side effects in patients.

The monospecific 4-1BB agonist Urelumab induced a dose-dependent grade 4 hepatitis in patients [116, 139, 140]. The side effects of Urelumab and other clinically developed IgGs were most likely induced by FcγR-mediated immobilization [141-143]. Bispecific antibodies aimed to overcome the limitations of monospecific antibodies by simultaneously targeting 4-1BB and a tumor antigen. As a result, various 4-1BB bispecific antibodies or fusion-proteins were developed with the intention to restrict 4-1BB stimulation to a given tumor site [115, 266-269].

3.3.1 Generation of novel anti-4-1BB antibodies

A panel of novel anti-4-1BB antibodies was initially generated and characterized for the use in a bispecific format. These novel generated clones were either hybridoma derived or generated via phage display technology. As briefly discussed in 0, both methods have theoretical and practical limitations and advantages. Julian Weischedel characterized the phage display derived antibodies as part of his Master thesis [254], and his results will be discussed in the context of the results of the hybridoma derived antibodies.

As expected, hybridoma derived clones were of higher affinity in comparison to the phage display derived clones. Due to missing affinity maturation *in vivo*, phage display derived antibodies are more likely to result in clones with low affinity. However, despite this limitations, all antibody clones obtained *via* phage display technology were of relatively high affinity.

Previous research revealed that it is more likely for an antibody with membrane-distant epitope to be a TNFR agonist [258]. For example, Yu and colleagues identified agonistic anti-CD40 antibodies binding the Cys1 domain and antagonistic antibodies binding to Cys3 and Cys4. Therefore, a panel of truncated 4-1BB-Fc fusion proteins was generated for the identification of the epitopes of all generated 4-BB antibodies. Nearly all hybridoma derived antibodies are binding the Cys1 domain of 4-1BB while the phage display derived antibodies demonstrated a higher distribution of their epitopes throughout the extracellular domain of 4-1BB.

The alignment of the extracellular domain of the human and mouse 4-1BB amino acid sequence revealed sequence identity of 60%. The domains Cys2 and Cys3 showed 65% and 71% identity between both species, respectively [270]. Higher immunogenicity of the Cys1 and Cys4 domains arises as a result of the inherent lower sequence identity. Eliciting a robust immune response is crucial only during the immunization in the hybridoma generation but not in the phage display technology. This appears to explain the tendency of generating anti-Cys1 and anti-Cys4 targeting antibodies.

The identification of agonistic clones was the main focus in the characterization of 4-1BB specific antibodies. Initial experiments led to the identification of 5 hybridoma derived antibodies, and 13 phage display derived antibodies.

Neither phage display technology nor hybridoma technology resulted in a higher percentage of 4-1BB agonists. In addition, no correlation between format, affinity, epitope, and isotype could be identified as a predictive marker or as an exclusion criteria for 4-1BB directed agonism. Interestingly, the phage display derived antibodies demonstrated a significantly higher activation of 4-1BB when being compared to the hybridoma derived clones. The exact reason for this difference in 4-1BB activation maintains unclear. Since the mouse IgG1κ 4B4-1 was used as a positive control and therefore, at least for the IgG1κ, these differences appear to be unlikely induced by the isotype

A loss in affinity became abundantly clear throughout all clones upon reformatting from scFv-Fc into IgG(scFv)$_2$ Hc+L format. Besides the loss of affinity, all bispecific antibodies exhibited a tumor cell restricted 4-1BB agonism. The strength of 4-1BB activation correlated strongly with the height of the affinity. However, IgG(scFv)$_2$ Hc+L muKro-22xSH1689-C3 did not further increase TAAxCD3 mediated T cell lysis, which indicates a minimum threshold needed for 4-1BB agonism to enhance further TAAxCD3 anti-tumor activity.

As previously discussed, 4-1BB costimulatory antibodies did so far not succeed in cancer immunotherapy due to severe side-effects in patients. Claus and colleagues generated a bispecific molecule, comprising a trimeric 4-1BBL in combination with either CD19 or FAP specific antibodies [115]. These proteins successfully stimulated T cells in the presence of tumor cells and improved survival in multiple mouse models. However, the 4-1BBL fusion proteins demonstrated minimal activation of 4-1BB in the absence of tumor cells.

In contrast to the proteins described by Claus et al., all endoglinx4-1BB molecules described in this work provided tumor cell-specific hyperclustering of 4-1BB without systemic activation by FcγR binding. In addition, TAAxCD3 mediated T cell proliferation, and tumor cell killing was selectively increased in combination with the endoglinx4-1BB antibodies described in this work.

3.4 Development of a bispecific immunomodulating antibody targeting PD-1

In contrast to CD28 and 4-1BB, PD-1 is described as an inhibitory receptor. PD-1 is expressed on T cells upon their activation [32], and the interaction with its ligands PD-L1/PD-L2 suppresses CD3/CD28 signaling [45]. Increased expression of PD-L1 was identified as a potential immune escape mechanism in a patient with refractory B-precursor ALL [271]. estoring T cell function by blocking the activities of these proteins with monoclonal anti-bodies has delivered a breakthrough in the therapy against cancer in recent years. Nonetheless, anti-PD-1 directed monotherapy demonstrated great therapeutic success while also exhibiting strong systemic side effects in patients [261]. Up to date, several approaches combine bispecific antibodies with anti-PD-1 directed monotherapy [225, 226]. Employing bispecific antibodies for a restricted blockade of PD-1 represents a promising approach in cancer immunotherapy to avoid systemic side effects.

For the screening of PD-L1 or PD-L2 blocking antibodies, a panel of several anti-PD-1 antibodies was generated via hybridoma technology and phage display technology. This resulted in antibodies with varying affinity with the hybridoma derived antibodies being of higher affinities, unlike the results for the 4-1BB specific antibodies. No prediction for antagonsim could be determined based on differences in their affinity. A total of 4 Hybridoma and one single phage display derived antagonist could be Identified when screening for PD-1 directed antagonism.

Structural analysis of the interaction of PD-1 with its two cognate ligands revealed similar epitopes for both ligands [272]. The crystal structure of the PD-1 extracellular domain and Pembrolizumab Fab fragments has shown a significant overlap between the epitope of Pembrolizumab and PD-L1 [220, 272, 273]. Surprisingly, TIM4-E6 demonstrated antagonistic properties despite its low affinity. Demonstrating the high importance of the epitope for antagonistic PD-1 antibodies.

Upon reformatting into IgG(scFv)$_2$ format, TIM4-E6 did not show any antagonistic characteristics which were previously seen in the scFv-Fc format. The question remains whether or not the difference in the affinity between the high affine Pembrolizumab and the low affine TIM4-E6 are the reason for the loss of antagonistic properties in the bispecific format. In addition, as long as the exact epitope of TIM4-E6 is not identified, format-specific hindrance can not be excluded as the reason for PD-1 specific antagonism.

In conclusion, target-cell restricted blockade could not be archived. However, the designed assay proved to be fully functional. Unfortunately, TIM4-E6 was the only antibody available for the screening of bispecific antagonistic antibodies. Therefore, a future screening including multiple antibodies, together with the successfully established test system may be more rewarding.

Nonetheless, other work indicates the usefulness of a bispecific approach, potentially limiting systemic side effects. The only PD-1 blocking bispecific known up to date is described in the work of Sun et al. [191]. Sun and his colleagues combined a PD-1 specific antibody with an antibody specific to c-MET. These bispecific antibodies rescued T cell activation and, furthermore, markedly inhibited the growth of subcutaneously implanted tumors and chronic inflammation in xenograft mouse models. Unfortunately, a missing affinity assessment of the PD-1 binding limits the possible comparison between the described molecule and the bispecific antibodies analyzed in this work.

3.4.1 Conclusions

In summary, the costimulatory bispecific IgG(scFv)2 antibodies targeting 4-1BB or CD28 that are presented in this work, provided the beneficial effect of activating T cells only in the presence and proximity of target cells. Thus, eliminate the potential of off-target related side effects. Therefore, in certain oncological settings, these molecules might be applied in addition to established anti-CD3 therapy [109, 113, 115, 190] to improve and sustain T cell activation.

4. Methods

4.1.1 Microbiology and Molecular biology methods

4.1.1.1 Electrocompetent *E. coli*

To generate electrocompetent *E. coli* DH5α, the bacteria were plated on LB plates without antibiotics and cultivated at 31°C overnight. The next day, a single colony from the LB plate was used to inoculate 5 ml of LB medium and the cells were incubated at 250 rpm and 37°C. In the morning, the incubated cells were diluted 1:100 in 100 ml and incubated for an additional 1 to 2 h at 250 rpm with 37°C. The cells were incubated until an optical density (OD) of 0.2-0.3 at 550 nm. After centrifugation for 10 min at 1619 x g at 4°C, the supernatant of the cells was discarded and the cell pellet resuspended in 20 ml of ice-cold TfbI-buffer and incubated on ice for 20-30 min. The cells were centrifuged again for 5 min at 719 x g at 4°C and then immediately frozen and stored at -80°C with aliquots of 100 or 200 µl of suspension.

4.1.1.2 Transformation via heat shock

Chemically competent bacteria were slowly thawed on ice prior to the transformation. The thawed bacteria were gently mixed with approximately 1 µg of plasmid DNA or complete reaction mix (see 4.1.1.12 on page 83). After an incubation of 45 min, the heat shock was performed for 1 min at 42°C. Immediately afterward, the tube was placed on ice. 300 µl of LB-media was added and incubated at 37°C for one hour to ensure the development of antibiotic resistance. 100 µl of the cell suspension was plated on LB plates containing the appropriate antibiotic. The plates were incubated overnight at 37°.

4.1.1.3 Cultivation of bacteria

The amplification of plasmid DNA was performed by cultivating the specific bacterial clone. Single bacterial colonies were picked from a selective plate and transferred onto a new master plate and into a tube with LB medium containing 100 µg/ml of the appropriate antibiotic. For a small quantity plasmid isolation used with the QIAGEN® Plasmid-DNA Miniprep Kit, the volume of the culture was set to 6 ml or 300 ml for larger quantities with QIAGEN® Plasmid-DNA Maxiprep Kit. The cultures were incubated for 12 to 16 h at 37°C with vigorous shaking.

4.1.1.4 Isolation and purification of plasmid DNA

Isolation of Plasmid-DNA from bacterial cultures was performed using commercial kits from Qiagen. Depending on the required amount of DNA different kits were used. Isolation was performed according to the QIAprep® Spin Plasmid-DNA Miniprep Kit or QIAGEN® Plasmid-DNA Maxiprep Kit manufacturer's instructions. QIAGEN plasmid purification protocols are based on a modified alkaline lysis procedure [274].

4.1.1.5 Agarose gel electrophorese

DNA fragments were separated and purified by agarose gel electrophoresis. An appropriate amount of agarose powder was mixed with TAE buffer to obtain concentrations of 1 % to 1.5 % (w/v). The mix was heated in the microwave oven for 1 to 5 min until the agarose powder was completely dissolved and after cooling, ethidium bromide (EtBr) was added to a final concentration of 0.5-1 µg/ml. A molecular weight ladder (GeneRuler^{TM} 1kb plus DNA ladder) was added for the determination of the size of the DNA-fragments. Agarose gel electrophoresis was performed using TAE buffer at 80 to 150 V. DNA fragments were visualized using UV light (254 nm).

4.1.1.6 Purification of DNA from agarose-gel electrophoreses

Gel purification was performed to isolate DNA fragments from agarose gel electrophoresis according to its size. After separating DNA fragments via agarose gel electrophoresis, bands were cut out of the gel and fragments were purified using the commercial gel purification kits Qiaquick® Gel Extraction Kit. The protocol was followed according to the manufacturer's instructions.

4.1.1.7 Quantification of nucleic acids and proteins

The concentration of nucleic acids in aqueous solution and proteins in PBS was determined by spectrophotometric analysis at the wavelength of 230 nm, 260 nm and 280 nm using Nanodrop™ 1000 UV-Vis spectrophotometer. The ratio of absorbance at 260 and 280 nm was used to assess the purity and concentration of DNA. To determine the concentration of proteins, absorbance at 280 nm was measured using the specific extinction coefficient and the molecular weight of the measured protein.

4.1.1.8 Sequence analysis

To analyze DNA sequences, prepared samples were sent to GATC Biotech for sequencing. The prepared samples contained 2 µM of either forward (pGH1_fv) or reverse primer (pGH1_rv), 400-500 ng DNA and were filled up to 10 µl with ddH2O.

4.1.1.9 Polymerase chain reaction

DNA fragments were amplified via polymerase chain reaction (PCR). DNA fragments specific sense and anti-sense primers complementary to the DNA sequences were generated [275, 276]. PCR reaction was performed using KAPA HiFi DNA polymerase and following cycling parameters:

Initial denaturation	95°C 5 min
Denaturation	98°C 30 sec
Primer annealing	Tm ±10°C 30 sec
Extension	72°C 30 sec/kb
Final extension	72°C 5 min
Cooling	4°C Hold

4.1.1.10 Restriction digest

DNA was subjected to digestion for 1 h at an appropriate temperature recommended by the manufacturer, depending on the respective restriction enzyme [274].

4.1.1.11 Cloning Strategy

The genes of all obtained antibodies were cloned into pGH1.2 Vector (Figure S 2) using the BamHI/XbaI restriction sides. Inserts were generated via PCR or by restriction digest of either a parental vector or gene synthesis.

4.1.1.12 Ligation

Ligation was used to join dsDNA fragments with blunt or sticky ends to insert DNA fragments into the plasmids or expression vectors. Reaction-mix for the ligation was as follows:

50 ng	vector
1:5	molar ratio of vector to insert
2 µl	10 x buffer
1 µl	T4 DNA Ligase (5 U/µl)
fill to 20 µl	ddH2O

The reaction mix was incubated at room temperature for at least 20min.

4.1.1.13 Humanization of antibodies

Amino acid sequences for the variable heavy (VH) and variable light chain (VL) were aligned to human IgG germline genes by using the Ig-BLAST algorithm of the NCBI website (http://www.ncbi.nlm.nih.gov/igblast/) with the IMGT database for reference. To validate the humanness, all chosen sequences were evaluated based on the t20-score (https://dm.lakepharma.com/bioinformatics/) [277] and z-score [247]. The CDR sequences of the antibodies were defined by the overlapping CDR definitions of Kabat [278], Chothia [279, 280] and Contact [281]. The identified CDR sequences of the mouse antibody were inserted onto the human backbone sequences. Not only the CDR sequence but also framework residues can play an essential role in maintaining the proper CDR conformation, such as amino acids in the Vernier zone [85]. Therefore, these amino acids were identified according to the list shown in Table 8.

Table 8 Residues in the Vernier zone according to Kabat numbering [278].

Heavy chain	Light Chain
2	2
27-30	4
47-49	35-36
67	46-49
69	64
71	66
73	68-69
78	71
93-94	98
103	-

Identification of mismatches between the mouse and parental backbone sequence let to the selection of mouse Vernier amino acids to obtain the final humanized sequence. DNA encoding for the humanized variable domains was ordered from GeneArt AG (Regensburg, Germany) and used for cloning into its respective vector.

4.1.2 Eukaryotic cell biology methods

4.1.3 Protein biochemistry and analytical methods

4.1.3.1 Protein Purification

All antibodies were purified using ProteinA affinity chromatography and the ÄKTA system.

Cell culture supernatants prepared and filtered and were applied to the column (MabSelect Sure) at the flow rate of 1 mL/min using a peristaltic pump. All unbound material was removed by washing with at least 10 column volumes of DPBS. Bound protein was eluted with 0.1 M glycine buffer at pH 2.5.

4.1.3.2 Polyacrylamide gel electrophoresis

Sodium dodecyl sulfate-polyacrylamide gel electrophoresis (SDS-PAGE) was performed according to [282] by using precast Mini-Protean® TGX™ polyacrylamide gels. Proteins are dissolved to the anionic detergent SDS. Due to a net negative charge within a wide pH range, the proteins can then be separated only due to their molecular weight.

For analysis, 2 µg of each sample was diluted 1:2 in loading buffer (Laemli-buffer) and denaturated for 5 min at 95°C. If the SDS-Page was run under reducing conditions, 2.5 % β-mercaptoethanol was added to the sample prior to denaturation. Separation of the samples was performed at 200 V. The gel was stained with Roti®-Blue colloidal coomassie staining solution following the electrophoresis to visualize the proteins. The gel was incubated with a staining solution with gentle agitation for 1 h and was then rinsed in a staining tray and destained for 1–3 h with ddH2O water.

4.1.3.3 Size exclusion chromatography

Size exclusion chromatography (SEC) was performed using a UHPLC-system “Dionex™ UltiMate™ 3000 BioRS” equipped with the Superdex 200 Increase 10/300 GL column. For analytical size-exclusion, 10 µg of protein in PBS was applied per run. The system was operated with a flow of 500 µL/min with DPBS. Proteins were detected via OD at 220 nm (OD220). Chromatograms were compared to an external gel filtration standard (Bio-Rad). Data acquisition and analysis was performed via control software Chromeleon 7.2.

4.1.3.4 Enzyme-linked immunosorbent assay (ELISA)

The coating of microtiter plates was performed over-night at 4°C with 100 µl of protein at 1 µg/ml in PBS. Residual binding sites were blocked with 1 % BSA in PBS at room temperature for 1 h with a total of 200 µl. Between each incubation step and in advance of the detection, the plates were washed two times with PBST (1 % Tween-20) and twice with PBS. A total of 100 µl per well of samples were diluted in PBS and incubated at room temperature for 1 h. For the detection of bound protein, 50 µl of the HRP conjugated detection antibodies in PBS were added. The bound detection antibody was detected with 100 µl TMB substrate solution, the HRP-reaction was stopped by the addition of 50 µl 1 M H_2SO_4 and the absorption at the wavelength of 450 nm was measured using the Infinite microtiter plate reader.

4.1.3.5 Binding kinetics

Binding kinetics of the mAbs to their respective antigen was analyzed by surface plasmon resonance *via* the BiaCore X instrument. To minimize the effect of unspecific interactions, the kinetic was performed using PBS including 0.05 % Tween-20 at pH 7.4 as running and dilution buffer with a flow of 30 µl/min. The antibodies were immobilized for 30 s on a sensor chip protein A. After immobilization of the antibody, a series of different dilutions of its antigen were prepared and injected for an association time of 100 s with a dissociation time of at least 1000 s. The chip was regenerated by injection of 10 mM glycine-HCl buffer at pH 1.5. The kinetic constants for association (k_A) and dissociation (k_D), as well as the equilibrium dissociation constant (KD), were calculated using steady-state affinity calculation at the BiaCore X evaluation software.

4.1.3.6 Flow cytometry

Binding of antibodies to the respective target protein on the cell surface was analyzed via flow cytometry (Fluorescence-activated cell sorter, FACS). Target cells were detached and transferred to a 96-well microtiter plate with a number of 100,000 to 250,000 cells per well in 100 µl FACS buffer. Samples were diluted in FACS buffer at double of the final desired concentration and 100 µl were added to the cells for a 1-hour incubation at 4°C. Cells were washed twice by centrifugation at 650 x g, 5 minutes and resuspension in 150 µl FACS buffer after each incubation step. Subsequently, the cells were incubated with secondary antibodies conjugated to fluorescent dyes for 1 h at 4°C in the dark prior to the detection. Analysis of cells was performed using the FACSCalibur flow cytometer together with the CellQuestPro software.

4.1.3.7 Differential scanning fluorimetry for assessment of thermal stability

Determination of the melting temperature T_m was analyzed by using the commercially available ProteoStat® Thermal Shift Stability Assay Kit. After binding to hydrophobic residues of a protein the fluorescence of the dye, used in the assay, is induced at a wavelCD105th of 610 nm. The increasing temperature is stressing the protein, leading to an unfolding and presentation of hydrophobic residues. Samples were diluted using a Fast optical 96-well reaction plate in PBS to a total of 22.5 µl with a final concentration of 1 mg/ml and 2.5 µL 10 x ProteoStat® TS Detection Reagent was added. The experiments were performed in a 7500 Fast Real-Time PCR system. The temperature was increased stepwise from 25 °C to 100 °C with 1 °C/min. Fluorescence was assessed at 610 nm. Fluorescence was plotted against temperature. The maximum of the first derivative of this plot represents the temperature, where half of the protein is unfolded and is referred to as melting temperature T_m.

4.1.3.8 Stable transfection of eukaryotic cells

For stable transfection, 2×10^7 Sp2/0-Ag14-cells were washed three times with 50 mL ice-cold IMDM medium without supplements. Centrifugation was performed at 200 × g. The cell pellet was resuspended in 200 µL IMDM, mixed with linearized expression vectors, and transferred into a cold electroporation cuvette with 0.4 cm gap width. Electroporation was performed at 230V und 975 µF. The cells were then transferred immediately into 12mL of warm IMDM complete medium and, after serial dilution, seeded into 96-well plates (50 µL/well). Selection for stably transfected cells was accomplished by adding the antibiotic G418 (end concentration: 1mg/mL) 24 h after transfection. 7-10 days after transfection, the cells were monitored for antibiotic-resistant clones. 14-20 days after transfection cell culture supernatants from growing clones were tested for the presence of recombinant antibodies by flow cytometry.

4.1.3.9 Cultivation of antibody-producing hybridoma cell lines

Antibody-producing Sp2/0 hybridoma cells were cultivated in IMDM Pan medium (IMDM supplemented with chemically defined serum substitute for suspension cells PANEXIN NTS) at a cell density of 2 - 3×105 cells/mL. The cells were expanded in TripleFlask™ cell culture flasks to a final volume of 1 - 2 L. Afterwards, the cells were kept in culture until approx. 50% of all cells were dead. Finally, the cell culture supernatant was harvested by centrifugation at 6000×g, supplemented with 0.02% (w/v) NaN3 and filtrated using 0.22 µm bottle-top filter. For purification with ProteinA, the supernatant was adjusted to pH8 and stored at 4°C.

4.1.4 Generation of hybridoma-derived antibodies

4.1.4.1 Immunization of mice

8-week old BALB/c were injected intraperitoneal (i.p.).with 150 µl of either 5-1 x 10^6 Sp2/0 cells stably expressing the antigen of interest or with 100 µg of recombinant protein. A total of up to 5 immunizations were repeated in an interval of 2 weeks. The final boost immunization was performed four days prior to the generation of the hybridoma.

4.1.4.2 Generation of hybridoma cells

Four days following the final boost immunization, the mice were terminated using lethal CO_2 inhalation. The spleen was removed under sterile conditions and briefly washed in PBS, and any residual tissue was removed. I order to obtain a homogeneous single-cell suspension, the spleen was pressed through a tea strainer into a sterile petri dish with preheated IMDM medium using a top of a 50 ml syringe plunger. The individual suspension was transferred to a 50 ml plastic centrifugation tube and left for about 3-5 minutes at room temperature to sedimentation of the larger pieces of tissue. The single-cell suspension was removed and transferred to a fresh 50 ml plastic centrifugation tube and washed at 10 min, 400 x g. The cell number was determined using a Turk' solution.

The fusion partners Sp2/0-Ag14 cells were cultivated in IMDM medium (with 5% FCS) at a cell density of maximum 0.5 x 10^6 per ml. For an optimal result, the fusion partners (Sp2/0-Ag14 cells) should be in a logarithmic growth phase on the day of the fusion. For the fusion, the fusion partners were washed three times with IMDM medium without additives (10 min, 200 x g) and the cell number was determined using trypan blue and a Neubauer counting chamber. For the fusion, 5 x 10^6 myeloma cells and 20 x 10^6 spleen cells were mixed in a 50 ml plastic centrifugation tube and centrifuged for 10 min at 400 x g.

The supernatant was removed, and the cell pellet was carefully resuspended. 1 ml of pre-warmed PEG 1500 solution was dropwise added, with constant shaking, and the mixture was incubated for 1 min. With continuous shaking, 10 ml of IMDM medium (without additives) was then added over 3 min and incubated for 5 min.

After gradual dilution of the PEG 1500 solution, the 50 ml plastic centrifugation tubes were filled up to 50 ml with IMDM medium (without additives) and centrifuged for 10 min at 200 x g. Immediately afterwards, 30 ml IMDM medium (20% FCS, 10% HCS) were added and distributed with the help of a multi-channel pipette on three 96-well flat-bottom plates with 100 µl/well and incubated at 37 ° C and 7% CO_2.

4.1.4.3 Selection of hybridoma cells

For the selection of the hybridoma cells, IMDM medium (2x HAT, 20% FCS, 10% HCS) was added to each well after 24 hours. The cells were then incubated for an additional 7-10 days at 37 ° C and 7% CO_2

4.1.4.4 Testing of hybridoma supernatants

After about 7-10 days, each well was visually checked for hybridoma colonies. Supernatants from these colonies were collected and then examined by flow cytometry for antibody production and antibody specificity. Positive clones were re-tested by flow cytometry 2-3 days later.

4.1.4.5 Subcloning positive hybridoma clones

Hybridoma clones, which were tested positive twice in flow cytometry, were subcloned using limited dilution series. The resulting individual clones were tested by flow cytometry for antibody production and antibody specificity. One part of the monoclonal hybridoma cells was cryopreserved, the other part for antibody production was transferred to advanced DMEM medium (1% FCS) and expanded for production.

4.1.5 Generation of phage display-derived antibodies

4.1.5.1 Immobilization of antigen

The recombinant antigen-Fc fusion protein was transferred into 2 blocked wells (150 µl per well, 1µg/ml) previously coated with goat anti-human (IgA, IgG, IgM) (109-005-064, Dianova, 1:500 in PBS) antibody, and were incubated for 2 h at RT. The excess protein was removed by washing three times with PBST (0.05%).

4.1.5.2 Selection of specifically bound phages

For the selection of specifically bound phages, two to three rounds of panning were performed using 2 x 10^{10} cfu phage library (in 150 µL MPBST) as input phage in round one and 100 µL of amplified phage (accounting for 3x 10^{11} cfu) as input in round two and three.

The phage were incubated with the immobilized antigens for 2 h at room temperature and unbound phage were removed by stringent washing (10, 20, 30 times with PBST (0.05 %). The bound phage were eluted with 200 µL phage elution buffer per well for 30 min at 37 °C. The eluted phage titer was determined using 10 µL of the elution and a 10-fold dilution series.

4.1.5.3 Amplification of eluted phages

For the next panning round, the eluted phage were amplified to use as input phage. The remaining 390 µL of the elution were used to infect 5 mL of an *E. coli* TOP10F' culture at an OD_{600} of 0.5 for 30 min at 37 °C. Cells were plated on 2 x YT-GA agar plates and incubated at 37 °C overnight. The cells were scraped using 5 mL 2 x YT-GA and used to inoculate a culture for phage amplification or was supplemented with 20 % (v/v) glycerol and stored at -80 °C. Phage amplification was performed in 30 mL.

30 mL of 2 x YT-GA were inoculated (OD600 < 0.1) and cultivated at 37 °C and 250 rpm (Infors HT) until logarithmic growth phase (OD600 = 0.5) was reached. Helperphage infection was performed for 30 min at 37 °C using 5 mL of the culture and a 20-fold excess (5x 1010 cfu) of the M13K07ΔgIII helperphage “Hyperphage”. After an additional incubation time of 30 min, the cells were pelleted (3,220 x g, 10 min) and subsequently resuspended in 30 mL 2x YT-AK following phage production at 30 °C and 250 rpm overnight. Amplified phage were precipitated (1 h on ice) after adding 1/5 volume phage precipitation buffer. After pelleting for 1 h at 4 °C, 3,220 x g, the phage were resuspended in 500 µL phage dilution buffer. The remaining bacteria were pelleted for 2 min at 16,100 x g. The supernatant containing the amplified phage was collected and stored at 4 °C until further use.

4.1.5.4 Screening of monoclonal phages

For the screening of monoclonal phage after panning, phage particles were produced in 96-well microtiter plate (MTP) scale. A 96-well MTP was supplemented with 180 µL 2x YT-GA medium, inoculated with single colonies bearing a phagemid and incubated at 34 °C and 800 rpm (Labnet Vortemp 56) overnight. For phage production, 175 µL 2x YT-GA per well were inoculated with 10 µL of the overnight culture and incubated for 2 h at 37 °C and 800 rpm to reach logarithmic growth. The cells were infected with 5 x 109 cfu “Hyperphage” (M13K07ΔgIII) for 30 min at 37 °C. To ensure antibiotic resistance, the cells were incubated for another 30 min at 37 °C and 800 rpm. In order to change the medium for phage production, the cells were pelleted for 10 min at 3,220 x g and resuspended in 180 µL 2x YT-AK followed by phage production at 30 °C and 800 rpm overnight. The cells were pelleted, and the phage were precipitated (1 h on ice) after adding 40 µL phage precipitation buffer to 150 µL phage containing supernatant. The phage particles were pelleted for 1 h at 3,220 x g an 4 °C, the supernatant was discarded and the phage were resuspended in 150 µL phage dilution buffer. The remaining bacteria were pelleted for 10 min at 3,220 x g. The cells were plated on2 x YT-GA agar plates and incubated at 37 °C overnight in order to obtain single colonies.

The monoclonal were and analyzed for their reactivity with immobilized antigen by ELISA.

4.1.5.5 Determination of phage titers

Phage titers were determined for the preparation of oligopeptide phage libraries and produced monoclonal oligopeptide phage as well as to monitor panning output. Phage titers were determined by infection of E. coli cells. Ten-fold serial dilutions of the phage were prepared in PBS. For infection, 50 µL of an E. coli XL1 Blue MRF' or E. coli TOP10F' culture at logarithmic growth (OD600 = 0.5 in 2xYT-T) was briefly mixed with 10 µL of a phage dilution and incubated for 30 min at 37°C. After the infection, 3x 10 µL of each dilution were spotted on 2x YT-GA agar plates. The plates were incubated at 37 °C overnight, and the colonies were counted the next day. To exclude phage contamination, a control with 50 µL E. coli culture and PBS was treated equally to the infection with phage. Also, the used PBS and E. coli culture alone was spotted on 2x YT-GA agar plates to exclude bacterial contamination of the PBS or ampicillin resistance of the E. coli culture. Another 50 µL of the E. coli culture were infected with 10 µL of a phage solution with known titer as a positive control.

4.1.6 Immunobiological assays

4.1.6.1 Thawing of cryopreserved cells

Cryovials containing cryopreserved cells were thawed in a water bath at 37°C. Subsequently, the cell suspension was transferred into a 15 ml PP tube. 10 ml of pre-warmed (37°C) basal medium was added slowly (approximately 1 min.). The suspension was centrifuged at 210 x g for 5 min and the supernatant was discarded. The cells were resuspended in 25 ml pre-warmed (37°C) basal medium and were transferred into a 125 ml disposable Erlenmeyer flask. After 24 h of cultivation, the cell culture medium was exchanged by centrifugation at 210 x g for 5 min by 25ml of new pre-warmed (37 °C) basal medium.

4.1.6.2 Cryopreservation of cells

The Cell suspension containing 10^7 cells was centrifuged at 210 x g for 5 min. Cells were resuspended in 1 ml cold cryopreservation medium (4°C) and transferred to a 2 ml cryovial. The cryovial was transferred to a Nalgene™ Cryo 1°C Freezing Container and stored at -80°C. The next day, the cryovial was transferred to the vapor phase of liquid nitrogen at -140°C.

4.1.6.3 Isolation of human PBMCs

PMBC were extracted from heparinized blood from human donors (mandatory premise: ethics approval). 12.5 ml blood was diluted with 12.5 ml DPBS and carefully applied to 12.5 ml Biocoll separating solution L. The preparation was centrifuged at 670 x g for 30 min. without brake. PBMCs were extracted with a 10 ml serological pipette and the same volume of DPBS was added. The PBMC solution was centrifuged at 210 x g for 10 min. and PBMC were resuspended in 25 ml DPBS. The cells were washed two times with 25 ml DPBS via centrifugation at 210 x g for 10 min and were subsequently resuspended in IMDM complete medium to obtain desired cell density.

4.1.6.4 Cell count via Neubauer counting chamber

The viability of cells was assessed by trypan blue staining. Trypan blue solution was added to cell suspension in a 96-well-plate in a ratio of 1:2. Subsequently, the number of viable cells was determined with a Neubauer counting chamber and an inverse microscope. The number of viable cells per large square multiplied with 10^4 and the dilution factor results in the viable cell density per mL cell culture medium.

4.1.6.5 Magnetic cell separation of T cells

Cells were separated through their expression of specific surface molecules via high gradient magnetic cell separation [283]. An antibody cocktail binding T cell excluding antigens was added. Cells labeled with antibody were coupled on magnetic beads and separated from unlabeled cells by trapping the cells in a separation column within a magnetic field. Thus, T cells could be negatively selected and separated. All steps were performed at 4°C or on ice following the manufacture's protocol of manufactures MACS® Pan T Cell Isolation Kit.

4.1.6.6 Thymidine uptake

For the determination of antibody-dependent proliferation, target cells were incubated with varying concentrations of different antibodies with and without PBMC or purified T cells. The cells were incubated for 48 h in 96well plates in a total of 200 µl of RMPI complete. After 2 days of incubation, the cells were pulsed with 0.5 µCi/well [methyl-3H]-thymidine in 50 µl of RPMI complete. Following 17 h, the cells were harvested on a Printed FiltermateA and the precipitated radioactivity was determined in a liquid scintillation counter.

4.1.6.7 Inactivation of tumor cells

Inactivation of tumor cells was performed by γ-radiation. Radiation was performed by a source of ^{137}caesium. The γ-radiation damages the DNA of the radiated cells which inhibits any further proliferation. Thus, tumor cell proliferation does not affect measurements of T cell proliferation. To achieve total radiation of about 120 Gy, the total time of radiation of about 20 min.

4.1.6.8 Real-time cytotoxicity via the xCELLigence system

Real-time cytotoxicity and cell adhesion can be measured with the xCELLigence system. The cytotoxicity is measured by continuous measurement of electrical impedance [284]. Cells adherent to the plate decreases the impedance of electric current in the electrodes at the bottom of each well in a 96-well E-plate. The killing of adherent cells by cytotoxic T-cell clones decreases the impedance. These changes in the electrical impedance were converted into dimensionless cell index (CI) values by the RTCA software v1.1. The cytotoxicity assays were performed in RPMI complete medium. Prior to the assay, the background was assessed by measuring 50 µl of medium for 10 s. LN-18 cells were seeded in a 96-well E-plate at a concentration of 30,000 cells in 100 µl of medium per well. Cells were allowed to adhere for about 48 hours. 100,000 PBMCs were selected as effector cells and added together with antibodies in the indicated concentrations to a final volume of 200 µl. 100 µl of Triton-X 100 was added as a positive control for complete cell lysis. CI values were assessed for up to 140 h with an impedance measurement every 15 min. All experiments were performed in triplicates. As further controls, untreated cells were used.

4.1.6.9 Luciferase bioassay.

For determination of agonistic and antagonistic properties of anti-4-1BB and anti-PD-1 antibodies, the commercially available Promega 4-1BB Bioassay and Promega PD-1/PD-L1 and PD-1/PD-L2 Blockade Bioassay were performed according to manufactures protocol. The Bioassays were performed in white 96-well plates for luminescence analysis. In the Promega 4-1BB Bioassay, either CHO CD32b positive cells were used for immobilization of antibodies according to the protocol or a total of 30,000 LN-18 cells were used. In the Promega PD-1/PD-L1 and PD-1/PD-L2 Blockade either CHO PD-L1/PD-L2 positive cells were used or 30,000 LN-18 were used. CHO PD-L1/PD-L2 positive cells express a TCR-stimulating domain on the surface for initial stimulation of the Jurkat reporter cell line. 5 nM immobilized anti-CD3 antibody was added to LN-18 cells to archive a similar initial stimulation. The final volume of the cell suspension in the well was 100 µl. All reaction components were prepared in RPMI 1640 medium supplemented with 10% fetal calf serum. After the addition of all the components, the plates were incubated for 7 h at 37°C in 5% CO_2, then the luminescence intensity was measured in the wells using ONE Glo assay system and plate reader.

4.2 Materials

4.2.1 Instruments

Äkta pure 25 L1	GE Healthcare Life Sciences, Chicago, USA
Cell harvester	Inotech Biosystems International, Inc. Rockville, USA
Biacore®X	GE Healthcare Life Sciences, Chicago, USA
Centrifuge Heraeus Biofuge fresco	Thermo Electron, Waltham, USA
Centrifuge Heraeus Megafuge 1.0	Thermo Electron, Waltham, USA
Centrifuge Heraeus Megafuge 2.0 R	Thermo Electron, Waltham, USA
Centrifuge ROTINA 420R	Andreas Hettich GmbH & Co.KG, Tuttlingen, Germany
Clean bench 3F120-II GS	Integra Biosciences GmbH, Fernwald, Germany
DIONEX UltiMAte*TM* 3000 Bio RSLC	Thermo Fisher Scientific, Schwerte Germany
Electrophoresis power supply EPS 200	Pharmacia Biotech, Stockholm, Sweden
FACS Calibur/Canto II	BD Biosciences, Heidelberg, Germany
Freezer Colora E80	Colora Messtechnik GmbH, Lorch, Germany
Gammacell 1000 Elite	MDS Nordion, Ottawa, Canada
Incubator APT.line CB	Binder GmbH, Tuttlingen, Germany
Incubator Heraeus function line	Thermo Electron, Waltham, USA
Laboratory balances	Sartorius, Göttingen, Germany
Light microscope Axiovert 25	Zeiss, Jena, Germany
Magnetic stirrer	Heidolph Instruments, Schwabach, Germany
Mini-PROTEAN Tetra Cell	Bio Rad, Hercules, USA
Multichannel pipette	Abimed GmbH, Langenfeld, Germany
Nanodrop™1000	Thermo Fisher Scientific GmbH, Schwerte, Germany
Neubauer counting chamber	Brand GmbH & Co KG, Weinheim, Germany
pH-meter Seven Multi	Mettler-Toledo GmbH, Giessen, Germany
Pipetboy acu	Integra Biosciences GmbH, Fernwald, Germany
Pipettes DV1000, DV200, DV100, DV20, DV10	Abimed GmbH, Langenfeld, Germany
Refrigerator	Liebherr Premium Liebherr Hausgeräte GmbH, Ochsenhausen, Germany
Sterile bank Tecnoflow	Integra Biosciences, Chur, Switzerland
Vortex Vibro-Fix VF2	IKA-Werke GmbH& Co. KG, Staufen, Germany
Water bath MP 19	Julabo Labortechnik GmbH, Seelbach, Germany
7500 Fast Real-Time PCR System	Applied Biosystems, Foster City, California, USA

4.2.2 Software

Biacore Control Software
Bicaore Evaluation
Chamelion (Dionex
Geneius
FLowJo
Microsoft Office
Unicorn (
Prism
Software Melting point

4.2.3 Consumables

Bottletop filter 500 ml (0.22 µm pore size)	SCGPT05RE	Millipore, Schwalbach, Germany
Bottletop filter 250 ml (0.22 µm pore size)	SCGPT02RE	Millipore, Schwalbach, Germany
Cellstar® Culture Flasks 175 cm^2	60175	Greiner Bio-One, Frickenhausen, Germany
Cellstar® Culture Flasks 75 cm^2	658175	Greiner Bio-One, Frickenhausen, Germany
Cellstar® Culture Flasks 25 cm^2	690175	Greiner Bio-One, Frickenhausen, Germany
Cellstar® 6-well Cell culture plates	657160	Greiner Bio-One, Frickenhausen, Germany
Cellstar® 96-well Cell culture plates, flat bottom	655180	Greiner Bio-One, Frickenhausen, Germany
Cellstar® 96-well Cell culture plates, round bottom	650160	Greiner Bio-One, Frickenhausen, Germany
Cellstar® 50 ml tubes, PP	227261	Greiner Bio-One, Frickenhausen, Germany
Cellstar® 50 ml tubes, skirted bottom, PP	210270	Greiner Bio-One, Frickenhausen, Germany
Cellstar® 15 ml tubes, PP	188271	Greiner Bio-One, Frickenhausen, GermanyClassic Nitrile powder-free examination gloves
Classic Nitrile powder-free examination gloves	290720-24	Abena, Aabenraa, Denmark
Costar® universal lid without corner notch	3098	Corning, Kaiserslautern, Germany
Costar® 96-well assay plate, clear,round bottom	C9018	Corning, Kaiserslautern, Germany
Costar® 50 ml Stripette	4501	Corning, Kaiserslautern, Germany
CryoBox*TM*	BCS-220G	Merck, Darmstadt, Germany
Cryo vials Cryo.S 2 ml	121278	Greiner Bio-One, Frickenhausen, Germany

Erlenmeyer flask Simax 1 L	251000	Bohemia Cristal, Selb, Germany
Falcon® 15 ml tubes, conical bottom, PS	352095	Corning, Kaiserslautern, Germany
Falcon® 25 ml Serological Pipet	357525	Corning, Kaiserslautern, Germany
Falcon® 10 ml Serological Pipet	357551	Corning, Kaiserslautern, Germany
Falcon® 5 ml Serological Pipet	357543	Corning, Kaiserslautern, Germany
Freezing Container Mr. Frosty®	5100-0001	Thermo Fischer Scientific GmbH, Schwerte, Germany
Glass Beaker	Z305197	Schott AG, Mainz, Germany
Glass bottles 2 l, 1 l, 500 ml, 250 ml		Schott AG, Mainz, Germany
LS Columns	130-042-401	Miltenyi Biotec, B. Gladbach, Germany
Measuring cylinder 500 ml, 250 ml	651081	Vitalab, Großostheim, Germany
MicroAmp® Fast Optical 96-Well Reaction Plate with Barcode	4346906	Applied Biosystems, Waltham, Massachusetts, USA
Parafilm® M	BR701605	Pechiney Plastic Packaging, Chicago, USA
Pasteur pipettes	S6268	WU, Mainz, Germany
PD Midi-Trap G-10 columns	28-9180-11	GE Healthcare Life Sciences, Chicago, USA
Petri Dish 94x16, without vents, with greiner, heavy version, sterile	632161	Greiner Bio-One, Frickenhausen, Germany
Plastic Beaker		Vitlab GmbH, Großostheim, GER
Printed Filtermats A	1450-421	Perkin Elmer, Rodgau, Germany
Reagents Reservoir Costar	4870	Corning, Kaiserslautern, Germany
Safe-Lock tubes 2 ml	30120094	Eppendorf, Hamburg, Germany
Safe-Lock tubes 1.5 ml	30120086	Eppendorf, Hamburg, Germany
Safe-Lock tubes 0.5 ml	30121023	Eppendorf, Hamburg, Germany
Single-use needle Sterican®	4657683	BD Biosciences, Heidelberg, Germany
Syringe filter Millex-GV, 0.22 µm	SLGV033RS	Millipore, Schwalbach, Germany
Syringe 3 ml Luer-Lok*TM* Tip	309657	BD, Heidelberg, Germany
TipOne® Pipette tips 1000 µl, 200 µl, 20 µl, 10 µl	S1111-0800	STARLAB, Hamburg, Germany
TipOne® Pipette tips with filter 1000 µl, 200 µl, 20 µl, 10 µl	S1120-8810	STARLAB, Hamburg, Germany
Tube 1.3 ml, pp,	102201	Greiner Bio-One,

8.5/44 mm, round bottom, natural		Frickenhausen, Germany
Zentricon Amicon Ultra 30 kDa	UFC903024	Milipore, Schwalbach, Germany

4.2.4 Reagents

Ampicillin	HP62.2	Roth, Karlsruhe, Germany
Ampuwa® destilled water	B23067A	Fresenius Kabi, Bad Homburg, Germany
Bacto agar	214050	BD, Heidelberg, Germany
Bacto trypton	211705	BD, Heidelberg, Germany
Bacto yeast extract	212750	BD, Heidelberg, Germany
_-mercaptoethanol	28625.01	Serva, Heidelberg, Germany
Biocoll separating solution L	6113	Biochrom GmbH, Berlin, Germany
Bovine serum albumin	A2058	Sigma, Steinheim, Germany
Coomassie blue stain	1610786	Bio-Rad, Munich, Germany
Dimethyl sulfoxid (DMSO)	A994.2	Roth, Karlsruhe, Germany
Ethanol 100%	100983	Merck, Darmstadt, Germany
Ethanol 96%	159010	Merck, Darmstadt, Germany
Ethylenediaminetetraacetic acid (EDTA)	431788	Sigma, Steinheim, Germany
FACS-Clean	340345	BD, Heidelberg, Germany
FACS-Flow	342003	BD, Heidelberg, Germany
FACS-Rinse	340346	BD, Heidelberg, Germany
Gibco® 1x DPBS	14190144	life technologies*TM*, Carlsbad, USA
Isopropyl alcohol	19634	Merck, Darmstadt, Germany
Methanol	106009	Merck, Darmstadt, Germany
PageRuler prestained protein ladder	26616	Thermo Fischer Scientific, Waltham, USA
Sodium azide	822335	Merck, Darmstadt, Germany
Sodium chloride	106482	Merck, Darmstadt, Germany
Trypan blue 0.4%	T8154	Sigma, Steinheim, Germany
Tween® 20	P2287	Sigma, Steinheim, Germany
10x Tris/Glycine/SDS buffer	1610772	Bio-Rad, Munich, Germany
2x Laemmli Sample Buffer	1610737	Bio-Rad, Munich, Germany

4.2.5 Cell Culture

BioWhittaker® Iscove's Modified Dulbecco's Medium (IMDM)	12-726	Lonza, Basel, Switzerland
Fetal calf serum	F4135	Sigma, Steinheim, Germany
Geneticin® G418	A1720	Sigma, Steinheim, Germany
Gibco® 1x DPBS	14190144	life technologies*TM*, Carlsbad, USA
Gibco® Roswell Park Memorial Institute 1640 medium (RPMI 1640)	11875093	life technologies*TM*, Carlsbad, USA
L-Glutamine (200 nM)	17-605	Lonza, Basel, Switzerland
Minimum essential medium nonessential amino acids (100x)	11140050	life technologies*TM*, Carlsbad, USA
Penicillin	13752	Sigma, Steinheim, Germany
Sodium Pyruvate (100 nM)	S8636	Sigma, Steinheim, Germany
Streptomycin	S9137	Sigma, Steinheim, Germany
Tuerk Solution	93770	Sigma, Steinheim, Germany

4.2.6 Kits

BD® CompBead Anti-mouse Ig κ	Becton Dickinson GmbH, Heidelberg
CloneJET PCR Cloning Kit	Thermo Fisher Scientific, Inc., Vilnius, Lithuania
KAPA HiFi PCR Kit	KAPA Biosystems, Cape Town, South Africa
QIAprep® Spin Miniprep Kit	Qiagen GmbH, Hilden
QIAGEN® Plasmid Maxi Kit	Qiagen GmbH, Hilden
QIAquick® Gel Extraction Kit	Qiagen GmbH, Hilden
QIFIKIT®	DAKO Deutschland GmbH, Hamburg

4.2.7 Cell lines

NALM-16	DSMZ, Braunschweig
JURKAT	DSMZ, Braunschweig
SP2/0-Ag-14	ATCC, Manassas, USA

4.2.8 Mouse lines

BALB/C	Charles River Laboratories, Wilmingtionm USA

4.2.9 Media, buffer, stocks

Media	
Freezing medium	90% (v/v) FCS 10% (v/v) DMSO
IMDM medium	10% (v/v) FCS L-Glutamine (1x) MEM non-essential amino acids (1x) Sodium pyruvate (1mM) Penicillin (100 U/mL) Streptomycin (100 µg/mL) 50 µM β-mercaptoethanol
RPMI 1640 medium	10% (v/v) FCS L-Glutamine (1x) MEM non-essential amino acids (1x) Sodium pyruvate (1mM) Penicillin (100 U/mL) Streptomycin (100 µg/mL) 50 µM β-mercaptoethanol
LB-Medium	10 g Bacto-tryptone 5 g Bacto-yeast extract 5 g NaCl ad 1 L ddH2O pH7
LB-Plates	10 g Bacto-tryptone 5 g Bacto-yeast extract 5 g NaCl 15 g Bacto-Agar ad 1 L ddH2O
LB-Amp-Plates	10 g Bacto-tryptone 5 g Bacto-yeast extract 5 g NaCl 15 g Bacto-Agar ad 1 L ddH2O pH7 1mL ampicillin stock solution
LB-Kan-Plates	10 g Bacto-tryptone 5 g Bacto-yeast extract 5 g NaCl 15 g Bacto-Agar ad 1 L ddH2O pH7 1mL kanamycin stock solution
Buffers	
Acetate buffer pH4	0.06M Sodium acetate 0.07M Acetic acid 0.1M NaCl pH adjusted with 37%HCl
0.1M Glycine/0.1M Citrate-Buffer pH2.4 and pH4.2	0.05M Trisodium citrate dehydrate

	0.05M Citric acid 0.1M Glycine 0.15M NaCl in ddH2O pH adjusted with HCl
0.1M Glycine-Buffer pH2.3	0.1M Glycine pH2.3 in ddH2O adjusted with HCl
0.1M Phosphate-Buffer pH7.2-7.3	0.07M Disodium phosphate 0.03M Sodium Dihydrogen Phosphate Monohydrate 0.1M NaCl in ddH2O pH adjusted with NaOH
0.01 M NaOH	1% (v/v) 1M NaOH buffer in ddH2O 20% ethanol 20% (v/v)
FACS-Buffer	DPBS 0.02% (w/v) Sodium azide 1% (v/v) FCS
ELISA blocking buffer	10% (v/v) BSA in ddH2O
ELISA wash buffer	0,05% Tween-20 in DPBS
ELISA stop solution	1M Phosphoric acid (H3PO4)
Ampicillin stock solution (100mg/m)]	Ampicillin in ddH2O
Kanamycin stock solution (100mg/mL)	Kanamycin in ddH2O
dNTP-stock solution (10mM)	dATP, dCTP, dGTP, dTTP (each 10mM) in ddH2O
Gel Loading Dye, Purple (6 x)	New CD105land Biolabs GmbH, Frankfurt
TfbI	30mM potassium acetate 50mM MnCl2 100mM KCl 10mM CaCl2 15% (w/v) Glycerine adjusted with 0.2M acetic acid to pH5.8 sterile-filtered
TfbII	10mM MOPS pH7 75mM CaCl2 10mM KCl 15% (w/v) Glycerol sterile-filtered

4.2.10 Single letter amino acid code

A	Alanine
R	Arginine
N	Asparagine
D	Aspartic Acid
C	Cysteine
Q	Glutamine
E	Glutamic Acid
G	Glycine
H	Histidine
I	Isoleucine
L	Leucine
K	Lysine
M	Methionine
F	Phenylalanine
P	Proline
S	Serine
T	Threonine
W	Tryptophan
Y	Tyrosine
V	Valine

5. Appendix

5.1 Supplementary Figures and Tables

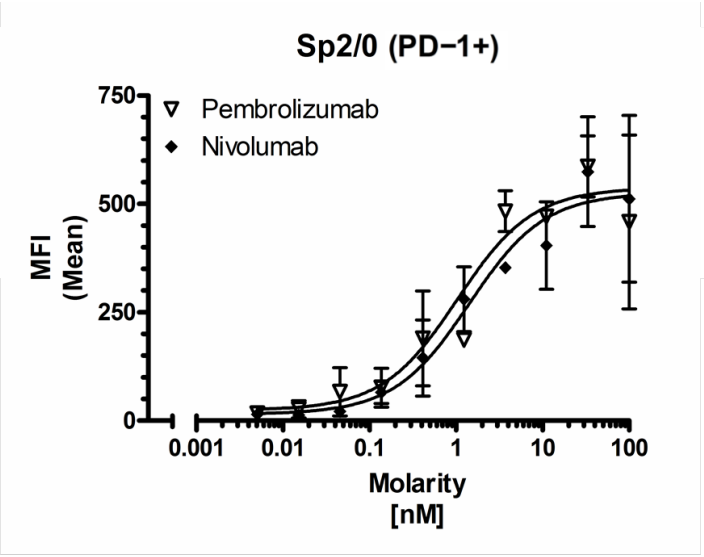

	EC_{50} [nM]
Pembrolizumab	1.04
Nivolumab	1.42

Figure S 1: Binding analysis of anti-PD-1 IgG to cell-bound PD-1. Antigen binding was analyzed by flow cytometry with their respective half-maximum binding. Mean ± SD n=1.

5.1.1 Vector

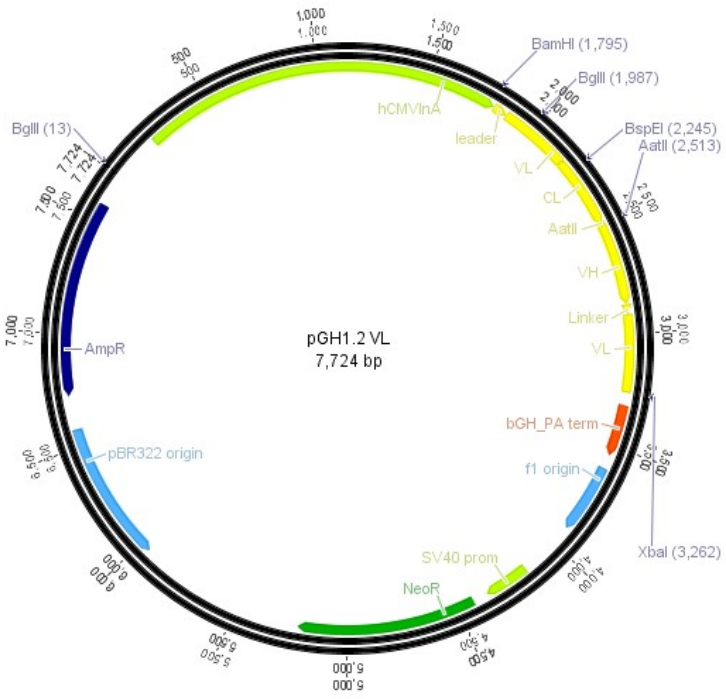

Figure S 2: Genetic elements of the pGH1.2 vector exemplary for Vl chain. AmpR – β-lactamase gene conferring resistance to ampicillin; pBR322 origin – responsible for the replication of pGH1.2; SV40 prom – SV40 Promotor region; NeoR – gene conferring neomycin resistance; hCMVInA – human CMV promotor region with human CMV insert A; Gene conferring for an exemplary antibody is colored in yellow; bGH_PA term – C – terminal poly A part.

Table S 1: List of all generated antibody clones during the work of this thesis

anti-4-1BB mAbs	
Hybridoma	**Phage**
TIM1	TIM5-A3
TIM2	TIM5-A4
TIM7-F10	TIM5-A8
TIM9-C2	TIM5-B5
TIM9-F9	TIM5-B12
TIM9-G6	TIM5-C2
TIM9-H9	TIM5-C3
TIM10-B1	TIM5-C5
TIM10-F4	TIM5-C8
TIM11-A2	TIM5-D6
TIM11-B3	TIM5-E4
TIM11-C1.1	TIM5-E11
TIM11-D2	TIM5-G8
TIM11-D4	TIM5-H1
TIM11-E4	TIM5-H11
TIM11-G4	SH1689-B12
	SH1689-C3
	SH1689-E12

anti-PD-1 mAbs	
Hybridoma	**Phage**
TIM7-A9	TIM4-A6
TIM7-G2	TIM4-B12
TIM9-E6	TIM4-C7
TIM10-B7	TIM4-D8
TIM10-C1	TIM4-E6
TIM10-D10	TIM4-F4
TIM11-A8	TIM4-G1
TIM11-B9	TIM4-G4
TIM11-C1.2	TIM4-H8
TIM11-E12	TIM4-H11
TIM11-F3.1	SH1716-A1
TIM11-H5	SH1716-A3
TIM11-H1	SH1716-B2
	SH1716-B4

anti-B7H3 mAbs
Hybridoma
TIM7-E10
TIM7-C4
TIM7-E11
TIM8-D4
TIM8-D9
TIM8-H8
TIM10-A7
TIM11-G3
TIM11-D11
TIM11-E2
TIM11-A7
TIM11-C8
TIM11-A7
TIM11-H2
TIM11-H5.1
TIM11-H5.2
TIM11-B8
TIM11-F3.2
TIM11-B11

anti-Fc mAbs
Hybridoma
TIM7-C3
TIM9-G9
TIM9-B9
TIM10-F5
TIM10-D5
TIM11-H9
TIM11-B1
TIM11-G1
TIM11-H4
TIM11-C9
TIM11-C7
TIM11-A11
TIM11-G5

5.2 List of Figures

List of Tables

Abbrevations

°C	Degree celsius
-L	without linker
+L	with linker
7-AAD	7-aminoactinomycin D
Amp	Ampicillin
AFCC	Antibody-dependent cytotoxicity
APCs	Antigen presenting cells
BCR	B cell receptor
bp	Base pair
CAR	Chimeric antigen receptor
CDC	Complement-dependent cytotoxicity
CDR	Complementary determining region
CI	Cell index
CRT	Control
CTLA-4	Cytotoxic T lymphocyte-associated antigen 4
Cys	Cysteine rich domain
D	Diversity
ddH2O	Double-distilled water
DMSO	Dimethyl sulfoxide
DNA	Deoxyribonucleic acid
DPBS	Dulbecco's phosphate buffered saline
EC50	Half maximal effective concentration
EDTA	Ethylenediaminetetraacetic acid
ELISA	Enzyme-linked immunosorbend assay
ENG	Endoglin
EtBr	Ethidium bromide
Fab	Fragment antigen binding
FACS	Fluorescence activated cell sorter
Fc	Fragment crystallizable
Fcγ	Fc gamma receptor
FcγR	Fc gamma receptor
FCS	Fetal calf serum
x g	Times earth's gravitational force
HAMA	Human anti-mouse antibodies
Hc	heavy chain
Hi	Hinge
Ig	Immunoglobulins
IMDM	Iscove's Modified Dulbecco's Medium
J	Joining
ka	association constant
kd	dissociation constant
KD	equilibrium dissociation constant
Lc	light chein
Li	Linker

mAb	Monoclonal antibody
MHC	Major histocompatiblity complex
ml	Milliliter
min	Minute
NKT	Natural killer T cell
OD	Optical density
µg	Microgram
µl	Microliter
µM	Micromol
UV	Ultraviolet
nm	Nanometer
NR	Reducing
OD	Optical density
PAA	Polyacrylamide
PD-1	Programmed death receptor 1
PD-L1	Programmed death receptor ligand 1
PD-L2	Programmed death receptor ligand 2
PCR	Polymerase chain reaction
PRRs	pattern recognition receptors
PSMA	Prostate specific membrane antigen
R	Reducing
SA	Superagonist
scFv	Single chain Fragment variable
SDS-Gel	sulfate-polyacrylamide gel electrophoresis
SEC	Size exclusion chromatography
TAA	Tumor associated antigen
TCR	T cell receptor
Tm	Melting Temperature
TMR	T cell modulating receptor
TNFα	Tumor necrosis factor α
TNFR	Tumor necrosis family receptors
V	Variable
VH	Variable heavy chain sequence
VL	Variable light chain sequence
w/o	without
wt	Wildtype
w/v	Weight/Volume

Acknowledgments

First of all, I want to express my sincere gratitude to Prof. Hans-Georg Rammensee and Prof. Gundram Jung. I am very grateful both of them for the substantial support and guidance I obtained throughout my PhD and for the trust in letting me pursue this highly explorative and challenging project. My deepest gratitude for the familiar and open atmosphere I felt throughout my work.

Thank you to all former and present members of the AG Jung for the productive and friendly atmosphere inside and outside the lab. I am grateful for the various good times.

Furthermore, I thank Latifa Zekri-Metref, for the close and thus fruitful work in our joint projects. I have greatly enjoyed our scientific exchange and brainstorming when trying to tackle our projects, and I wish there had been enough time to finalize them.

I also thank Beate Pömmel and Carolin Walker for the help with their animal husbandry and support in the laboratory work. I thank Yacine Mahringer and Julian Weischedel for their support in generating and characterizing several of the characterized antibodies in this work.

Besides, I want to thank Ana Marcu, Ferdinand Salomon, Yacine Mahringer, Annika Nelde, Maren Lübke, Yamel, and Felix Pagallies for sometimes more or less scientific discussions, breaking the lab routine and the obtained friendship over the years.

Finally, I want to express my gratitude for my friends and family for their immense support, love, and inspiration during the last couple of years in every possible manner.

Thank you all!

Bibliography

1. Moser, M. and O. Leo, *Key concepts in immunology.* Vaccine, 2010. **28 Suppl 3**: p. C2-13.

2. Saphire, E.O., et al., *Crystal structure of a neutralizing human IGG against HIV-1: a template for vaccine design.* Science, 2001. **293**(5532): p. 1155-9.

3. Dranoff, G., *Cytokines in cancer pathogenesis and cancer therapy.* Nat Rev Cancer, 2004. **4**(1): p. 11-22.

4. Kontermann, R.E., *Dual targeting strategies with bispecific antibodies.* MAbs, 2012. **4**(2): p. 182-97.

5. Kambayashi, T. and T.M. Laufer, *Atypical MHC class II-expressing antigen-presenting cells: can anything replace a dendritic cell?* Nat Rev Immunol, 2014. **14**(11): p. 719-30.

6. Brinkmann, U. and R.E. Kontermann, *The making of bispecific antibodies.* MAbs, 2017. **9**(2): p. 182-212.

7. Hoffmann, J.A., et al., *Phylogenetic perspectives in innate immunity.* Science, 1999. **284**(5418): p. 1313-8.

8. Spirig, R., J. Tsui, and S. Shaw, *The Emerging Role of TLR and Innate Immunity in Cardiovascular Disease.* Cardiol Res Pract, 2012. **2012**: p. 181394.

9. Bowie, A.G. and L. Unterholzner, *Viral evasion and subversion of pattern-recognition receptor signalling.* Nat Rev Immunol, 2008. **8**(12): p. 911-22.

10. Gordon, S., *Pattern recognition receptors: doubling up for the innate immune response.* Cell, 2002. **111**(7): p. 927-30.

11. Brack, C., et al., *A complete immunoglobulin gene is created by somatic recombination.* Cell, 1978. **15**(1): p. 1-14.

12. Harris, L.J., E. Skaletsky, and A. McPherson, *Crystallographic structure of an intact IgG1 monoclonal antibody.* J Mol Biol, 1998. **275**(5): p. 861-72.

13. Janin, J. and C. Chothia, *The structure of protein-protein recognition sites.* J Biol Chem, 1990. **265**(27): p. 16027-30.

14. Chacko, S., et al., *Structure of an antibody-lysozyme complex unexpected effect of conservative mutation.* J Mol Biol, 1995. **245**(3): p. 261-74.

15. Davies, D.R. and S. Chacko, *Antibody Structure.* Accounts of Chemical Research, 1993. **26**(8): p. 421-427.

16. Babbitt, B.P., et al., *Binding of immunogenic peptides to Ia histocompatibility molecules.* Nature, 1985. **317**(6035): p. 359-61.

17. Allen, P.M. and E.R. Unanue, *Antigen processing and presentation by macrophages.* Am J Anat, 1984. **170**(3): p. 483-90.

18. Curtsinger, J.M., D.C. Lins, and M.F. Mescher, *CD8+ memory T cells (CD44high, Ly-6C+) are more sensitive than naive cells to (CD44low, Ly-6C-) to TCR/CD8 signaling in response to antigen.* J Immunol, 1998. **160**(7): p. 3236-43.

19. Curtsinger, J.M., et al., *Inflammatory cytokines provide a third signal for activation of naive CD4+ and CD8+ T cells.* J Immunol, 1999. **162**(6): p. 3256-62.

20. Schwartz, R.H., et al., *T-cell clonal anergy.* Cold Spring Harb Symp Quant Biol, 1989. **54 Pt 2**: p. 605-10.

21. Appleman, L.J., et al., *Helper T cell anergy: from biochemistry to cancer pathophysiology and therapeutics.* J Mol Med (Berl), 2001. **78**(12): p. 673-83.

22. Lechler, R., et al., *The contributions of T-cell anergy to peripheral T-cell tolerance.* Immunology, 2001. **103**(3): p. 262-9.

23. Yang, Y. and J.M. Wilson, *CD40 ligand-dependent T cell activation: requirement of B7-CD28 signaling through CD40.* Science, 1996. **273**(5283): p. 1862-4.

24. McLellan, A.D., et al., *Human dendritic cells activate T lymphocytes via a CD40: CD40 ligand-dependent pathway.* Eur J Immunol, 1996. **26**(6): p. 1204-10.

25. Grewal, I.S., et al., *Requirement for CD40 ligand in costimulation induction, T cell activation, and experimental allergic encephalomyelitis.* Science, 1996. **273**(5283): p. 1864-7.

26. Higgins, L.M., et al., *Regulation of T cell activation in vitro and in vivo by targeting the OX40-OX40 ligand interaction: amelioration of ongoing inflammatory bowel disease with an OX40-IgG fusion protein, but not with an OX40 ligand-IgG fusion protein.* J Immunol, 1999. **162**(1): p. 486-93.

27. Akiba, H., et al., *CD28-independent costimulation of T cells by OX40 ligand and CD70 on activated B cells.* J Immunol, 1999. **162**(12): p. 7058-66.

28. Hurtado, J.C., et al., *Potential role of 4-1BB in T cell activation. Comparison with the costimulatory molecule CD28.* J Immunol, 1995. **155**(7): p. 3360-7.

29. Hurtado, J.C., Y.J. Kim, and B.S. Kwon, *Signals through 4-1BB are costimulatory to previously activated splenic T cells and inhibit activation-induced cell death.* J Immunol, 1997. **158**(6): p. 2600-9.

30. Pollok, K.E., et al., *Inducible T cell antigen 4-1BB. Analysis of expression and function.* J Immunol, 1993. **150**(3): p. 771-81.

31. Ishida, Y., et al., *Induced Expression of Pd-1, a Novel Member of the Immunoglobulin Gene Superfamily, Upon Programmed Cell-Death.* Embo Journal, 1992. **11**(11): p. 3887-3895.

32. Agata, Y., et al., *Expression of the PD-1 antigen on the surface of stimulated mouse T and B lymphocytes.* International Immunology, 1996. **8**(5): p. 765-772.

33. Zhang, J.Y., et al., *PD-1 up-regulation is correlated with HIV-specific memory CD8(+) T-cell exhaustion in typical progressors, but not in long-terrn nonprogressors.* Blood, 2007. **109**(11): p. 4671-4678.

34. Yao, S., et al., *PD-1 on dendritic cells impedes innate immunity against bacterial infection.* Blood, 2009. **113**(23): p. 5811-5818.

35. Freeman, G.J., et al., *Engagement of the PD-1 immunoinhibitory receptor by a novel B7 family member leads to negative regulation of lymphocyte activation.* J Exp Med, 2000. **192**(7): p. 1027-34.

36. Freeman, G.J., et al., *Reinvigorating exhausted HIV-specific T cells via PD-1-PD-1 ligand blockade.* Journal of Experimental Medicine, 2006. **203**(10): p. 2223-2227.

37. Yamazaki, T., et al., *Expression of programmed death 1 ligands by murine T cells and APC.* Journal of Immunology, 2002. **169**(10): p. 5538-5545.

38. Latchman, Y.E., et al., *PD-L1-deficient mice show that PD-L1 on T cells, antigen-presenting cells, and host tissues negatively regulates T cells.* Proceedings of the National Academy of Sciences of the United States of America, 2004. **101**(29): p. 10691-10696.

39. Probst, H.C., et al., *Resting dendritic cells induce peripheral CD8+T cell tolerance through PD-1 and CTLA-4.* Immunology, 2005. **116**: p. 43-43.

40. Keir, M.E., G.J. Freeman, and A.H. Sharpe, *PD-1 regulates self-reactive CD8(+) T cell responses to antigen in lymph nodes and tissues.* Journal of Immunology, 2007. **179**(8): p. 5064-5070.

41. Latchman, Y., et al., *PD-L2 is a second ligand for PD-I and inhibits T cell activation.* Nature Immunology, 2001. **2**(3): p. 261-268.

42. Okazaki, T., et al., *PD-1 immunoreceptor inhibits B cell receptor-mediated signaling by recruiting src homology 2-domain-containing tyrosine phosphatase 2 to phosphotyrosine.* Proceedings of the National Academy of Sciences of the United States of America, 2001. **98**(24): p. 13866-13871.

43. Chemnitz, J.M., et al., *SHP-1 and SHP-2 associate with immunoreceptor tyrosine-based switch motif of programmed death 1 upon primary human T cell*

stimulation, but only receptor ligation prevents T cell activation. Journal of Immunology, 2004. **173**(2): p. 945-954.

44. Hui, E.F., et al., *T cell costimulatory receptor CD28 is a primary target for PD-1-mediated inhibition.* Science, 2017. **355**(6332): p. 1428-+.

45. Parry, R.V., et al., *CTLA-4 and PD-1 receptors inhibit T-cell activation by distinct mechanisms.* Molecular and Cellular Biology, 2005. **25**(21): p. 9543-9553.

46. Bennett, F., et al., *Program death-1 engagement upon TCR activation has distinct effects on costimulation and cytokine-driven proliferation: Attenuation of ICOS, IL-4, and IL-21, but not CD28, IL-7, and IL-15 responses.* Journal of Immunology, 2003. **170**(2): p. 711-718.

47. Carter, L.L., et al., *PD-1 : PD-L inhibitory pathway affects both CD4(+)and CD8(+) T cells and is overcome by IL-2.* European Journal of Immunology, 2002. **32**(3): p. 634-643.

48. Skalli, O., et al., *A monoclonal antibody against alpha-smooth muscle actin: a new probe for smooth muscle differentiation.* J Cell Biol, 1986. **103**(6 Pt 2): p. 2787-96.

49. Burke, B., et al., *A monoclonal antibody against a 135-K Golgi membrane protein.* EMBO J, 1982. **1**(12): p. 1621-8.

50. Purtscher, M., et al., *A broadly neutralizing human monoclonal antibody against gp41 of human immunodeficiency virus type 1.* AIDS Res Hum Retroviruses, 1994. **10**(12): p. 1651-8.

51. Fisher, C.J., Jr., et al., *Initial evaluation of human monoclonal anti-lipid A antibody (HA-1A) in patients with sepsis syndrome.* Crit Care Med, 1990. **18**(12): p. 1311-5.

52. Kuhn, H.M., et al., *Characterization of the epitope specificity of murine monoclonal antibodies directed against lipid A.* Infect Immun, 1992. **60**(6): p. 2201-10.

53. Schuster, B.G., et al., *Production of antibodies against phosphocholine, phosphatidylcholine, sphingomyelin, and lipid A by injection of liposomes containing lipid A.* J Immunol, 1979. **122**(3): p. 900-5.

54. Gonchoroff, N.J., et al., *A monoclonal antibody reactive with 5-bromo-2-deoxyuridine that does not require DNA denaturation.* Cytometry, 1985. **6**(6): p. 506-12.

55. Naruse, I., H. Keino, and Y. Kawarada, *Antibody against single-stranded DNA detects both programmed cell death and drug-induced apoptosis.* Histochemistry, 1994. **101**(1): p. 73-8.

56. Seguela, P., et al., *Antibodies against gamma-aminobutyric acid: specificity studies and immunocytochemical results.* Proc Natl Acad Sci U S A, 1984. **81**(12): p. 3888-92.

57. Singh, K.V., et al., *Synthesis and characterization of hapten-protein conjugates for antibody production against small molecules.* Bioconjug Chem, 2004. **15**(1): p. 168-73.

58. Emini, E.A., et al., *Induction of hepatitis A virus-neutralizing antibody by a virus-specific synthetic peptide.* J Virol, 1985. **55**(3): p. 836-9.

59. Pantarotto, D., et al., *Immunization with peptide-functionalized carbon nanotubes enhances virus-specific neutralizing antibody responses.* Chem Biol, 2003. **10**(10): p. 961-6.

60. Strockbine, N.A., et al., *Characterization of monoclonal antibodies against Shiga-like toxin from Escherichia coli.* Infect Immun, 1985. **50**(3): p. 695-700.

61. Viscidi, R., et al., *Serum antibody response to toxins A and B of Clostridium difficile.* J Infect Dis, 1983. **148**(1): p. 93-100.

62. Volk, W.A., et al., *Neutralization of tetanus toxin by distinct monoclonal antibodies binding to multiple epitopes on the toxin molecule.* Infect Immun, 1984. **45**(3): p. 604-9.

63. Peitsch, M.C. and J. Tschopp, *Assembly of macromolecular pores by immune defense systems.* Curr Opin Cell Biol, 1991. **3**(4): p. 710-6.

64. Cassel, D.L., et al., *Differential expression of Fc gamma RIIA, Fc gamma RIIB and Fc gamma RIIC in hematopoietic cells: analysis of transcripts.* Mol Immunol, 1993. **30**(5): p. 451-60.

65. Kellner, C., et al., *Boosting ADCC and CDC activity by Fc engineering and evaluation of antibody effector functions.* Methods, 2014. **65**(1): p. 105-13.

66. Kohler, G. and C. Milstein, *Continuous cultures of fused cells secreting antibody of predefined specificity.* Nature, 1975. **256**(5517): p. 495-7.

67. Koren, E., L.A. Zuckerman, and A.R. Mire-Sluis, *Immune responses to therapeutic proteins in humans--clinical significance, assessment and prediction.* Curr Pharm Biotechnol, 2002. **3**(4): p. 349-60.

68. Schellekens, H., *Bioequivalence and the immunogenicity of biopharmaceuticals.* Nat Rev Drug Discov, 2002. **1**(6): p. 457-62.

69. Schellekens, H., *Immunogenicity of therapeutic proteins: clinical implications and future prospects.* Clin Ther, 2002. **24**(11): p. 1720-40; discussion 1719.

70. Shawler, D.L., et al., *Human immune response to multiple injections of murine monoclonal IgG.* J Immunol, 1985. **135**(2): p. 1530-5.

71. Schroff, R.W., et al., *Human anti-murine immunoglobulin responses in patients receiving monoclonal antibody therapy.* Cancer Res, 1985. **45**(2): p. 879-85.

72. Lubeck, M.D., et al., *The interaction of murine IgG subclass proteins with human monocyte Fc receptors.* J Immunol, 1985. **135**(2): p. 1299-304.

73. Carson, D.A. and B.D. Freimark, *Human lymphocyte hybridomas and monoclonal antibodies.* Adv Immunol, 1986. **38**: p. 275-311.

74. Morrison, S.L., et al., *Chimeric human antibody molecules: mouse antigen-binding domains with human constant region domains.* Proc Natl Acad Sci U S A, 1984. **81**(21): p. 6851-5.

75. Neuberger, M.S., et al., *A hapten-specific chimaeric IgE antibody with human physiological effector function.* Nature, 1985. **314**(6008): p. 268-70.

76. Boulianne, G.L., N. Hozumi, and M.J. Shulman, *Production of functional chimaeric mouse/human antibody.* Nature, 1984. **312**(5995): p. 643-6.

77. Liu, A.Y., et al., *Production of a mouse-human chimeric monoclonal antibody to CD20 with potent Fc-dependent biologic activity.* J Immunol, 1987. **139**(10): p. 3521-6.

78. Khazaeli, M.B., et al., *Frequent anti-V-region immune response to mouse B72.3 monoclonal antibody.* J Clin Immunol, 1992. **12**(2): p. 116-21.

79. Brüggemann, M., et al., *The immunogenicity of chimeric antibodies.* J Exp Med, 1989. **170**(6): p. 2153-7.

80. Jones, P.T., et al., *Replacing the complementarity-determining regions in a human antibody with those from a mouse.* Nature, 1986. **321**(6069): p. 522-5.

81. Reichert, J.M., *Monoclonal antibodies in the clinic.* Nat Biotechnol, 2001. **19**(9): p. 819-22.

82. Yoon, S.O., et al., *Construction, affinity maturation, and biological characterization of an anti-tumor-associated glycoprotein-72 humanized antibody.* J Biol Chem, 2006. **281**(11): p. 6985-92.

83. Verhoeyen, M., C. Milstein, and G. Winter, *Reshaping human antibodies: grafting an antilysozyme activity.* Science, 1988. **239**(4847): p. 1534-6.

84. Saito, R., et al., *Impact in stability during sequential CDR grafting to construct camelid VHH antibodies against zinc oxide and gold.* J Biochem, 2018. **164**(1): p. 21-25.

85. Foote, J. and G. Winter, *Antibody framework residues affecting the conformation of the hypervariable loops.* J Mol Biol, 1992. **224**(2): p. 487-99.

86. de Haard, H., et al., *Vernier zone residue 4 of mouse subgroup II kappa light chains is a critical determinant for antigen recognition.* Immunotechnology, 1999. **4**(3-4): p. 203-15.

87. Makabe, K., et al., *Thermodynamic consequences of mutations in vernier zone residues of a humanized anti-human epidermal growth factor receptor murine antibody, 528.* J Biol Chem, 2008. **283**(2): p. 1156-66.

88. Ewert, S., A. Honegger, and A. Pluckthun, *Stability improvement of antibodies for extracellular and intracellular applications: CDR grafting to stable frameworks and structure-based framework engineering.* Methods, 2004. **34**(2): p. 184-99.

89. Ewert, S., A. Honegger, and A. Pluckthun, *Structure-based improvement of the biophysical properties of immunoglobulin VH domains with a generalizable approach.* Biochemistry, 2003. **42**(6): p. 1517-28.

90. Weinblatt, M.E., et al., *CAMPATH-1H, a humanized monoclonal antibody, in refractory rheumatoid arthritis. An intravenous dose-escalation study.* Arthritis Rheum, 1995. **38**(11): p. 1589-94.

91. Smith, G.P., *Filamentous fusion phage: novel expression vectors that display cloned antigens on the virion surface.* Science, 1985. **228**(4705): p. 1315-7.

92. Hoet, R.M., et al., *Generation of high-affinity human antibodies by combining donor-derived and synthetic complementarity-determining-region diversity.* Nat Biotechnol, 2005. **23**(3): p. 344-8.

93. Tiller, T., et al., *A fully synthetic human Fab antibody library based on fixed VH/VL framework pairings with favorable biophysical properties.* MAbs, 2013. **5**(3): p. 445-70.

94. Schofield, D.J., et al., *Application of phage display to high throughput antibody generation and characterization.* Genome Biol, 2007. **8**(11): p. R254.

95. Vaughan, T.J., et al., *Human antibodies with sub-nanomolar affinities isolated from a large non-immunized phage display library.* Nat Biotechnol, 1996. **14**(3): p. 309-14.

96. Hust, M., et al., *A human scFv antibody generation pipeline for proteome research.* J Biotechnol, 2011. **152**(4): p. 159-70.

97. McCafferty, J., et al., *Phage antibodies: filamentous phage displaying antibody variable domains.* Nature, 1990. **348**(6301): p. 552-4.

98. Breitling, F., et al., *A surface expression vector for antibody screening.* Gene, 1991. **104**(2): p. 147-53.

99. Barbas, C.F., 3rd, et al., *Assembly of combinatorial antibody libraries on phage surfaces: the gene III site.* Proc Natl Acad Sci U S A, 1991. **88**(18): p. 7978-82.

100. Marks, J.D., et al., *By-passing immunization. Human antibodies from V-gene libraries displayed on phage.* J Mol Biol, 1991. **222**(3): p. 581-97.

101. Low, N.M., P.H. Holliger, and G. Winter, *Mimicking somatic hypermutation: affinity maturation of antibodies displayed on bacteriophage using a bacterial mutator strain.* J Mol Biol, 1996. **260**(3): p. 359-68.

102. Frenzel, A., T. Schirrmann, and M. Hust, *Phage display-derived human antibodies in clinical development and therapy.* MAbs, 2016. **8**(7): p. 1177-1194.

103. Kung, P., et al., *Monoclonal antibodies defining distinctive human T cell surface antigens.* Science, 1979. **206**(4416): p. 347-9.

104. Hooks, M.A., C.S. Wade, and W.J. Millikan, Jr., *Muromonab CD-3: a review of its pharmacology, pharmacokinetics, and clinical use in transplantation.* Pharmacotherapy, 1991. **11**(1): p. 26-37.

105. Van Wauwe, J.P., J.R. De Mey, and J.G. Goossens, *OKT3: a monoclonal anti-human T lymphocyte antibody with potent mitogenic properties.* J Immunol, 1980. **124**(6): p. 2708-13.

106. Sgro, C., *Side-effects of a monoclonal antibody, muromonab CD3/orthoclone OKT3: bibliographic review.* Toxicology, 1995. **105**(1): p. 23-9.

107. Suntharalingam, G., et al., *Cytokine storm in a phase 1 trial of the anti-CD28 monoclonal antibody TGN1412.* N Engl J Med, 2006. **355**(10): p. 1018-28.

108. Beyersdorf, N., et al., *Superagonistic anti-CD28 antibodies: potent activators of regulatory T cells for the therapy of autoimmune diseases.* Ann Rheum Dis, 2005. **64 Suppl 4**: p. iv91-5.

109. Otz, T., et al., *A bispecific single-chain antibody that mediates target cell-restricted, supra-agonistic CD28 stimulation and killing of lymphoma cells.* Leukemia, 2009. **23**(1): p. 71-7.

110. Grosse-Hovest, L., et al., *A recombinant bispecific single-chain antibody induces targeted, supra-agonistic CD28-stimulation and tumor cell killing.* Eur J Immunol, 2003. **33**(5): p. 1334-40.

111. Brandl, M., et al., *Bispecific antibody fragments with CD20 X CD28 specificity allow effective autologous and allogeneic T-cell activation against malignant cells in peripheral blood and bone marrow cultures from patients with B-cell lineage leukemia and lymphoma.* Exp Hematol, 1999. **27**(8): p. 1264-70.

112. Brown, K.E., *Revisiting CD28 Superagonist TGN1412 as Potential Therapeutic for Pediatric B Cell Leukemia: A Review.* Diseases, 2018. **6**(2).

113. Hinner, M.J., et al., *Tumor-Localized Costimulatory T-Cell Engagement by the 4-1BB/HER2 Bispecific Antibody-Anticalin Fusion PRS-343.* Clin Cancer Res, 2019. **25**(19): p. 5878-5889.

114. Compte, M., et al., *A tumor-targeted trimeric 4-1BB-agonistic antibody induces potent anti-tumor immunity without systemic toxicity.* Nat Commun, 2018. **9**(1): p. 4809.

115. Claus, C., et al., *Tumor-targeted 4-1BB agonists for combination with T cell bispecific antibodies as off-the-shelf therapy.* Sci Transl Med, 2019. **11**(496).

116. Segal, N.H., et al., *Results from an Integrated Safety Analysis of Urelumab, an Agonist Anti-CD137 Monoclonal Antibody.* Clin Cancer Res, 2017. **23**(8): p. 1929-1936.

117. Lum, L.G., et al., *In vitro regulation of immunoglobulin synthesis by T-cell subpopulations defined by a new human T-cell antigen (9.3).* Cell Immunol, 1982. **72**(1): p. 122-9.

118. Ledbetter, J.A., et al., *CD28 ligation in T-cell activation: evidence for two signal transduction pathways.* Blood, 1990. **75**(7): p. 1531-9.

119. Truitt, K.E., C.M. Hicks, and J.B. Imboden, *Stimulation of CD28 triggers an association between CD28 and phosphatidylinositol 3-kinase in Jurkat T cells.* J Exp Med, 1994. **179**(3): p. 1071-6.

120. Thompson, C.B., et al., *CD28 activation pathway regulates the production of multiple T-cell-derived lymphokines/cytokines.* Proc Natl Acad Sci U S A, 1989. **86**(4): p. 1333-7.

121. Baroja, M.L., et al., *The anti-T cell monoclonal antibody 9.3 (anti-CD28) provides a helper signal and bypasses the need for accessory cells in T cell activation with immobilized anti-CD3 and mitogens.* Cell Immunol, 1989. **120**(1): p. 205-17.

122. Bischof, A., et al., *Autonomous induction of proliferation, JNK and NF-alphaB activation in primary resting T cells by mobilized CD28.* Eur J Immunol, 2000. **30**(3): p. 876-82.

123. Luhder, F., et al., *Topological requirements and signaling properties of T cell-activating, anti-CD28 antibody superagonists.* J Exp Med, 2003. **197**(8): p. 955-66.

124. Evans, E.J., et al., *Crystal structure of a soluble CD28-Fab complex.* Nat Immunol, 2005. **6**(3): p. 271-9.

125. Tacke, M., et al., *CD28-mediated induction of proliferation in resting T cells in vitro and in vivo without engagement of the T cell receptor: evidence for functionally distinct forms of CD28.* Eur J Immunol, 1997. **27**(1): p. 239-47.

126. Levin, S.E., et al., *Inhibition of ZAP-70 kinase activity via an analog-sensitive allele blocks T cell receptor and CD28 superagonist signaling.* J Biol Chem, 2008. **283**(22): p. 15419-30.

127. Dennehy, K.M., et al., *Mitogenic CD28 signals require the exchange factor Vav1 to enhance TCR signaling at the SLP-76-Vav-Itk signalosome.* J Immunol, 2007. **178**(3): p. 1363-71.

128. Romer, P.S., et al., *Preculture of PBMCs at high cell density increases sensitivity of T-cell responses, revealing cytokine release by CD28 superagonist TGN1412.* Blood, 2011. **118**(26): p. 6772-82.

129. Elflein, K., et al., *Rapid recovery from T lymphopenia by CD28 superagonist therapy.* Blood, 2003. **102**(5): p. 1764-70.

130. Eastwood, D., et al., *Monoclonal antibody TGN1412 trial failure explained by species differences in CD28 expression on CD4+ effector memory T-cells.* Br J Pharmacol, 2010. **161**(3): p. 512-26.

131. Tabares, P., et al., *Human regulatory T cells are selectively activated by low-dose application of the CD28 superagonist TGN1412/TAB08.* Eur J Immunol, 2014. **44**(4): p. 1225-36.

132. Chester, C., et al., *Immunotherapy targeting 4-1BB: mechanistic rationale, clinical results, and future strategies.* Blood, 2018. **131**(1): p. 49-57.

133. Shuford, W.W., et al., *4-1BB costimulatory signals preferentially induce CD8+ T cell proliferation and lead to the amplification in vivo of cytotoxic T cell responses.* J Exp Med, 1997. **186**(1): p. 47-55.

134. Hernandez-Chacon, J.A., et al., *Costimulation through the CD137/4-1BB pathway protects human melanoma tumor-infiltrating lymphocytes from activation-induced cell death and enhances antitumor effector function.* J Immunother, 2011. **34**(3): p. 236-50.

135. Saoulli, K., et al., *CD28-independent, TRAF2-dependent costimulation of resting T cells by 4-1BB ligand.* J Exp Med, 1998. **187**(11): p. 1849-62.

136. Wilcox, R.A., et al., *Ligation of CD137 receptor prevents and reverses established anergy of CD8+ cytolytic T lymphocytes in vivo.* Blood, 2004. **103**(1): p. 177-84.

137. Kawalekar, O.U., et al., *Distinct Signaling of Coreceptors Regulates Specific Metabolism Pathways and Impacts Memory Development in CAR T Cells.* Immunity, 2016. **44**(2): p. 380-90.

138. Aznar, M.A., et al., *CD137 (4-1BB) Costimulation Modifies DNA Methylation in CD8(+) T Cell-Relevant Genes.* Cancer Immunol Res, 2018. **6**(1): p. 69-78.

139. Perez-Ruiz, E., et al., *Anti-CD137 and PD-1/PD-L1 Antibodies En Route toward Clinical Synergy.* Clin Cancer Res, 2017. **23**(18): p. 5326-5328.

140. Ascierto, P.A., et al., *Clinical experiences with anti-CD137 and anti-PD1 therapeutic antibodies.* Semin Oncol, 2010. **37**(5): p. 508-16.

141. Li, F. and J.V. Ravetch, *Antitumor activities of agonistic anti-TNFR antibodies require differential FcgammaRIIB coengagement in vivo.* Proc Natl Acad Sci U S A, 2013. **110**(48): p. 19501-6.

142. Xu, Y., et al., *Fc gamma Rs modulate cytotoxicity of anti-Fas antibodies: implications for agonistic antibody-based therapeutics.* J Immunol, 2003. **171**(2): p. 562-8.

143. Li, F. and J.V. Ravetch, *A general requirement for FcgammaRIIB co-engagement of agonistic anti-TNFR antibodies.* Cell Cycle, 2012. **11**(18): p. 3343-4.

144. Iwai, Y., et al., *Involvement of PD-L1 on tumor cells in the escape from host immune system and tumor immunotherapy by PD-L1 blockade.* Proc Natl Acad Sci U S A, 2002. **99**(19): p. 12293-7.

145. Dong, H., et al., *Tumor-associated B7-H1 promotes T-cell apoptosis: a potential mechanism of immune evasion.* Nat Med, 2002. **8**(8): p. 793-800.

146. Strome, S.E., et al., *B7-H1 blockade augments adoptive T-cell immunotherapy for squamous cell carcinoma.* Cancer Res, 2003. **63**(19): p. 6501-5.

147. Hamid, O., et al., *Safety and tumor responses with lambrolizumab (anti-PD-1) in melanoma.* N Engl J Med, 2013. **369**(2): p. 134-44.

148. Topalian, S.L., et al., *Survival, durable tumor remission, and long-term safety in patients with advanced melanoma receiving nivolumab.* J Clin Oncol, 2014. **32**(10): p. 1020-30.

149. Brahmer, J.R., et al., *Safety and activity of anti-PD-L1 antibody in patients with advanced cancer.* N Engl J Med, 2012. **366**(26): p. 2455-65.

150. Borghaei, H., et al., *Nivolumab versus Docetaxel in Advanced Nonsquamous Non-Small-Cell Lung Cancer.* N Engl J Med, 2015. **373**(17): p. 1627-39.

151. Garon, E.B., et al., *Pembrolizumab for the treatment of non-small-cell lung cancer.* N Engl J Med, 2015. **372**(21): p. 2018-28.

152. Zhou, Q., et al., *Program death-1 signaling and regulatory T cells collaborate to resist the function of adoptively transferred cytotoxic T lymphocytes in advanced acute myeloid leukemia.* Blood, 2010. **116**(14): p. 2484-93.

153. Weber, J.S., K.C. Kahler, and A. Hauschild, *Management of immune-related adverse events and kinetics of response with ipilimumab.* J Clin Oncol, 2012. **30**(21): p. 2691-7.

154. Herbst, R.S., et al., *Predictive correlates of response to the anti-PD-L1 antibody MPDL3280A in cancer patients.* Nature, 2014. **515**(7528): p. 563-7.

155. Robert, C., et al., *Nivolumab in previously untreated melanoma without BRAF mutation.* N Engl J Med, 2015. **372**(4): p. 320-30.

156. Min, L. and F.S. Hodi, *Anti-PD1 following ipilimumab for mucosal melanoma: durable tumor response associated with severe hypothyroidism and rhabdomyolysis.* Cancer Immunol Res, 2014. **2**(1): p. 15-8.

157. Wolchok, J.D., et al., *Nivolumab plus ipilimumab in advanced melanoma.* N Engl J Med, 2013. **369**(2): p. 122-33.

158. Robert, C., et al., *Anti-programmed-death-receptor-1 treatment with pembrolizumab in ipilimumab-refractory advanced melanoma: a randomised dose-comparison cohort of a phase 1 trial.* Lancet, 2014. **384**(9948): p. 1109-17.

159. Liao, B., et al., *Atypical neurological complications of ipilimumab therapy in patients with metastatic melanoma.* Neuro Oncol, 2014. **16**(4): p. 589-93.

160. Neri, D., et al., *High-affinity antigen binding by chelating recombinant antibodies (CRAbs).* J Mol Biol, 1995. **246**(3): p. 367-73.

161. Lu, D., et al., *Acquired antagonistic activity of a bispecific diabody directed against two different epitopes on vascular endothelial growth factor receptor 2.* J Immunol Methods, 1999. **230**(1-2): p. 159-71.

162. Cheong, H.S., et al., *Affinity enhancement of bispecific antibody against two different epitopes in the same antigen.* Biochem Biophys Res Commun, 1990. **173**(3): p. 795-800.

163. Staerz, U.D. and M.J. Bevan, *Hybrid hybridoma producing a bispecific monoclonal antibody that can focus effector T-cell activity.* Proc Natl Acad Sci U S A, 1986. **83**(5): p. 1453-7.

164. Lindhofer, H., et al., *Preferential species-restricted heavy/light chain pairing in rat/mouse quadromas. Implications for a single-step purification of bispecific antibodies.* J Immunol, 1995. **155**(1): p. 219-25.

165. Jung, G., J.A. Ledbetter, and H.J. Muller-Eberhard, *Induction of cytotoxicity in resting human T lymphocytes bound to tumor cells by antibody heteroconjugates.* Proc Natl Acad Sci U S A, 1987. **84**(13): p. 4611-5.

166. Karpovsky, B., et al., *Production of target-specific effector cells using hetero-cross-linked aggregates containing anti-target cell and anti-Fc gamma receptor antibodies.* J Exp Med, 1984. **160**(6): p. 1686-701.

167. Perez, P., et al., *Specific targeting of human peripheral blood T cells by heteroaggregates containing anti-T3 crosslinked to anti-target cell antibodies.* J Exp Med, 1986. **163**(1): p. 166-78.

168. Nisonoff, A. and M.M. Rivers, *Recombination of a mixture of univalent antibody fragments of different specificity.* Arch Biochem Biophys, 1961. **93**: p. 460-2.

169. Holliger, P., T. Prospero, and G. Winter, *"Diabodies": small bivalent and bispecific antibody fragments.* Proc Natl Acad Sci U S A, 1993. **90**(14): p. 6444-8.

170. Alt, M., R. Muller, and R.E. Kontermann, *Novel tetravalent and bispecific IgG-like antibody molecules combining single-chain diabodies with the immunoglobulin gamma1 Fc or CH3 region.* FEBS Lett, 1999. **454**(1-2): p. 90-4.

171. Jendreyko, N., et al., *Intradiabodies, bispecific, tetravalent antibodies for the simultaneous functional knockout of two cell surface receptors.* J Biol Chem, 2003. **278**(48): p. 47812-9.

172. Dangl, J.L., et al., *Segmental flexibility and complement fixation of genetically engineered chimeric human, rabbit and mouse antibodies.* EMBO J, 1988. **7**(7): p. 1989-94.

173. Dall'Acqua, W.F., P.A. Kiener, and H. Wu, *Properties of human IgG1s engineered for enhanced binding to the neonatal Fc receptor (FcRn).* J Biol Chem, 2006. **281**(33): p. 23514-24.

174. Hinton, P.R., et al., *Engineered human IgG antibodies with longer serum half-lives in primates.* J Biol Chem, 2004. **279**(8): p. 6213-6.

175. Hinton, P.R., et al., *An engineered human IgG1 antibody with longer serum half-life.* J Immunol, 2006. **176**(1): p. 346-56.

176. Jain, R.K. and L.T. Baxter, *Mechanisms of heterogeneous distribution of monoclonal antibodies and other macromolecules in tumors: significance of elevated interstitial pressure.* Cancer Res, 1988. **48**(24 Pt 1): p. 7022-32.

177. Idusogie, E.E., et al., *Engineered antibodies with increased activity to recruit complement.* J Immunol, 2001. **166**(4): p. 2571-5.

178. Lazar, G.A., et al., *Engineered antibody Fc variants with enhanced effector function.* Proc Natl Acad Sci U S A, 2006. **103**(11): p. 4005-10.

179. Schaefer, W., et al., *Immunoglobulin domain crossover as a generic approach for the production of bispecific IgG antibodies.* Proc Natl Acad Sci U S A, 2011. **108**(27): p. 11187-92.

180. Regula, J.T., et al., *Targeting key angiogenic pathways with a bispecific CrossMAb optimized for neovascular eye diseases.* EMBO Mol Med, 2016. **8**(11): p. 1265-1288.

181. Sahni, J., et al., *Simultaneous Inhibition of Angiopoietin-2 and Vascular Endothelial Growth Factor-A with Faricimab in Diabetic Macular Edema: BOULEVARD Phase 2 Randomized Trial.* Ophthalmology, 2019. **126**(8): p. 1155-1170.

182. Heiss, M.M., et al., *The trifunctional antibody catumaxomab for the treatment of malignant ascites due to epithelial cancer: Results of a prospective randomized phase II/III trial.* Int J Cancer, 2010. **127**(9): p. 2209-21.

183. Haas, C., et al., *Mode of cytotoxic action of T cell-engaging BiTE antibody MT110.* Immunobiology, 2009. **214**(6): p. 441-53.

184. Molhoj, M., et al., *CD19-/CD3-bispecific antibody of the BiTE class is far superior to tandem diabody with respect to redirected tumor cell lysis.* Mol Immunol, 2007. **44**(8): p. 1935-43.

185. Kipriyanov, S.M., et al., *Bispecific CD3 x CD19 diabody for T cell-mediated lysis of malignant human B cells.* Int J Cancer, 1998. **77**(5): p. 763-72.

186. Staerz, U.D., O. Kanagawa, and M.J. Bevan, *Hybrid antibodies can target sites for attack by T cells.* Nature, 1985. **314**(6012): p. 628-31.

187. Portell, C.A., C.M. Wenzell, and A.S. Advani, *Clinical and pharmacologic aspects of blinatumomab in the treatment of B-cell acute lymphoblastic leukemia.* Clin Pharmacol, 2013. **5**(Suppl 1): p. 5-11.

188. Bargou, R., et al., *Tumor regression in cancer patients by very low doses of a T cell-engaging antibody.* Science, 2008. **321**(5891): p. 974-7.

189. Grosse-Hovest, L., et al., *Supraagonistic, bispecific single-chain antibody purified from the serum of cloned, transgenic cows induces T-cell-mediated killing of glioblastoma cells in vitro and in vivo.* Int J Cancer, 2005. **117**(6): p. 1060-4.

190. Skokos, D., et al., *A class of costimulatory CD28-bispecific antibodies that enhance the antitumor activity of CD3-bispecific antibodies.* Sci Transl Med, 2020. **12**(525).

191. Sun, Z.J., et al., *A novel bispecific c-MET/PD-1 antibody with therapeutic potential in solid cancer.* Oncotarget, 2017. **8**(17): p. 29067-29079.

192. Correnti, C.E., et al., *Simultaneous multiple interaction T-cell engaging (SMITE) bispecific antibodies overcome bispecific T-cell engager (BiTE) resistance via CD28 co-stimulation.* Leukemia, 2018. **32**(5): p. 1239-1243.

193. Koopmans, I., et al., *A novel bispecific antibody for EGFR-directed blockade of the PD-1/PD-L1 immune checkpoint.* Oncoimmunology, 2018. **7**(8): p. e1466016.

194. Mittal, D., et al., *Blockade of ErbB2 and PD-L1 using a bispecific antibody to improve targeted anti-ErbB2 therapy.* Oncoimmunology, 2019. **8**(11): p. e1648171.

195. Foran, J.M., et al., *European phase II study of rituximab (chimeric anti-CD20 monoclonal antibody) for patients with newly diagnosed mantle-cell lymphoma and previously treated mantle-cell lymphoma, immunocytoma, and small B-cell lymphocytic lymphoma.* J Clin Oncol, 2000. **18**(2): p. 317-24.

196. Foran, J.M., et al., *A UK multicentre phase II study of rituximab (chimaeric anti-CD20 monoclonal antibody) in patients with follicular lymphoma, with PCR monitoring of molecular response.* Br J Haematol, 2000. **109**(1): p. 81-8.

197. Pallasch, C.P., et al., *Sensitizing protective tumor microenvironments to antibody-mediated therapy.* Cell, 2014. **156**(3): p. 590-602.

198. Baker, J.H.E., et al., *Heterogeneous distribution of trastuzumab in HER2-positive xenografts and metastases: role of the tumor microenvironment.* Clin Exp Metastasis, 2018. **35**(7): p. 691-705.

199. Bhutani, D. and U.N. Vaishampayan, *Monoclonal antibodies in oncology therapeutics: present and future indications.* Expert Opin Biol Ther, 2013. **13**(2): p. 269-82.

200. Thurber, G.M., M.M. Schmidt, and K.D. Wittrup, *Antibody tumor penetration: transport opposed by systemic and antigen-mediated clearance.* Adv Drug Deliv Rev, 2008. **60**(12): p. 1421-34.

201. Thurber, G.M., S.C. Zajic, and K.D. Wittrup, *Theoretic criteria for antibody penetration into solid tumors and micrometastases.* J Nucl Med, 2007. **48**(6): p. 995-9.

202. Nessler, I., et al., *Increased Tumor Penetration of Single-Domain Antibody Drug Conjugates Improves In Vivo Efficacy in Prostate Cancer Models.* Cancer Res, 2020.

203. Schmidt, M.M. and K.D. Wittrup, *A modeling analysis of the effects of molecular size and binding affinity on tumor targeting.* Mol Cancer Ther, 2009. **8**(10): p. 2861-71.

204. Lee, S.H., et al., *Pivotal role of vascular endothelial growth factor pathway in tumor angiogenesis.* Ann Surg Treat Res, 2015. **89**(1): p. 1-8.

205. Vredenburgh, J.J., et al., *Phase II trial of bevacizumab and irinotecan in recurrent malignant glioma.* Clin Cancer Res, 2007. **13**(4): p. 1253-9.

206. Zhu, A.X., et al., *A phase II and biomarker study of ramucirumab, a human monoclonal antibody targeting the VEGF receptor-2, as first-line monotherapy in patients with advanced hepatocellular cancer.* Clin Cancer Res, 2013. **19**(23): p. 6614-23.

207. St Croix, B., et al., *Genes expressed in human tumor endothelium.* Science, 2000. **289**(5482): p. 1197-202.

208. Gougos, A. and M. Letarte, *Identification of a human endothelial cell antigen with monoclonal antibody 44G4 produced against a pre-B leukemic cell line.* J Immunol, 1988. **141**(6): p. 1925-33.

209. Letamendia, A., et al., *Role of endoglin in cellular responses to transforming growth factor-beta. A comparative study with betaglycan.* J Biol Chem, 1998. **273**(49): p. 33011-9.

210. Burrows, F.J., et al., *Up-regulation of endoglin on vascular endothelial cells in human solid tumors: implications for diagnosis and therapy.* Clin Cancer Res, 1995. **1**(12): p. 1623-34.

211. Wang, J.M., et al., *Irradiation induces up-regulation of E9 protein (CD105) in human vascular endothelial cells.* Int J Cancer, 1995. **62**(6): p. 791-6.

212. Miller, D.W., et al., *Elevated expression of endoglin, a component of the TGF-beta-receptor complex, correlates with proliferation of tumor endothelial cells.* Int J Cancer, 1999. **81**(4): p. 568-72.

213. Vo, M.N., et al., *Elevated plasma endoglin (CD105) predicts decreased response and survival in a metastatic breast cancer trial of hormone therapy.* Breast Cancer Res Treat, 2010. **119**(3): p. 767-71.

214. Tanaka, F., et al., *Evaluation of angiogenesis in non-small cell lung cancer: comparison between anti-CD34 antibody and anti-CD105 antibody.* Clin Cancer Res, 2001. **7**(11): p. 3410-5.

215. Svatek, R.S., et al., *Preoperative plasma endoglin levels predict biochemical progression after radical prostatectomy.* Clin Cancer Res, 2008. **14**(11): p. 3362-6.

216. Li, C., et al., *Both high intratumoral microvessel density determined using CD105 antibody and elevated plasma levels of CD105 in colorectal cancer patients correlate with poor prognosis.* Br J Cancer, 2003. **88**(9): p. 1424-31.

217. Kumar, S., et al., *Breast carcinoma: vascular density determined using CD105 antibody correlates with tumor prognosis.* Cancer Res, 1999. **59**(4): p. 856-61.

218. El-Gohary, Y.M., et al., *Endoglin (CD105) and vascular endothelial growth factor as prognostic markers in prostatic adenocarcinoma.* Am J Clin Pathol, 2007. **127**(4): p. 572-9.

219. Apolo, A.B., et al., *A Phase II Clinical Trial of TRC105 (Anti-Endoglin Antibody) in Adults With Advanced/Metastatic Urothelial Carcinoma.* Clin Genitourin Cancer, 2017. **15**(1): p. 77-85.

220. Na, Z., et al., *Structural basis for blocking PD-1-mediated immune suppression by therapeutic antibody pembrolizumab.* Cell Res, 2017. **27**(1): p. 147-150.

221. Chodorge, M., et al., *A series of Fas receptor agonist antibodies that demonstrate an inverse correlation between affinity and potency.* Cell Death Differ, 2012. **19**(7): p. 1187-95.

222. Rudolf, D., et al., *Potent costimulation of human CD8 T cells by anti-4-1BB and anti-CD28 on synthetic artificial antigen presenting cells.* Cancer Immunol Immunother, 2008. **57**(2): p. 175-83.

223. Luo, H., et al., *Anti-CD28 antibody- and IL-4-induced human T cell proliferation is sensitive to rapamycin.* Clin Exp Immunol, 1993. **94**(2): p. 371-6.

224. Jenkins, M.K., et al., *CD28 delivers a costimulatory signal involved in antigen-specific IL-2 production by human T cells.* J Immunol, 1991. **147**(8): p. 2461-6.

225. Osada, T., et al., *CEA/CD3-bispecific T cell-engaging (BiTE) antibody-mediated T lymphocyte cytotoxicity maximized by inhibition of both PD1 and PD-L1.* Cancer Immunol Immunother, 2015. **64**(6): p. 677-88.

226. Krupka, C., et al., *Blockade of the PD-1/PD-L1 axis augments lysis of AML cells by the CD33/CD3 BiTE antibody construct AMG 330: reversing a T-cell-induced immune escape mechanism.* Leukemia, 2016. **30**(2): p. 484-91.

227. Singh-Jasuja, H., N.P. Emmerich, and H.G. Rammensee, *The Tubingen approach: identification, selection, and validation of tumor-associated HLA peptides for cancer therapy.* Cancer Immunol Immunother, 2004. **53**(3): p. 187-95.

228. Dudley, M.E., et al., *Adoptive cell therapy for patients with metastatic melanoma: evaluation of intensive myeloablative chemoradiation preparative regimens.* J Clin Oncol, 2008. **26**(32): p. 5233-9.

229. Turtle, C.J., et al., *CD19 CAR-T cells of defined CD4+:CD8+ composition in adult B cell ALL patients.* J Clin Invest, 2016. **126**(6): p. 2123-38.

230. Chavez, J.C., C. Bachmeier, and M.A. Kharfan-Dabaja, *CAR T-cell therapy for B-cell lymphomas: clinical trial results of available products.* Ther Adv Hematol, 2019. **10**: p. 2040620719841581.

231. Bai, X.F., et al., *Antigenic drift as a mechanism for tumor evasion of destruction by cytolytic T lymphocytes.* J Clin Invest, 2003. **111**(10): p. 1487-96.

232. Strand, S., et al., *Lymphocyte apoptosis induced by CD95 (APO-1/Fas) ligand-expressing tumor cells--a mechanism of immune evasion?* Nat Med, 1996. **2**(12): p. 1361-6.

233. Nitta, T., et al., *Induction of cytotoxicity in human T cells coated with anti-glioma x anti-CD3 bispecific antibody against human glioma cells.* J Neurosurg, 1990. **72**(3): p. 476-81.

234. Mezzanzanica, D., et al., *Human ovarian carcinoma lysis by cytotoxic T cells targeted by bispecific monoclonal antibodies: analysis of the antibody components.* Int J Cancer, 1988. **41**(4): p. 609-15.

235. Mack, M., G. Riethmuller, and P. Kufer, *A small bispecific antibody construct expressed as a functional single-chain molecule with high tumor cell cytotoxicity.* Proc Natl Acad Sci U S A, 1995. **92**(15): p. 7021-5.

236. Hoffmann, P., et al., *Serial killing of tumor cells by cytotoxic T cells redirected with a CD19-/CD3-bispecific single-chain antibody construct.* Int J Cancer, 2005. **115**(1): p. 98-104.

237. Schwartz, K., *Generierung, präklinische Charakterisierung und Optimierung monoklonaler Antikörper zur anti-angiogenetischen Therapie solider Tumoren*, in *Biology*. 2013, University of Tübingen: Mathematisch-Naturwissenschaftliche Fakultät.

238. Hansen, J.A.M., P. J.

Nowinski, R. C., *Monoclonal antibodies identifying a novel T-Cell antigen and Ia antigens of human lymphocytes.* Immunogenetics, 1980. **10**(1-4): p. 247-260.

239. Coloma, M.J. and S.L. Morrison, *Design and production of novel tetravalent bispecific antibodies.* Nat Biotechnol, 1997. **15**(2): p. 159-63.

240. June, C.H., et al., *T-cell proliferation involving the CD28 pathway is associated with cyclosporine-resistant interleukin 2 gene expression.* Mol Cell Biol, 1987. **7**(12): p. 4472-81.

241. Soos, M.A., et al., *A Panel of Monoclonal-Antibodies for the Type-I Insulin-Like Growth-Factor Receptor - Epitope Mapping, Effects on Ligand-Binding, and Biological-Activity.* Journal of Biological Chemistry, 1992. **267**(18): p. 12955-12963.

242. Hefta, L.J., M. Neumaier, and J.E. Shively, *Kinetic and affinity constants of epitope specific anti-carcinoembryonic antigen (CEA) monoclonal antibodies for CEA and engineered CEA domain constructs.* Immunotechnology, 1998. **4**(1): p. 49-57.

243. Hawkins, R.E., S.J. Russell, and G. Winter, *Selection of phage antibodies by binding affinity. Mimicking affinity maturation.* J Mol Biol, 1992. **226**(3): p. 889-96.

244. Antonelli, G., *In vivo development of antibody to interferons: an update to 1996.* J Interferon Cytokine Res, 1997. **17 Suppl 1**: p. S39-46.

245. Mahringer, Y., *Pre-clinical development of a combinatorial approach in cancer therapy using bispecific antibodies and the optimization thereof.*, in *Biology*. 2018, University of Tübingen: Mathematisch-Naturwissenschaftliche Fakultät.

246. Al-Lazikani, B., A.M. Lesk, and C. Chothia, *Standard conformations for the canonical structures of immunoglobulins.* J Mol Biol, 1997. **273**(4): p. 927-48.

247. Abhinandan, K.R. and A.C. Martin, *Analyzing the "degree of humanness" of antibody sequences.* J Mol Biol, 2007. **369**(3): p. 852-62.

248. Jayaram, N., P. Bhowmick, and A.C. Martin, *Germline VH/VL pairing in antibodies.* Protein Eng Des Sel, 2012. **25**(10): p. 523-9.

249. Gram, H., et al., *In vitro selection and affinity maturation of antibodies from a naive combinatorial immunoglobulin library.* Proc Natl Acad Sci U S A, 1992. **89**(8): p. 3576-80.

250. Wörn, A. and A. Pluckthun, *Stability engineering of antibody single-chain Fv fragments.* J Mol Biol, 2001. **305**(5): p. 989-1010.

251. Glockshuber, R., et al., *A comparison of strategies to stabilize immunoglobulin Fv-fragments.* Biochemistry, 1990. **29**(6): p. 1362-7.

252. Miller, B.R., et al., *Stability engineering of scFvs for the development of bispecific and multivalent antibodies.* Protein Eng Des Sel, 2010. **23**(7): p. 549-57.

253. Stonehouse, T.J., et al., *Molecular characterization of U937-dependent T-cell co-stimulation.* Immunology, 1999. **96**(1): p. 35-47.

254. Weischedel, J.D.A., *Characterisation of novel phage display generated CD137 directed antibodies for cancer immunotherapy*, in *Faculty of Medicine*. 2018, University of Tübingen.

255. Carpenito, C., et al., *Control of large, established tumor xenografts with genetically retargeted human T cells containing CD28 and CD137 domains.* Proc Natl Acad Sci U S A, 2009. **106**(9): p. 3360-5.

256. Li, Y., et al., *Limited Cross-Linking of 4-1BB by 4-1BB Ligand and the Agonist Monoclonal Antibody Utomilumab.* Cell Rep, 2018. **25**(4): p. 909-920 e4.

257. Chin, S.M., et al., *Structure of the 4-1BB/4-1BBL complex and distinct binding and functional properties of utomilumab and urelumab.* Nat Commun, 2018. **9**(1): p. 4679.

258. Yu, X., et al., *Complex Interplay between Epitope Specificity and Isotype Dictates the Biological Activity of Anti-human CD40 Antibodies.* Cancer Cell, 2018. **33**(4): p. 664-675 e4.

259. White, A.L., et al., *Fcgamma receptor dependency of agonistic CD40 antibody in lymphoma therapy can be overcome through antibody multimerization.* J Immunol, 2014. **193**(4): p. 1828-35.

260. White, A.L., S.A. Beers, and M.S. Cragg, *FcgammaRIIB as a key determinant of agonistic antibody efficacy.* Curr Top Microbiol Immunol, 2014. **382**: p. 355-72.

261. Wang, C., et al., *In vitro characterization of the anti-PD-1 antibody nivolumab, BMS-936558, and in vivo toxicology in non-human primates.* Cancer Immunol Res, 2014. **2**(9): p. 846-56.

262. Croasdale, R., et al., *Development of tetravalent IgG1 dual targeting IGF-1R-EGFR antibodies with potent tumor inhibition.* Arch Biochem Biophys, 2012. **526**(2): p. 206-18.

263. Schanzer, J., et al., *Development of tetravalent, bispecific CCR5 antibodies with antiviral activity against CCR5 monoclonal antibody-resistant HIV-1 strains.* Antimicrob Agents Chemother, 2011. **55**(5): p. 2369-78.

264. Le Gall, F., et al., *Effect of linker sequences between the antibody variable domains on the formation, stability and biological activity of a bispecific tandem diabody.* Protein Eng Des Sel, 2004. **17**(4): p. 357-66.

265. Fransson, J., et al., *Human framework adaptation of a mouse anti-human IL-13 antibody.* J Mol Biol, 2010. **398**(2): p. 214-31.

266. Liu, R., et al., *Efficient inhibition of human B-cell lymphoma in SCID mice by synergistic antitumor effect of human 4-1BB ligand/anti-CD20 fusion proteins and anti-CD3/anti-CD20 diabodies.* J Immunother, 2010. **33**(5): p. 500-9.

267. Muller, D., K. Frey, and R.E. Kontermann, *A novel antibody-4-1BBL fusion protein for targeted costimulation in cancer immunotherapy.* J Immunother, 2008. **31**(8): p. 714-22.

268. Schrand, B., et al., *Reducing toxicity of 4-1BB costimulation: targeting 4-1BB ligands to the tumor stroma with bi-specific aptamer conjugates.* Oncoimmunology, 2015. **4**(3): p. e970918.

269. Schrand, B., et al., *Targeting 4-1BB costimulation to the tumor stroma with bispecific aptamer conjugates enhances the therapeutic index of tumor immunotherapy.* Cancer Immunol Res, 2014. **2**(9): p. 867-77.

270. Yi, L., et al., *Human and mouse CD137 have predominantly different binding CRDs to their respective ligands.* PLoS One, 2014. **9**(1): p. e86337.

271. Kohnke, T., et al., *Increase of PD-L1 expressing B-precursor ALL cells in a patient resistant to the CD19/CD3-bispecific T cell engager antibody blinatumomab.* J Hematol Oncol, 2015. **8**: p. 111.

272. Zak, K.M., et al., *Structural Biology of the Immune Checkpoint Receptor PD-1 and Its Ligands PD-L1/PD-L2.* Structure, 2017. **25**(8): p. 1163-1174.

273. Horita, S., et al., *High-resolution crystal structure of the therapeutic antibody pembrolizumab bound to the human PD-1.* Sci Rep, 2016. **6**: p. 35297.

274. Birnboim, H.C. and J. Doly, *A rapid alkaline extraction procedure for screening recombinant plasmid DNA.* Nucleic Acids Res, 1979. **7**(6): p. 1513-23.

275. Kleppe, K., et al., *Studies on polynucleotides. XCVI. Repair replications of short synthetic DNA's as catalyzed by DNA polymerases.* J Mol Biol, 1971. **56**(2): p. 341-61.

276. Mullis, K.B. and F.A. Faloona, *Specific synthesis of DNA in vitro via a polymerase-catalyzed chain reaction.* Methods Enzymol, 1987. **155**: p. 335-50.

277. Gao, S.H., et al., *Monoclonal antibody humanness score and its applications.* BMC Biotechnol, 2013. **13**: p. 55.

278. Kabat, E.A., T.T. Wu, and H. Bilofksy, Reid-Miller, M., Perry, H., *Sequence of Proteins of Immunological Interest.* 1983, National Institutes of Health, Bethesda.

279. Chothia, C. and A.M. Lesk, *Canonical structures for the hypervariable regions of immunoglobulins.* J Mol Biol, 1987. **196**(4): p. 901-17.

280. Chothia, C., et al., *Conformations of immunoglobulin hypervariable regions.* Nature, 1989. **342**(6252): p. 877-83.

281. MacCallum, R.M., A.C. Martin, and J.M. Thornton, *Antibody-antigen interactions: contact analysis and binding site topography.* J Mol Biol, 1996. **262**(5): p. 732-45.

282. Laemmli, U.K., *Cleavage of structural proteins during the assembly of the head of bacteriophage T4.* Nature, 1970. **227**(5259): p. 680-5.

283. Miltenyi, S., et al., *High gradient magnetic cell separation with MACS.* Cytometry, 1990. **11**(2): p. 231-8.

284. Peper, J.K., et al., *An impedance-based cytotoxicity assay for real-time and label-free assessment of T-cell-mediated killing of adherent cells.* J Immunol Methods, 2014. **405**: p. 192-8.

Eidesstattliche Erklärung

Mit meiner Unterschrift erkläre ich, dass die vorliegende Arbeit selbständig und nur unter Verwendung der im Literaturverzeichnis aufgeführten Quellen erarbeitet worden ist. Die Stellen meiner Arbeit, die dem Wortlaut oder dem Sinn nach anderen Werken entnommen sind, habe ich in jedem Fall unter Angabe der Quelle als Entlehnung kenntlich gemacht. Die Angaben sind für jede einzelne Quelle als Fußnote mit Verweis auf die Quelle aufgeführt. Dasselbe gilt sinngemäß für Tabellen, Karten und Abbildungen, auch solche, die aus Internetquellen stammen.

Ort, Datum

Unterschrift